ANALOGUE MODELLING OF THE SALT TECTONICS SYSTEM, OFFSHORE NOVA SCOTIA: INSIGHTS INTO INITIAL SALT MOBILIZATION AND AUTOCHTHONOUS SALT STRUCTURES

Cody J. MacDonald

Submitted in Partial Fulfillment of the Requirements for the Degree of Bachelor of Science, Honours

Department of Earth Sciences
Dalhousie University, Halifax, Nova Scotia

March, 2007

Abstract

Geological problems with offshore Nova Scotia are associated with complex salt deformation beneath the shelf and slope. Features in this area record highly variable tectono-sedimentary environments with high rates of sedimentation and progradation during the Jurassic and Early Cretaceous. These features have impacted petroleum exploration; particularly seismic imaging and hampers the structural interpretation of basement morphology beneath the rift-related salt basins. To address these problems dynamically scaled analogue models consisting of silica sand and silicone rubber simulate sedimentation, salt mobilization and deformation of the brittle overburden sediments and viscous salt.

The experimental results have led to three fundamental concepts. 1) The dominant mechanism for initial salt mobilization in rift basins with thick salt is channel flow within the salt layer driven by passive downbuilding of the landward salt withdrawal basins. 2) Initial landward mobilization and position of basinward salt inflation depends mainly on variations in salt thickness controlled by the basin floor geometry, rather than the geometry of the basinward rift shoulder. 3) The timing and extent of the allochthonous salt nappe advancement depends on the efficiency of early salt evacuation in the landward salt basin and sediment progradation on top of the inflated salt complex. Application of these concepts suggests that Subprovinces III and IV containing the Abenaki and Sable Subbasins have a basement floor geometry that results in highly variable salt thickness. With more in depth studies of seismic data these new concepts will make it possible to refine basement structure and its effect on the evolution of the salt-related structures and depositional systems at the Scotian Margin from early Jurassic to Cretaceous. This understanding is essential for the analysis of petroleum reservoir development, migration systems and potential plays.

Table of Contents

Table of Figures

Table of Tables

Acknowledgements

I would like to thank Juergen Adam and Csaba Krezsek for their mentorship and patience during the summer internship and school term. If it were not for them I would not have had the opportunity to study this interesting and important topic. Working with these two has been a wonderful experience.

I would also like to thank Shell Canada for the funding and opportunity to work with the Salt Dynamics Group at Dalhousie and for the great Structural Geology field trip that they hosted in the summer.

Thanks also go to Djordje Grujic for making structural geology so interesting to me and bringing to my attention the position with the Dalhousie Salt Dynamics Group.

Special thanks go to Grant Wach for helping me with organization of school work, applying for scholarships and guidance with building a career. Grant works very hard to get funding for students who rely on it and deserves thanks from us all.

Finally, I would like to thank Clarke Campbell for being a great person to work with, as well as being a great friend during not only the extent of the honours project but throughout my experience as an undergraduate student at Dalhousie University.

Chapter 1: Introduction

1.1 Background

The latest round of hydrocarbon exploration in the deepwater slope of the Scotian Margin has yielded unsatisfactory results. The problems associated with exploration in this area stem from an inadequate geological understanding of the tectonic and sedimentary evolution of the shelf-slope-basin transition (Enachescu and Wach, 2005). Many of the problems associated with understanding the geology of this area are related to the complex thin skinned salt deformation structures beneath the shelf and the slope (fig. 1-1) (Shimeld, 2004). The features observed in this area record a highly variable tectono-sedimentary environment with high rates of sedimentation and progradation during the Jurassic and Early Cretaceous. Factors which limit knowledge of the Scotian Margin include the lack of scientific drill holes, frequent overpressures and acoustic shadowing from salt present in the substratum. The number of wells is significant where water depths are less than 200 m and good data exists. However, at greater depths the risk and costs associated with drilling increases, resulting in the lack of wells and reliable data. Because of the lack of well data at greater depths most of the information detailing salt related deformation and structures come from 2D and 3D seismic data (Shimeld, 2004).

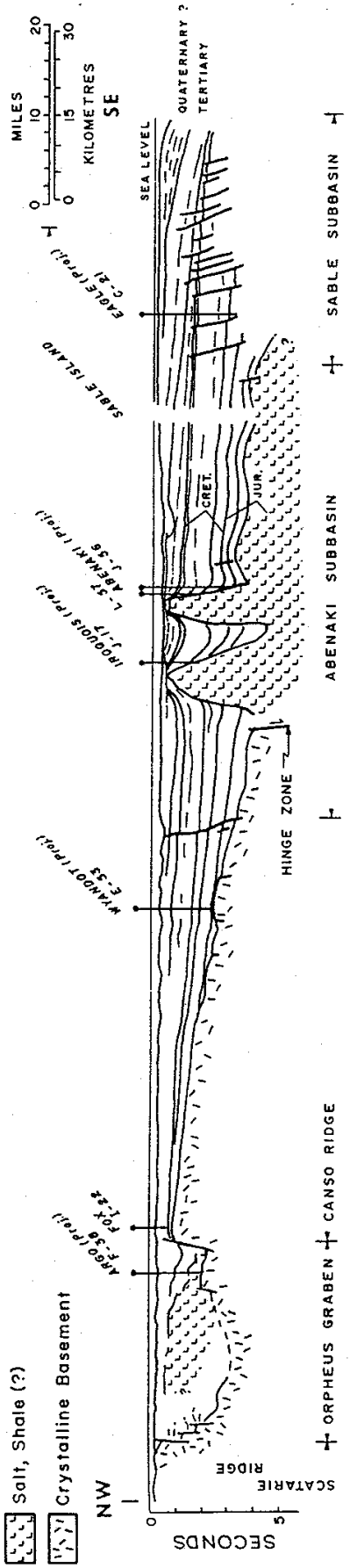

Figure 1-1: NW-SE cross section of the Scotian Margin displaying the Orpheus Graben, Canso Ridge, Abenaki Subbasin and Sable subbasin. (Modified from Wade, J. A. and B. C. MacLean, 1990)

1.2 Objective

The objective of the honours project is to improve the understanding of initial salt mobilization and salt/sediment interaction in the original salt basin/autochthonous region of the Abenaki and Sable Subbasins of the modern Scotian Shelf (fig. 1-2).

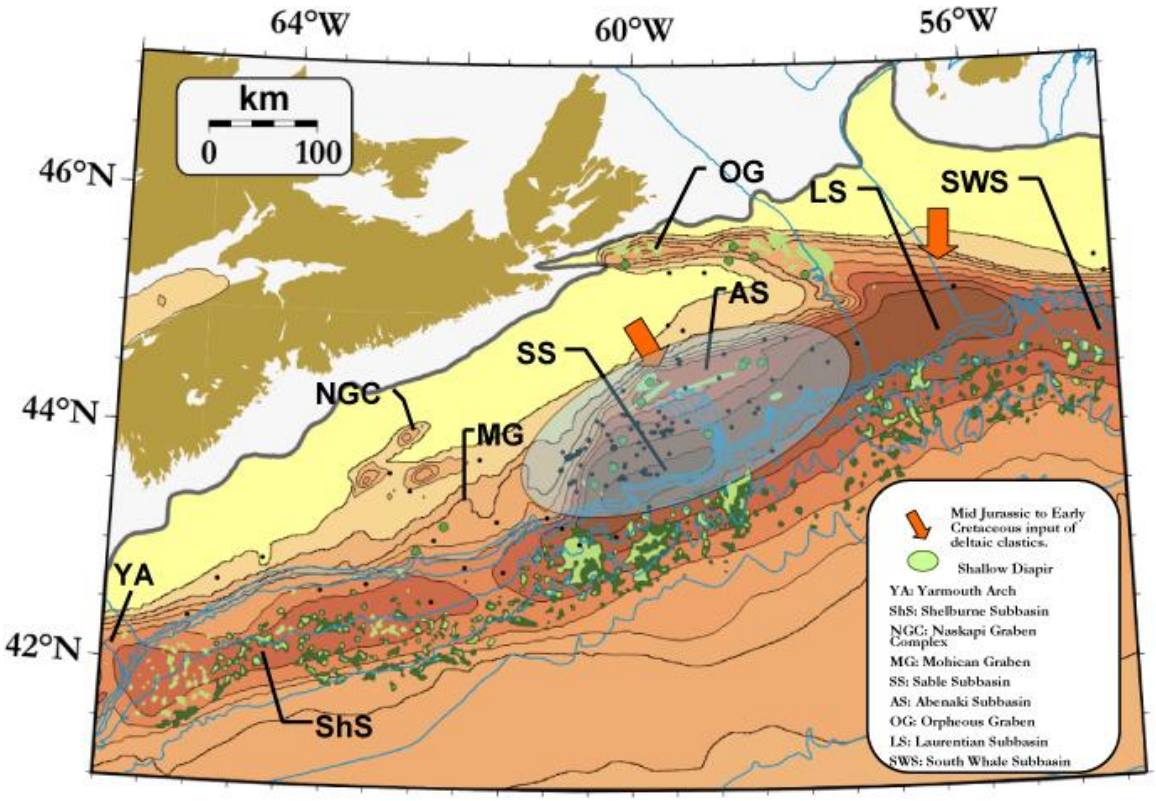

Figure 1-2: Map of the Scotian Basin. The blue circle denotes the study area of this thesis: Abenaki and Sable Subbasins. (Modified from Shimeld, 2004)

This project will have direct application to petroleum exploration as a better understanding of salt related structures will greatly benefit the identification and understanding of basin evolution. I will use state of the art physical simulation methods and structural modelling techniques to provide insight into coupled tectonic and depositional processes, fault mechanics, and salt mobilization in passive margin basins affected by gravity spreading on salt substratum. This will aid interpretation of dynamic

salt systems which have been affected by basement morphologies associated with rift basins (fig. 1-3), such as the Scotian Margin (Adam et al., 2006).

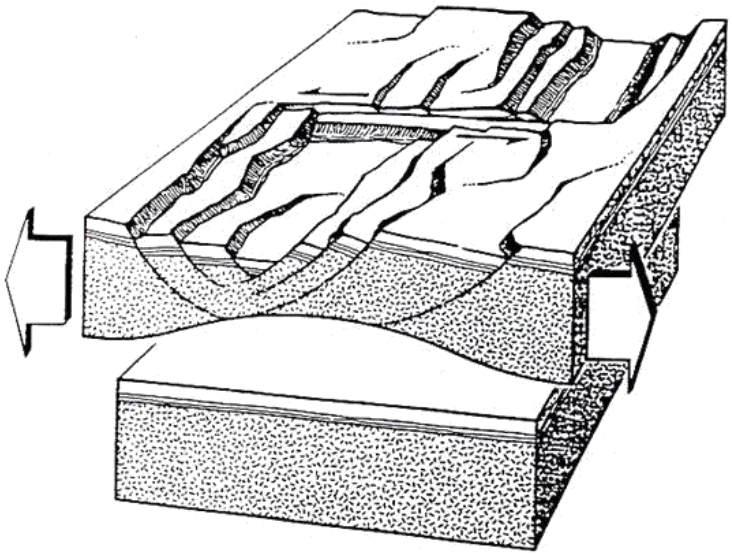

Figure 1-3: Regional structural elements of a rift basin. Present are: half graben steps, and symmetrical grabens. (Stonely, 1981)

With introduction of the scaling theory, dynamically scaled analogue experiments have been proven to faithfully reflect the evolution of natural geological systems (Hubbert, 1937). The models make use of brittle and ductile materials to simulate the evolution of thin skinned extension in a passive margin sedimentary wedge on a salt substratum. Interpretations of experiments will be made with data obtained from lateral 2D cross-sections and surface deformation with Particle Imaging Velocimetry (PIV) in order to gain a comprehensive and quantified account of the syn-sedimentary structural, kinematic, and dynamic evolution of sedimentary basins deformed on salt.

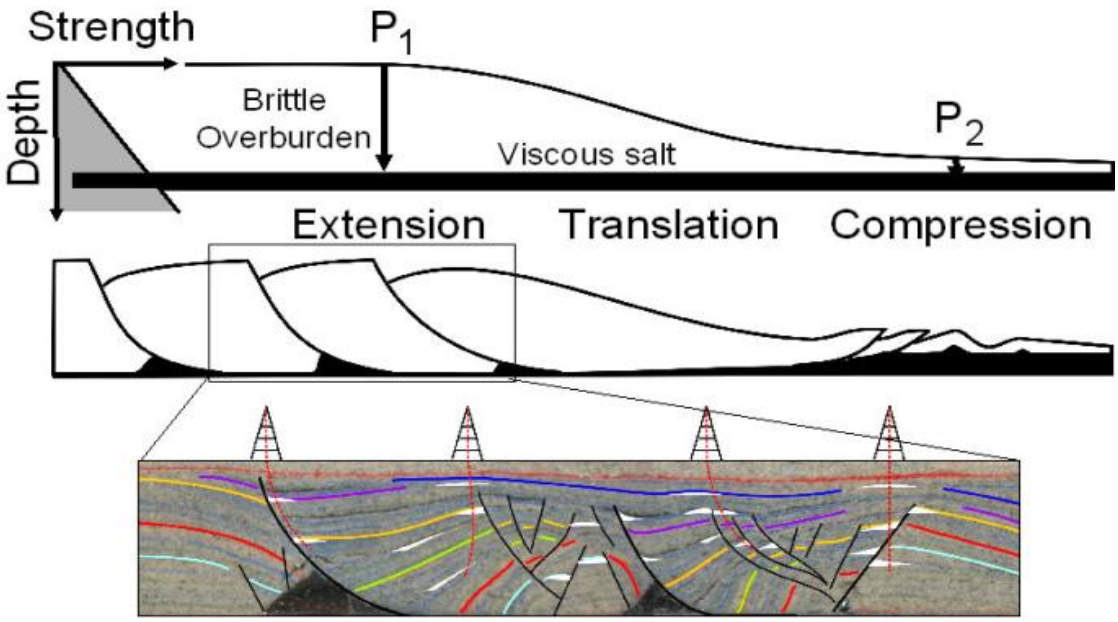

Figure 1-4: Thin-skinned extension in a passive margin sedimentary wedge on salt substratum. The top image illustrates pressure gradient (P_1-P_2) and strength profile. The kinematic segmentation due to basinward salt flow is illustrated in the centre image and growth fault rollover system and plays are represented by the lower image. (Adam et al. 2006)

The structures of focus in this study will be in the shelf region containing the initial salt basin in all models as there may still be plays in the Abenaki and Sable subbasins which are not yet recognized or understood in terms of timing and evolution. The focus of this thesis is centered on processes in the shelf area to study early salt mobilization and basin evolution. Clarke Campbell of the Salt Dynamics Group of Dalhousie University is doing an honours thesis on processes in the deepwater/allochthonous region of the Scotian Margin to investigate late stage evolution.

Chapter 2: Salt Tectonics and Regional Geology

2.1 History of Salt Tectonics

The concept of salt tectonics has undergone numerous stages including: the pioneering era, the fluid era and the brittle era. A very comprehensive overview of the history of salt tectonics with references of the milestones of scientific achievements is given by Jackson (1995) and briefly summarized here.

The pioneering era (1856-1933) focused on the search for a general hypothesis which would explain salt diapirism. At this time many of the ideas brought forth invoked bizarre situations, such as; igneous activity, residual islands, in situ crystallization, osmotic pressures and expansive crystallization. With data obtained from oil exploration new questions were generated concerning the effects of buoyancy versus orogeny, contact relations, salt glaciers. New concepts were also generated which included downbuilding and differential loading, two fundamental ideas still used today.

The fluid era (1933-1989) was centered on the dominant view that the evolution of salt diapirs was controlled by Rayleigh-Taylor instabilities, in which a dense fluid overburden having negligible yield strength sinks into a less dense fluid salt layer, displacing it upward. Factors related to this model include: density contrasts, viscosity contrasts and dominant wavelengths. This set of ideas however ignored the strength, and faulting of the rigid overburden. During this era many salt structures were recognized such as peripheral sinks, turtle structures and allochthonous salt sheets. Many concepts eventually evolved through the 1970's and 1980's involving salt allochthons, intrasalt minibasins, finite strains in diapirs, thermal convection in salt, glacial flow, etc.

The brittle era began in 1989 and is presently the prevalent model for salt tectonics. Major problems of the fluid era include the lack of faulting of overburden sediments and the observation that was made by Neddleton and Elkins (1947) which is that a diapir stops rising if its roof becomes too thick due to the strength of the overburden. As consequence of the increasing interest and data available from hydrocarbon exploration of salt-related structures in the sedimentary overburden, it became more and more clear that the structural evolution of brittle sediment structures in the overlying sediments cannot be described by a fluid-fluid concept. Various physical and computer modelling studies that tested the overburden with a brittle rheology and salt with a viscous rheology have successfully developed more realistic concepts regarding faults surrounding diapirs, regional detachments and evacuation surfaces (welds) along vanished salt allochthons, raft tectonics, salt flats, etc. During this recent era, viable rules of structural balancing of salt structures were introduced and the importance of differential loading and the influence of sedimentation rate versus salt thickness were emphasized.

2.2 Glossary of Terms related to Salt Tectonics

Salt tectonics uses a suite of terms to describe fundamental features, processes and structures. This section serves as a glossary of common terms to allow for quick reference when querying results.

Overburden – The upper part of a sedimentary deposit which compresses and consolidates material below (Bates and Jackson, 1987).

Substratum – In salt tectonics substratum is used to describe a ductile salt layer which is positioned below the brittle overburden and above the subsalt strata or basement (Jackson and Talbot, 1991).

Source Layer – The term feeder refers to a source layer of salt which readily replenishes a salt structure during its evolution (Jackson and Talbot, 1991). The source layer will only continue to supply salt to an adjoined salt body if it is not depleted. When the substratum becomes depleted, the conduit to the structure will form a weld (fig. 2-5) and the salt system will shutdown.

Graben (G) – Grabens are down-dropped blocks that are bounded on both sides by conjugate normal faults (Twiss and Moores, 1992). Graben formation is important in extensional systems associated with salt and is a key factor in raft tectonics. Horst blocks are associated with grabens and represent a relatively uplifted block bounded by two conjugate normal faults. Identification of grabens or horst blocks may be based on either topographic features or by structural features.

Half-Graben (HG) – Half-grabens, or asymmetric grabens, are down-dropped blocks bounded on one side by a major normal fault (Twiss and Moores, 1992).

Planar Fault – A linear surface or narrow zone along which one side has moved relative to the other in a direction parallel to the surface or zone (Twiss and Moores, 1992).

Listric Fault – A concave upward fault, whose dip decreases with increasing depth (fig. 2-1) (Twiss and Moores, 2007). The non-linear shape (i.e. listric) shape of the fault is formed due to rheological changes with depth.

Growth Strata – Growth strata, as seen in figure 2-1, is a result of syn-kinematic sedimentation. Apparent thickening of stratigraphic packages is evidence of areas in

which there was more accommodation space. Accommodation space may result from salt withdrawal, faulting, or tectonic events; such as rifting/extension.

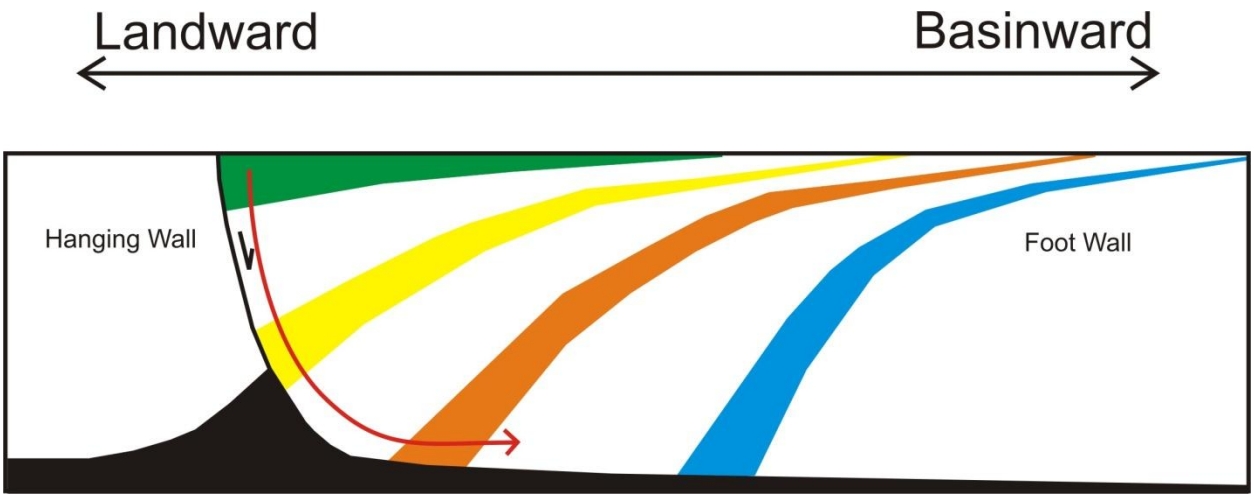

Figure 2-1: Basinward dipping growth normal fault. Thick packages of strata indicate growth of overburden from fault controlled subsidence. Salt is indicated by the color black and the sense of rotation is noted by the red arrow.

Growth Fault Rollover – A growth fault (fig. 2-1) is recognizable by displacement of strata which thicken towards the fault surface. The strata appears to roll as it is displaced vertically and laterally (rotating) along the listric fault surface.

Keystone Graben (KG) – Keystone grabens (fig. 2-2) are small-scale extensional structures that form in the crest of rollovers due to bending of brittle overburden. They are very common in nature and in the physical experiments. Keystone grabens often extend to the base of the salt as it acts as a detachment surface. Because they are commonly associated with rollovers, keystone grabens are representative of a regime of low sedimentation rate and thick salt thickness.

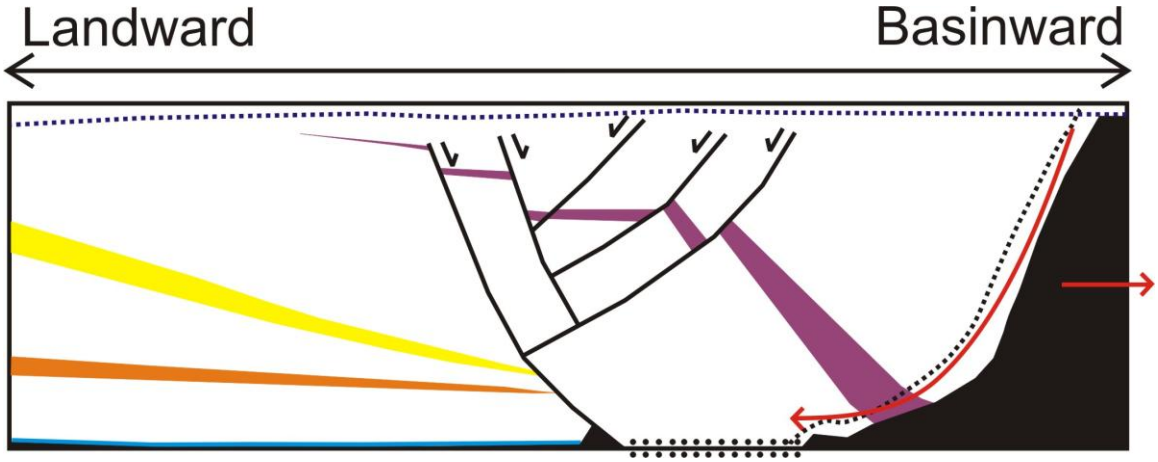

Figure 2-2: Keystone graben present in experiment 5-3. Salt withdrawal in the expulsion rollover is dominantly accommodated rollover formation inboard of the diapir; extension due to bending of the growth strata lead to formation of the keystone graben. The blue dashed line is the top-most limit of the strata and the sense of rotation and movement are given by the red arrows. The black dashed line marks the former position of the salt massif.

Basinward Listric Growth Fault Rollover Systems (BLS) –are generated by downbending of hangingwall strata due to displacement on a basinward listric fault (fig. 2-3). The dip of the listric fault is coincident with the downslope oriented gravity spreading direction. The listric shape of a growth fault is due to rheological changes of rock with depth and/or asymmetric extension. Basinward listric faults are typically associated with a high coupling between brittle and ductile layers.

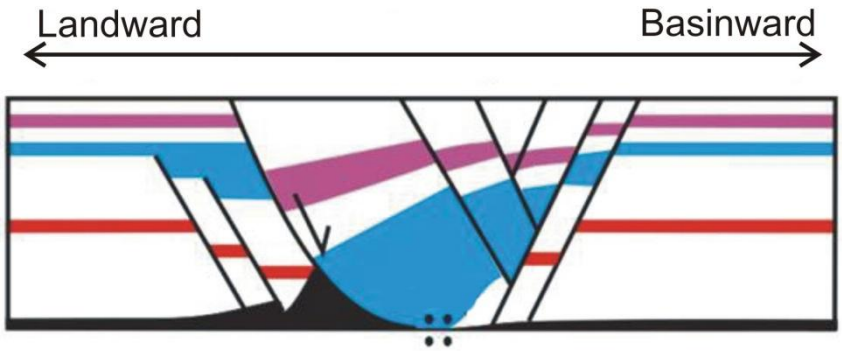

Figure 2-3: Basinward listric growth fault rollover system. (After Krezsek et al., 2006a)

Landward Listric Growth Fault Rollover Systems (LLS) - are created when there is a very high sedimentation rate or low salt thickness (fig. 2-4). They often start as a basinward listric fault system but become overridden later in their evolution. The dip of the listric fault is opposed to the gravity spreading direction.

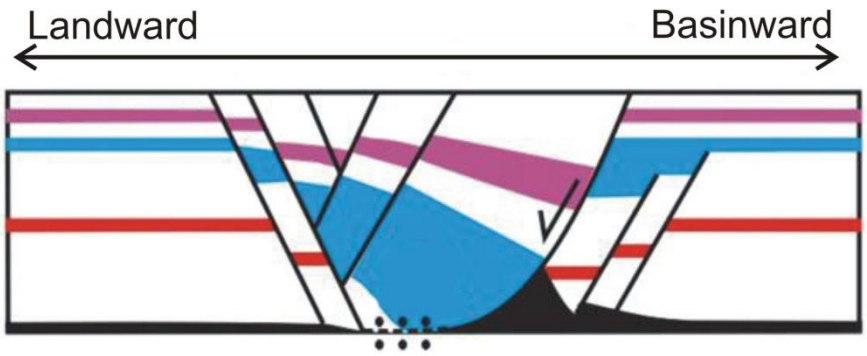

Figure 2-4: Landward listric growth fault rollover system. (After Krezsek et al., 2006a)

Expulsion Rollovers (ER) - Form due to "rolling" or growth (thickening packages of sediment accompanying accommodation space) of strata that occurs during lateral salt withdrawal, and therefore involves downbuilding of the overburden. No extension is accommodated by the rollover itself, but by the associated diapir. Typically with expulsion rollovers the initial basin touches down and welds out, with asymmetric flank collapse so that the depocenter shifts progressively in one direction, forming a growth monocline (Rowan, 2005). Like fault rollovers, expulsion rollovers are common as traps for petroleum as they are commonly in contact with an impermeable salt wall or diapir and form a closure which allows hydrocarbons to become trapped.

Weld – Welds form after the complete expulsion of salt from its original configuration and define the contact of overburden and subsalt stratigraphy. They may be identified by

discontinuous, high amplitude reflectors, with angular discordance between strata on either side (Rowan, 2005). There are three common classifications of salt welds; primary, secondary and tertiary. Primary welds occur where autochthonous salt has been evacuated and the overburden has come into contact with underlying strata, as seen in figure 2-5. Secondary welds are defined by salt stocks or diapirs which have been shutdown from lack of rejuvenation from a source layer and have been sealed. Tertiary welds are similar to primary welds, however they are found at allochthonous salt bodies, commonly canopies and nappes.

Salt Withdrawal Basin – Salt withdrawal basins (fig. 2-5) form from the displacement of salt from the area under differential load called the protobasin. Salt withdrawn form the protobasin moves laterally to flanking areas resulting in bathymetric highs. Accommodation space created in the basin low results in a positive feedback cycle, allowing for the accumulation of sediments and further salt withdrawal.

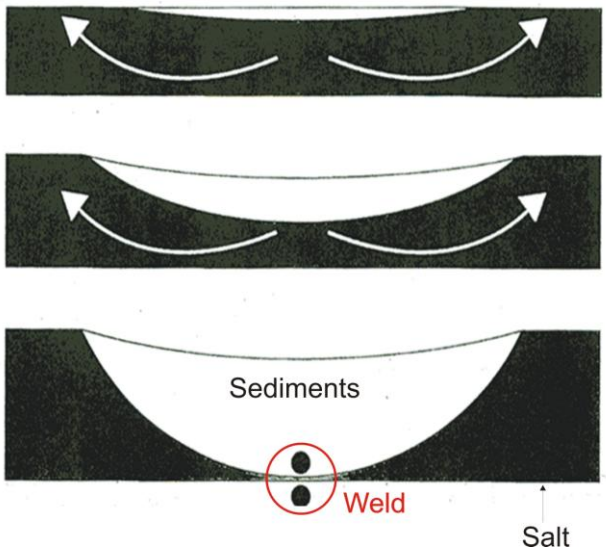

Figure 2-5: Salt withdrawal basin. Top: Initiation of the withdrawal basin. Middle: Subsidence and growth of the basin from differential load. Bottom: End of subsidence with weld formation. (Modified from Rowan, 2005)

Raft – Rafts are characterized by lateral breaks in strata with younger material separating displaced blocks (fig. 2-6).

Figure 2-6: Example of rafted sediments (brown strata). The system had begun its evolution with symmetrical graben formation and as the blocks separated from each other younger sediments infilled the accommodation space. (After Krezsek et al., 2006a)

Salt Pillows - Salt pillows are features that appear as subcircular upwellings of salt with a concordant overburden (Truschiem, 1960). Salt pillows do not pierce the overburden and usually result from salt accumulation in the seaward compressional part of the basin from salt withdrawal at the landward limit.

Salt Rollers (SR) - Salt rollers (fig. 2-7) are low-amplitude; asymmetric salt structures comprising two flanks. One is gently dipping and has conformable stratigraphic contact with the overburden. The other flank is usually more steeply dipping and in normal faulted contact with the overburden (Bally, 1981). Salt rollers are features that are definitive of regional thin-skinned extension and are essentially reactive diapirs which started to form to accommodate extension and local unloading of overburden created by grabens. They are shut down due to high sedimentation rate and decreasing salt thickness, in that the sedimentation rate is too great for the diapir to mature or rise passively.

Figure 2-7: Triangle shaped salt roller/reactive diapir (black) and associated faults. (After Krezsek et al., 2006a)

Diapir – Diapirs are the most well known salt structure, and ironically one of the least understood (Jackson and Vendeville, 1994). A diapir is defined by a dome or anticlinal fold in which the overburden has been ruptured by the squeezing out of a plastic core material, typically salt or shale (Bates and Jackson, 1987). There are three stages of diapir evolution: reactive diapirism, active diapirism and passive diapirism. Reactive diapirism is the first stage of diapir rise, and is dependant on regional extension resulting in growth fault/graben formation (fig. 2-8 a). This extensional faulting creates differential unloading on the salt from surface relief and also weakens the overburden by fracturing and thinning it (Jackson and Vendeville, 1994). It is only when the fault blocks shift that pressurized salt can rise into the space created from extension (fig. 2-8 b, c & d), and therefore the process is mostly independent of overburden lithology, thickness and density.

Diapiric rise must also be considered as a function of extension in the system rather than a function of differential loading. Although differential loading drives salt mobilization, it is the extension and unloading process that allows the salt to migrate upward through the overburden. Active diapirs are the least common in nature because the active diapirism stage needs specific requirements and is merely a transition from reactive diapirism to passive diapirism. Once the overburden becomes thin and weak enough and/or the pressure differential in the salt is great enough, a diapir can pierce through the surface. The final stage of diapirism is the passive stage (fig. 2-8 e). This terminology refers to the time when salt has already broken through the sea-floor. After a diapir becomes passive it will continue to grow as long as there is an adequate source of salt. This concept is essentially downbuilding which was proposed by Barton in 1933,

and states that a diapir keeps its crest at the sea floor as surrounding strata subside into the source layer of salt. If the source is depleted or obstructed by welding however, the diapir will not continue to grow because there is no longer a differential fluid pressure to drive salt flow (Rowan, 2005).

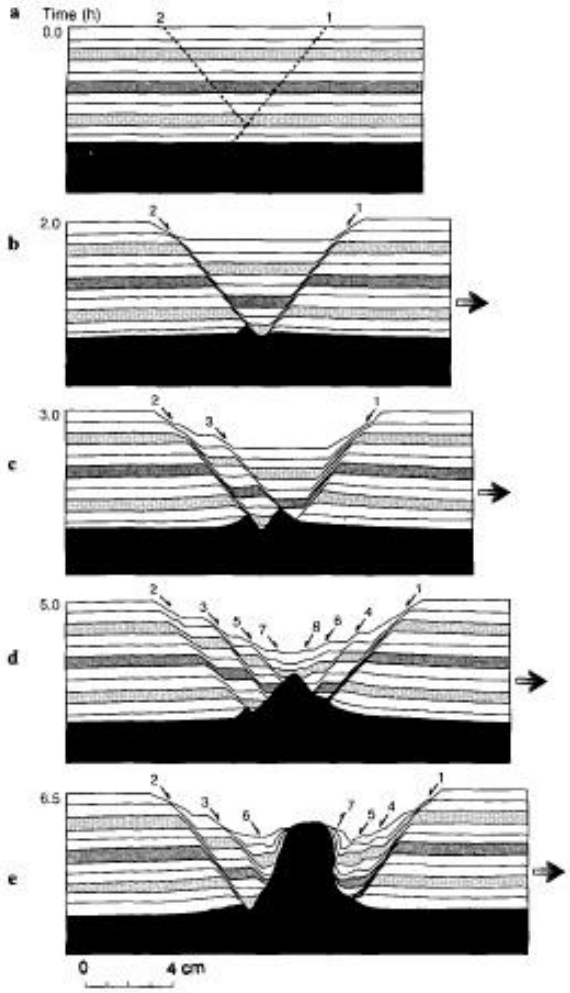

Figure 2-8: Evolution of a model diapir in an extensional setting with time. a: Graben initiation. b, c, d: Reactive diapirism. e: Diapir at the passive stage. The active stage occurs very briefly and is not shown in this figure. (Vendeville, and Jackson, 1992)

Passive diapirism is currently the dominant style of diapiric growth in passive margin basins throughout the world and is the longest lasting of the 3 stages.

When the source layer for the diapir is depleted growth will discontinue and there will be diapiric fall in the case that extension continues or salt is removed laterally. Typically the diapir will already be in its passive stage when the source is depleted. Because the salt is the weakest part of the system it will become the center of the extensional strain and will widen with time. At this point the diapir will begin to collapse and become a new topographic low/depocenter and at the extreme end-member, become a mock turtle structure or raft.

A particularly important type of diapir in petroleum systems is the "Christmas Tree" diapir. These diapirs have multiple branching salt overhangs which indicated periods when sedimentation rates were low enough for the diapir to flow to the surface. These diapirs evolved through all stages of diapirism and most of them were sealed by later sedimentation.

Canopy – Salt Canopies (C) are allochthonous salt bodies and occur in three forms: salt stock canopies, salt wall canopies and salt-tongue canopies from the coalescence of stocks, walls and tongues (fig. 2-9) (Jackson and Talbot, 1991). A salt stock is a plug-like salt diapir with subcircular planform (Truscheim, 1960). Salt walls are defined as laterally continuous diapirs. They may be bulbous at their vertical limit; however they are not subcircular in planform due to their lateral extent. Lastly, salt tongues are caused by extruded salt, usually basinward, from a leaning feeder (passive diapir). When two individual stocks, walls or tongues merge the surface which marks the amalgamation is called the suture (Rowan, 2005).

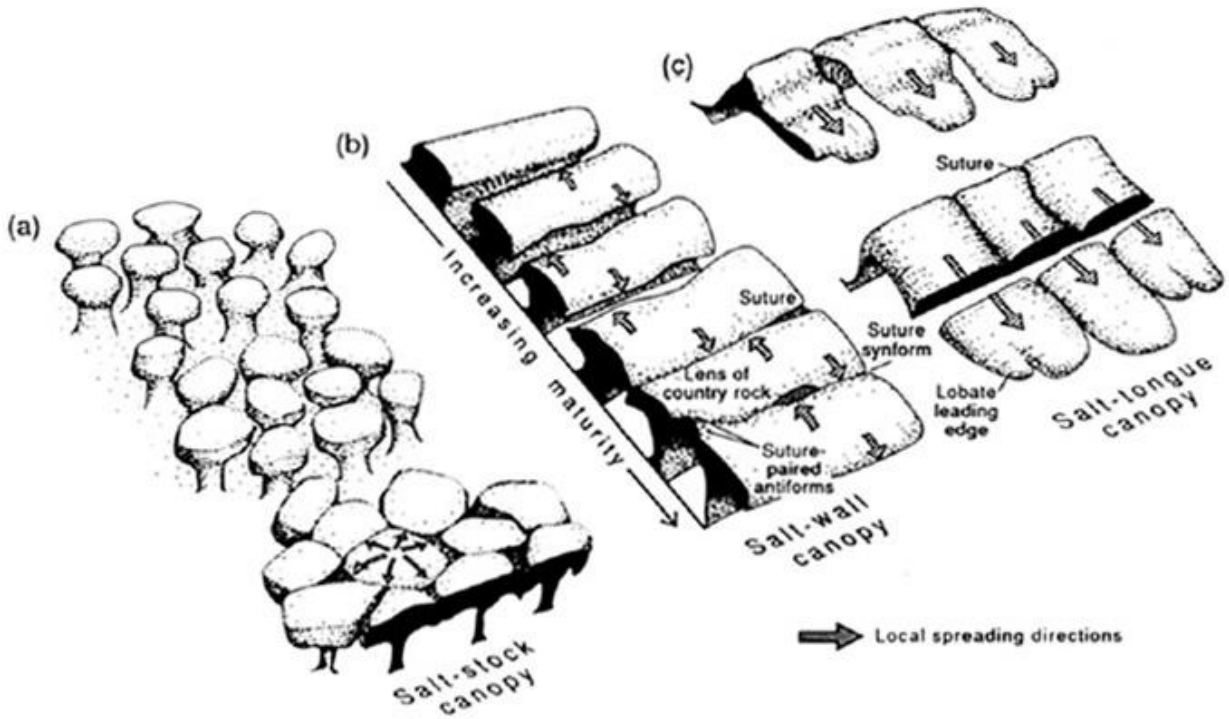

Figure 2-9: The three main forms of allochthonous salt canopies with local spreading directions shown by arrows. Note that the arrow below the illustrations is not the overall flow direction but is used as a legend symbol. (Modified from Jackson and Talbot, 1991)

Salt Nappe - Salt nappes (N) are very similar to canopies however they do not have multiple feeders, but rather flow basinward as a salt "glacier".

Rim Synclines - Rim synclines, termed purely on a structural basis, have folding with an arcuate or subcircular axial trace on the outer margin of a salt upwelling (Jackson and Talbot, 1991). Rim synclines are often a result of salt withdrawal in the source layer (Nettleton, 1934).

Turtle Structure (TS) – Turtle structures (fig 2-10) are a very common hydrocarbon play and are often exploited in petroleum exploration. Like expulsion rollovers, turtle structures are a result of downbuilding of the overburden into the underlying salt layer. In the case of turtle structures, however, the overburden touches down in the center as a

salt weld with salt underlying the overburden to either side. These salt flanks later touch down leaving an apparent anticline in the sedimentary record.

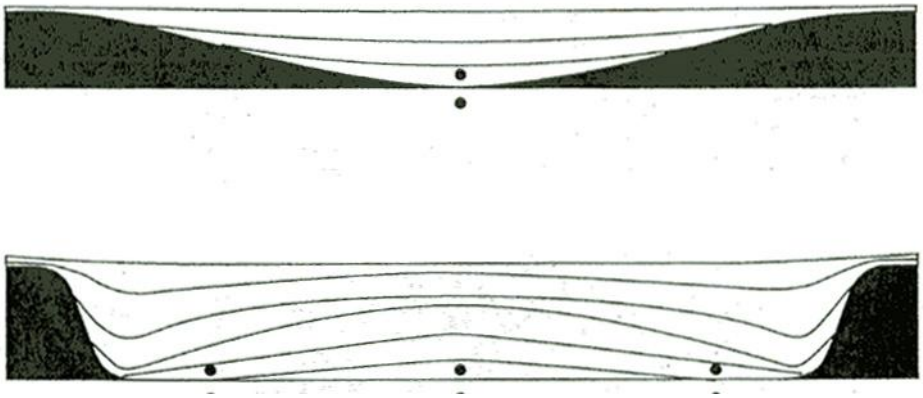

Figure 2-10: Formation of a turtle structure by flank collapse and inversion of a minibasin, of which the center has touched down and formed a salt weld (Rowan, M.G., 2005)

The age of a turtle structure is always defined as the age of touchdown in the center of the initial minibasin and the start of flank collapse. Turtle structures are indicative of a low sedimentation/salt thickness ratio.

2.3 Thin-Skinned Salt Tectonics of Passive Margins

2.3.1 Formation of Salt Basins

Salt Basins form primarily in rift basins, and occur today along passive margins and in deformed settings such as the Alpine/Himalayan system. Most salt basins were deposited during the late syn to early post-rift phase though others may form during rifting or lulls between distinct rift episodes (Jackson and Vendeville, 1994). Some intra-continental salt basins however are older than rifting, such as those located in the North Sea and Persian Gulf.

For rift related salt basins such as the Scotian Basin, deposition requires evaporite conditions, i.e. a hot climate. Extension in the continental crust forms grabens that are initially in-filled with non-marine clastics due to the high heat flow and associated regional uplift of the rift shoulders. Subsidence of the grabens which occurs during: rifting, post-rift thermal subsidence and loading subsidence, leads to frequent marine incursion. During this time there is a transition from a non-marine to marine setting and salt is deposited. Continued subsidence may finally lead to true marine conditions and initial shallow water carbonate deposition may initiate and eventually lead to deepwater marls and shales with increasing water depth (Rowan, 2005).

2.3.2 Thin-Skinned Deformation

The most important factor in the kinematics of salt mobilization is that rock salt acts with very different mechanics than other sedimentary types. There are two main factors which dictate its behavior; low strength and low density.

An important factor involving the viscous nature of salt is that it forms a low strength layer in contrast to brittle sedimentary layers that show a linear strength increase with depth (see fig. 2-11). As consequence, under sedimentary load, salt acts as a very effective detachment surface into which faults of the brittle overburden can sole out (Rowan, 2005).

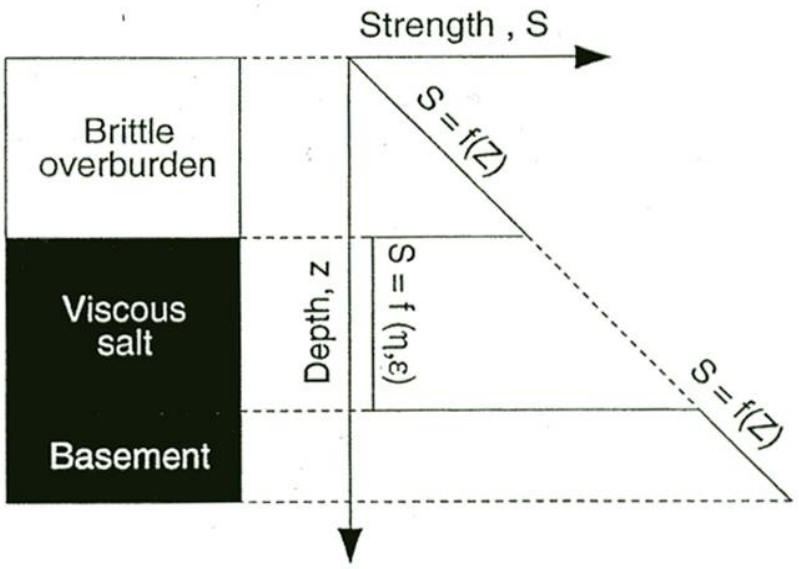

Figure 2-11: Strength of brittle overburden and salt with depth. The brittle overburden and basement show an increasing strength profile with depth. The viscous salt layer marks a drop in strength and remains constant throughout. (Vendeville and Jackson, 1993)

The density of salt (Halite) is approximately 2.2 g/cm^3 and decreases slightly with depth due to thermal expansion (fig. 2-12). Because other sediments become more compacted and dense with depth, salt is more dense than surrounding strata when it is near the surface but less dense starting at depths of around 1000 – 1500 m. Though density contrasts contribute to salt mobilization it plays a smaller role in salt tectonics than assumed in fluid-fluid models. The viscous nature of salt allows it to be viewed as more of a pressurized fluid and therefore salt flow is driven by differential fluid pressure (Vendeville and Jackson, 1992; Gemmer et al., 2005). Because it is driven by this fluid pressure, any differential load will cause salt mobilization; however, it needs to fit certain conditions. There are three constraints; (1) there must be an open path to a near-surface salt body, (2) the overburden must be weak or thin enough for the differential fluid pressure to overcome the overburden strength, and (3) some other process must create

space (Rowan, 2005). Most important to note from this is that salt does not drive extension or compression in a system, but flows into space created from both processes.

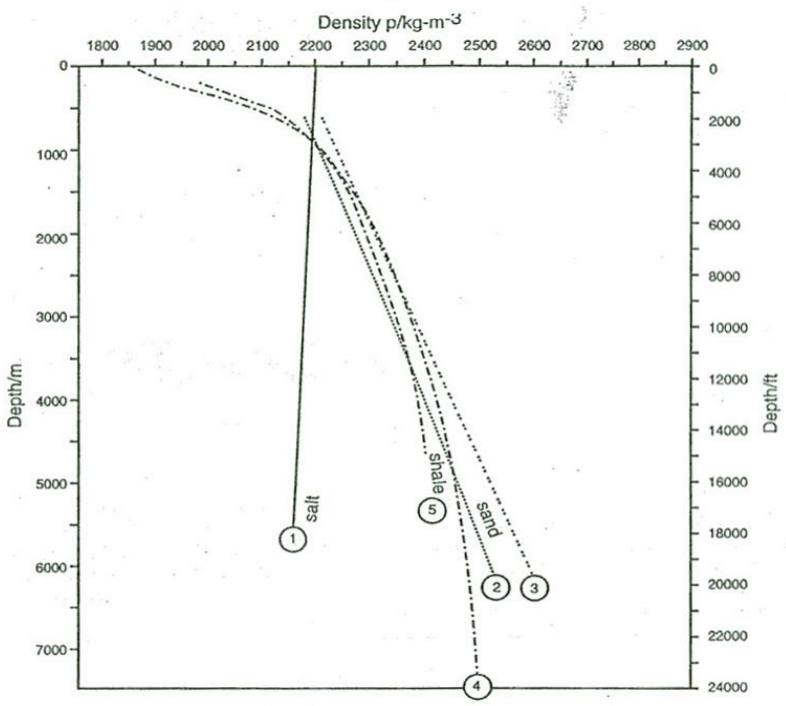

Figure 2-12: Density of different rock types with depth. (Jackson and Talbot, 1986)

Under both tension and compression salt is much weaker than other lithologies. This characteristic allows salt to deform as a viscous material, viscosity: 10^{18} Pa·s (Gemmer et al., 2005), that affectively flows in geological time scales (Rowan, 2005).

Flow of salt is a combination of Poiseuille flow and Couette flow. Poiseuille flow is a result of overburden loading, whereas Couette flow is a response of overburden translation. Poiseuille flow (fig. 2-13) has the highest velocity vectors in the center of the fluid medium (channel flow) whereas Couette flow has velocity increasing toward the fluid-brittle overburden interface (shear flow).

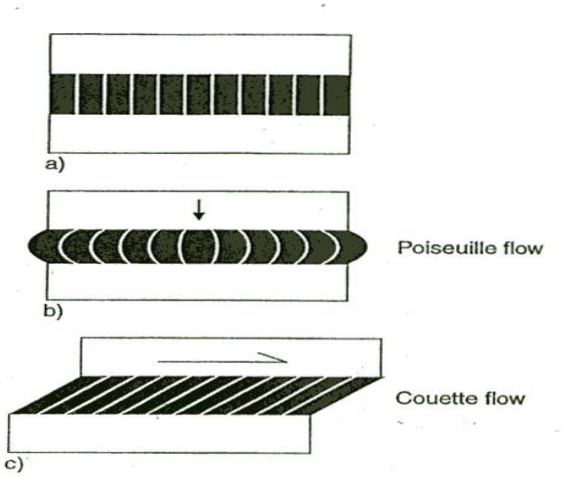

Figure 2-13: Types of salt flow. A) Undeformed medium. B) Poiseuille (channel) flow. C) Couette (shear) flow. (Rowan, 2005)

In a continental margin with a sedimentary wedge the balance between these flow types can be associated with deformation in the system (fig. 2-14) and can be described by the following equation:

$$F_1 + F_2 + F_P + F_C = 0 \qquad (2.0)$$

Where; F_1 and F_2 are forces that result from landward tensional and seaward compressional horizontal stresses in the frictional plastic overburden, and F_P and F_C are forces due to Poiseuille and Couette flow (Gemmer et al., 2005). The system is in balance and no deformation occurs if all forces equal 0 as shown, with only Poiseuille flow occurring. However, if there are more forces attributed from F_1 and F_P due to differential loading, such that:

$$F_1 + F_P > F_2 + F_C \qquad (2.1)$$

Deformation will begin, with basinward extension associated with an increase in Couette flow.

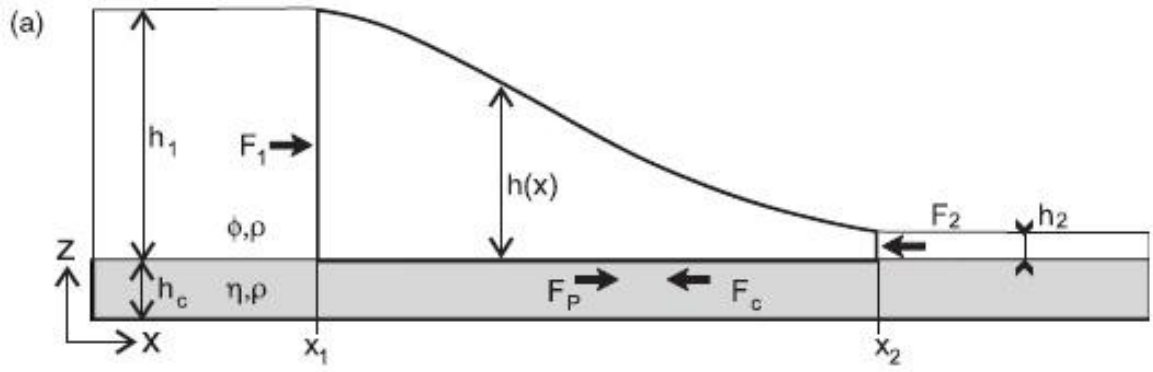

Figure 2-14: Force balance of the rigid overburden and the viscous salt layer. F_1 is the landward tensional force, F_2 is the seaward compressional force, F_P is the Poiseuille force and F_C is the resisting Couette drag force (Gemmer et al., 2005).

2.4 Regional Geology

The Scotian Basin began to develop during the Middle to Late Triassic when North America started to separate from Africa during the break-up of Pangea. Presently it is situated on the Atlantic continental margin offshore Nova Scotia and extends 1,200 km from the Yarmouth Arch in the south to the Avalon Uplift of the Grand Banks in the north (Wade et al., 1995).

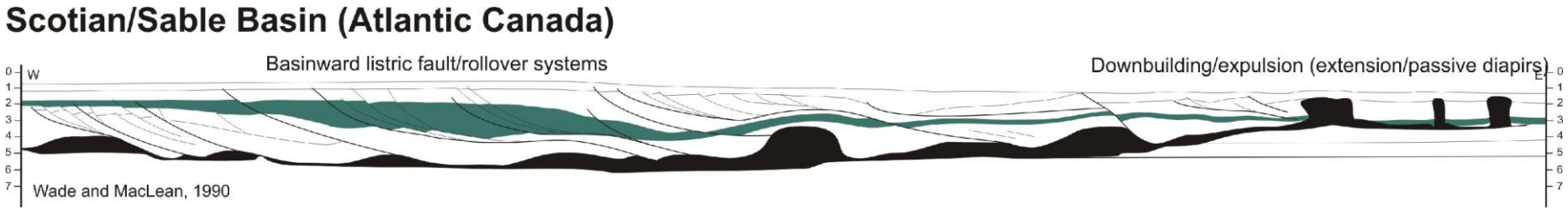

Figure 2-15: Generalized cross-section of salt related structures offshore Nova Scotia. (Modified by Krezek, 2006a after Wade and MacLean, 1990).

The basin is comprised of the Scotian Shelf, the Western Grand Banks and the Laurentian Channel with an areal extent of approximately 300,000 km^2 (Jansa and Wade, 1975; Kidston et al., 2002). The basin itself is subdivided into numerous smaller subbasins that reflect the rift-related basement structures: the Shelburne Subbasin, Naskapi Graben Complex, Mohican Graben, Sable Subbasin, Abenaki Subbasin, Orpheus Graben, Laurentian Subbasin and South Whale Subbasin (Wade et al., 1995). To date, the exploration activities of the Scotian Basin have been focused on the Abenaki, Sable and Laurentian subbasins.

The Stratigraphy of Offshore Nova Scotia (fig. 2-15) has been established by many studies, most notably by Jansa and Wade (1975). The Argo salt unit is responsible for most of the thin-skinned deformation in the Scotian Margin. It is thought to have been deposited when the rifted Middle to Late Triassic rift valley, which was in-filled with syn-rift fluvial lacustrine facies, underwent flooding in the Early Jurassic. The sedimentation during the Jurassic to Cretaceous continued with no significant interruption in the deeper parts of the Scotian Basin. Strong seismic reflectors beneath the lower slope and rise suggest the presence of turbidites and cherty and/or carbonate horizons. Landward, the deposition of the carbonate bank, known as the Abenaki Formation, was interrupted by a Late Jurassic-Early Cretaceous regression which resulted in more than 1220 m of terrigenous sediments Missisauga and Logan Canyon Fm. These sediments were deposited by delta systems and are believed to have been developed in response to tectonic uplift in the source area, including the Avalon Uplift. During the Aptian stage, regional uplift commenced and it was not until the Cenomanian-Turonian that rising sea level allowed most of the Avalon Uplift to be covered by sea. From correlating this event

with similarities found in Eastern Europe and the northern part of the Sahara it is believed that this transgression was the result of eustatic sea level rise. The result of this sea level rise was the deposition of mainly terrigenous sequences along the eastern margin of Canada with Carbonates of the Wyandot and Petrel Formations appearing in the Late Cretaceous and Early Tertiary during periods of transgression and maximum flooding events. Several sub-aerial unconformities (i.e. sequence boundaries) are present in nearshore tertiary sequences as a result of tectonics (e.g. tilting, uplift, etc.) or changes in global sea level. By the Late Oligocene, sedimentation was influenced across the Scotian Shelf as a result of regional regression, which culminated in the Latest Pliocene. During this regression there was a strong progradation of sediments which helped to shape the present day continental shelf and steepened the continental slope. These sediments can also be seen in the deepwater regions as turbidites and slump deposits with the deposition of pelagic carbonates and cherts.

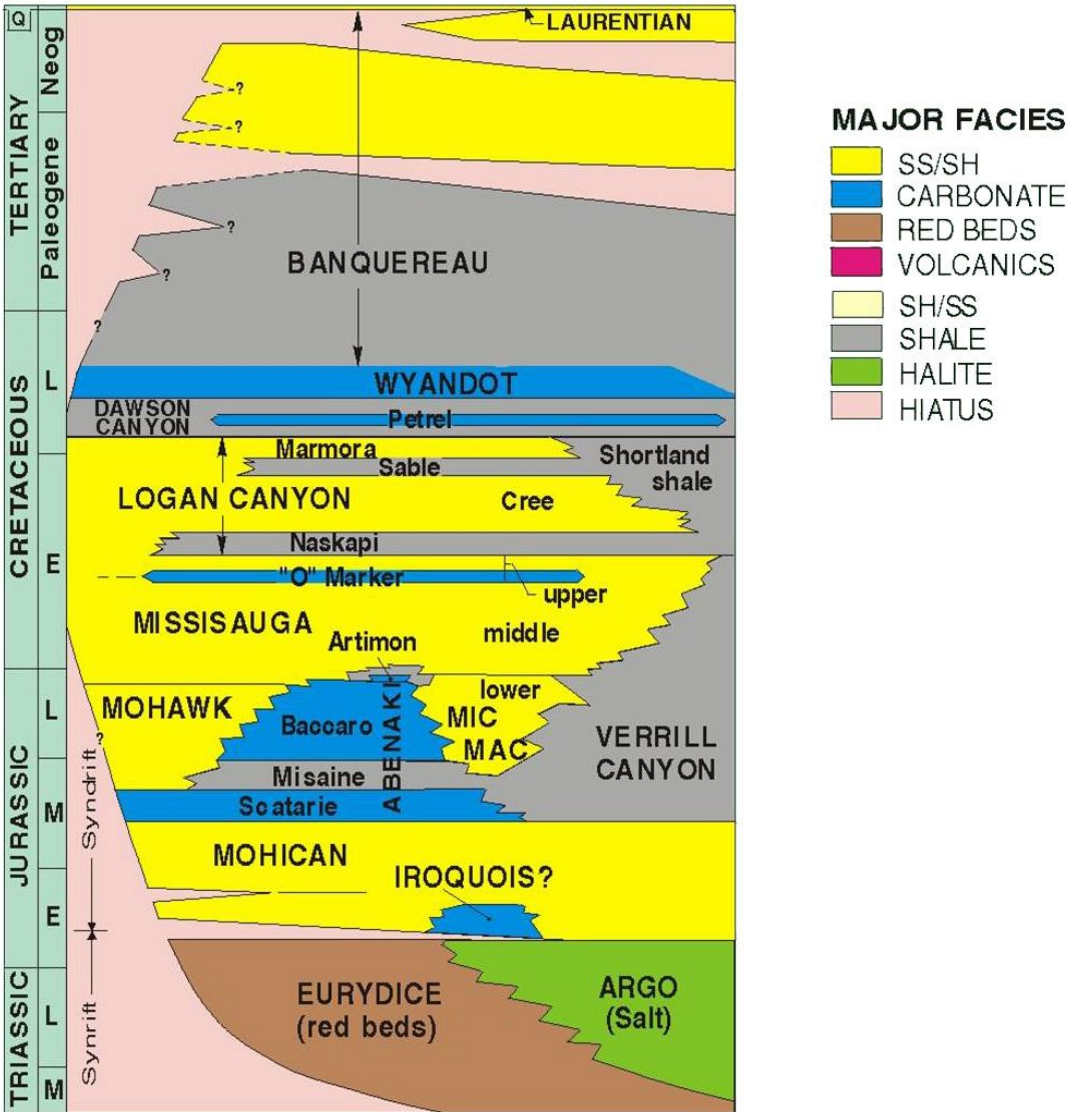

Figure 2-16: Generalized stratigraphic chart of the Scotian Basin. (Wade and MacLean, 1990)

The Abenaki Subbasin (fig. 2-16) was one of the locations of primary exploration focus. It lies south of the Canso Ridge, which is an elevated horst block situated between the Orpheus and Abenaki Grabens, and contains approximately 11 km of sediments. The northern limit of the Abenaki is defined by basement faults and the southern boundary toward the slope is not well defined. The basement at the southern limit, which is proximal to Sable Island, cannot be imaged with seismic surveys because of the substantial salt thickness and other sediments (Jansa and Wade, 1975).

The Sable Subbasin (fig. 2-16) is another focus area of hydrocarbon exploration. The northern and southwestern limits are the North Sable High and the basement hinge zone. The southern boundary of this area is also not determined due to sediment thickness and depth to basement, approximately 10-12 km. The Sable Subbasin may have been formed as a structurally controlled embayment in the North American continental margin, at the border of the developing North Atlantic Basin (Jansa and Wade, 1975).

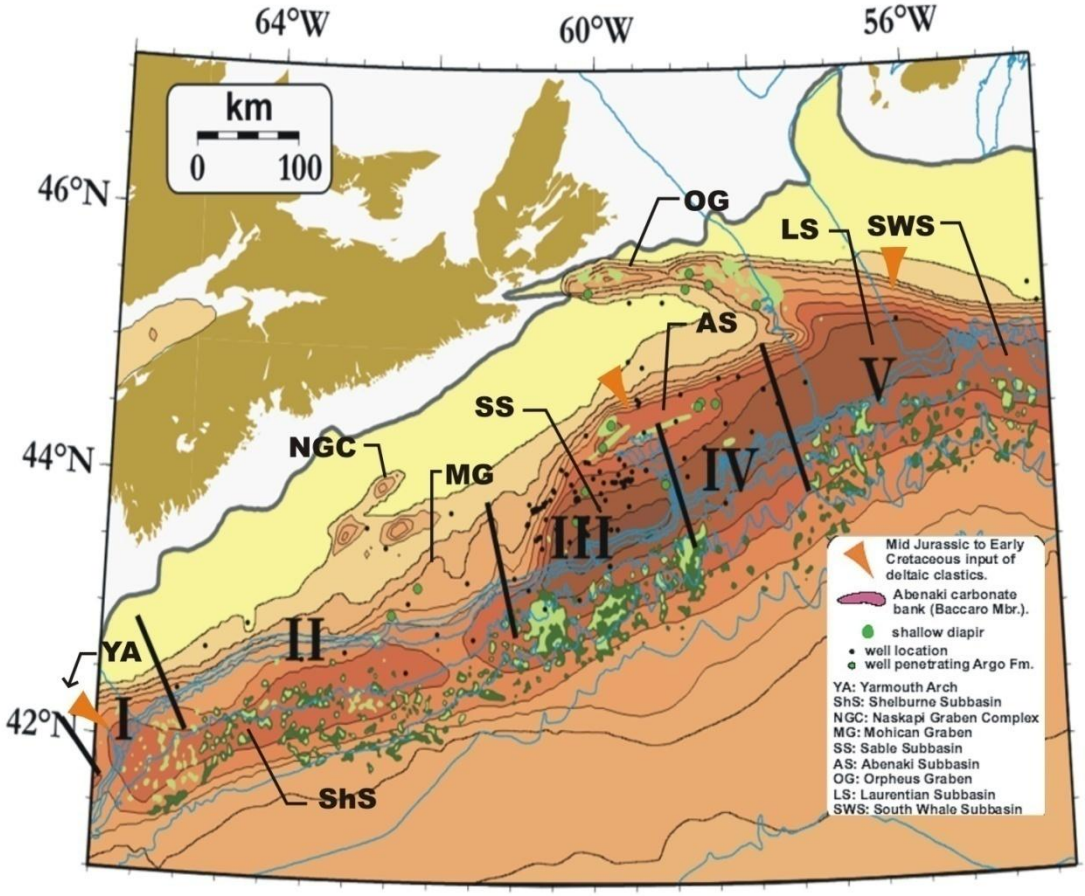

Figure 2-17: Major structural elements and salt subprovinces of the Scotian Basin. (Modified from Shimeld, 2004)

Within the deepwater region of the Scotian Basin there is an area with a prevalence of salt diapirs, which has been termed the Slope Diapir Province. The Slope Diapir Province has been divided into 5 distinct tectono-stratigraphic subprovinces by Shimeld (2004) (see Fig. 2-16). The subprovinces are defined by their salt tectonics style and sedimentation pattern. All subprovinces display distinctively different salt structure styles and syn-depositional environments. Shimeld (2004) suggests that the diverse evolution of subprovinces is related to variations in basement morphology, salt thickness and sedimentation patterns and rates during the Jurassic and Cretaceous Periods.

Subprovince I is characterized by diapirs in the form of elongated walls distributed in an arcuate trend and a seaward tongue canopy system that reaches approximately 15 to 20 km seaward. These passive diapirs are flanked by marginal synclines with Jurassic and Cretaceous siliclastic and carbonate sediments.

Subprovince II is transitionally bounded by Subprovince I and is characterized by linear salt walls that are aligned parallel to the edge of the Abenaki carbonate platform. Like Subprovince I, vertical diapirs and seaward tongues are present in the western portion of Subprovince II. In the eastern section there is a trend of mushroom-shaped to seaward verging, tongue shape diapirs predominant. There are also marginal synclines present between diapirs; however they are much broader than those seen flanking passive diapirs in Subprovince I.

Subprovince III is characterized by allochthonous tongue canopies estimated to be Cretaceous in age. The deformation of these sediments implies a variety of extensional syn-kinematic structures, such as turtles and expulsion grabens. The amalgamation and

degree of structural evolution of the allochthonous bodies appears to increase eastward. Because there is no clear evidence of feeders in the eastern region of this subprovince it is believed that the allochthonous salt bodies moved 80 to 100 km seaward. The Sable Subbasin lies within Subprovince III.

Subprovince IV is characterized by its lack of diapirs beneath the shelf break and upper slope of the present-day margin and the Banquereau syn-kinematic wedge (a package of sediments which lies immediately seaward of a bathymetric feature named Banquereau along the outer shelf). The Banquereau syn-kinematic wedge is comprised of an eastward thinning package of dominantly landward dipping reflectors, which converge causing individual units to thin, with little evidence for erosional truncation toward the top of the package. This feature is interpreted as a large-scale basinward listric rollover system developed on top of an allochthonous salt nappe (Ings and Shimeld, 2006). Isolated diapirs occur beneath the present day slope in this region with adjacent rim synclines which were created during the expulsion of an underlying ductile layer into the diapirs. The Abenaki Subbasin lies within Subprovince IV.

Subprovince V yields the most structurally complex 3D morphology of all Subprovinces. The Banquereau syn-kinematic wedge is obscured by the presence of overlying allochthonous salt tongues. Various complex extensional structures are present within the Cretaceous section of this area, with contraction and folding affecting the overlying uppermost Cretaceous and Neogene layers. Diapirs that are present beneath the upper slope have a thin post-kinematic cover, with crests of several diapirs within 100 m of the sea floor.

Chapter 3: Methodology

3.1 Overview of Analogue Modelling

Analogue modelling is an effective tool in the understanding and testing of brittle/ductile deformation systems with variable geological boundary conditions in 3D (Vendeville and Jackson, 1992). For this study, the scaled analogue experiments were conducted under normal gravity conditions. Brittle sediments are simulated with silica sand. Viscous salt, which deforms under gravitational loading, is simulated with silicone rubber. Silicone is justified as an analogue for salt deformation as it is a viscous material which deforms in the scaled experiment under similar strain rates by model sediment loading as natural prototypes (Vendeville and Cobbold, 1988).

The Salt Dynamics Group at Dalhousie University uses analogue experiments with high-resolution strain monitoring techniques (section 3.5.2), structural modelling and seismic interpretation to improve the understanding of passive margin sedimentary basin evolution and the structural evolution of salt tectonic structures and the depositional system present in the Scotian Basin.

3.2 Materials

All materials used in related experiments stay consistent throughout the honours project and are comprised of silica sand and silicone rubber. The following table summarizes the properties of each.

Property	Silica Sand	Silicone Rubber
Grain Size (mm)	0.02 - 0.45	--
Density (g/cm^2) (sifted)	1.6	0.99
Viscosity (Pas)	--	6x10^4
Angle of internal friction	34	--

Table 3-1: Table of material properties for silica sand and silicone rubber used in all experiments.

3.3 Scaling

Pilot and large scale experiments, are dynamically scaled such that geometries, kinematics and stresses observed in the model are quantitatively comparable to nature (Costa and Vendeville, 2002; Hubbert, 1937; Weijermars et al., 1993). The geometric scaling factor: $L^* = 10^{-5}$, is derived from the relation of cohesion, density of the sand in the model and sedimentary rocks in nature, and gravity acceleration. When applied, 1 cm in all experiments is equal to 1 km in nature. The time scaling factor is deduced from the viscosities of silicone and salt sediments, and the density of the respective overburden. With the given time scaling factor of $t^* = 1.4x10^9$, 1 hour in the model is approximately equivalent to 150,000 years in the geological record. Since the time interval under study for the honours project is the Jurassic to Cretaceous periods, the experiments usually run for ten to fourteen days to correspond to the natural evolution from initial salt mobilisation to final allochthonous salt nappe formation.

3.4 Experimental Procedures

There are two sets of experiments conducted for this honours project. One set is comprised of the pilot experiments, which are not PIV monitored and serve to give early insight into various controls. The other set of experiments is comprised of large scale

experiments which run continuously with no sedimentation breaks over night and are fully monitored.

To begin each experiment, the lateral boundaries and basement topography of the basins are built with sand on a base plate. Once the basement morphology is established, silicone rubber is placed evenly in the accommodation space and allowed to settle to establish the salt basin. It is important to manually disperse the silicone rubber with minimal space between chunks to ensure that there is little or no trapped air in the silicone to allow gravity spreading with minimal inclusion of air bubbles.

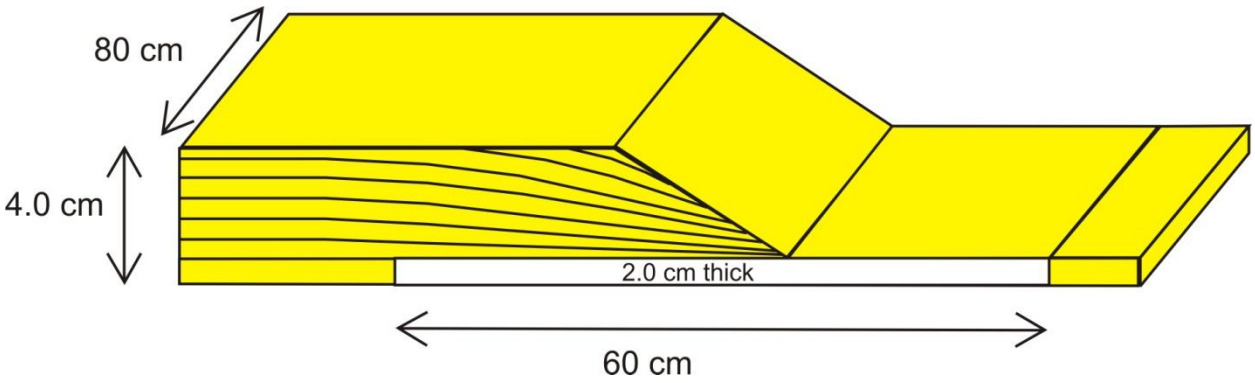

Figure 3-1: Simplified large scale experiment setup. All dimensions remain the same during the project with exception of the initial salt thickness which varies with basement geometry. In this figure sand is represented by yellow and silicone is represented by white.

In the pilot experiments sedimentation is simulated by sieving layers of coloured sand every two or four hours with a constant mass of either 200 or 250 g, which is equivalent to the amount of sand needed to deposit 250 m of strata on the landward shelf and landward salt basin areas during 300,000 or 600,000 years respectively. Sieving is done manually with the use of special sieves made of plastic cups with constant rates and material volumes starting from the landward side of the model to simulate sediment delivery by rivers from coast to deep water. Sieving is also performed in such a way that

accommodation space created from silicone withdrawal in the shelf area may be filled first, rather than a constant thickness for the extent of the model surface. During initial shelf build-up a total thickness of 4 cm of sand is allowed to accumulate in proximity to the shelf area, with each layer being only 0.25 cm thick. After the shelf build-up stage has reached this critical thickness progradation into the slope area begins, either maintaining the constant mass, or lowering it slightly to 175 g for each event until completion.

In the large-scale experiments sedimentation rates are similar to pilot experiments such that each interval results in the deposition of 0.25 cm of silica sand. However, the mass of sand deposited during each event is increased to 700 g as the area to undergo sedimentation and width of the margin in the experiments is much larger. A height adjustable guide and rail system combined with oblique lighting aids in the accurate sieving of each layer. The guides, present as a set of parallel strings, allow for shadows to be cast onto the experiment from an oblique light source. The shadows cast on the experiment should remain relatively straight on the surface to ensure that it is not bumpy or uneven. After the experiments are stopped they are covered with a layer of sand to protect the model surface during sectioning and to remove differential loading to prevent further salt mobilization. The experiments are then soaked with water to increase cohesion between sand grains and to allow for easier sectioning. After the sand has drained for some time the experiments are cut in parallel sections in intervals of 2.5 cm (pilot) or 5 cm (large experiment) with the use of cutting tools. Digital photos are taken after each section interval with a digital camera mounted on a tripod to record the variation of final structures in the cross-sections detailing the final salt structures, basin

architecture, and the lateral variations of brittle deformation structures in the overburden sand layer.

3.5 Monitoring

3.5.1 Pilot Experiments

Pilot experiments are monitored with a digital camera mounted on a tripod at a set location in the laboratory. Time-series overview photos which document oblique-view cross sections of the experiment are taken after every sedimentation event and after any nightly sedimentation breaks in order to document structures in cross section and at the surface. Detail photos are also taken to document additional interesting deformation structures and experiment stages. The time-series images are an important data source in the course of the project as they document the experiment evolution and aid in the interpretation and structural restoration of experimental results.

3.5.2 Particle Imaging Velocimetry (PIV) Monitoring

Particle Imaging Velocimetry is an optical deformation monitoring technique which is used to measure 3D surface flow and deformation of the lab scaled model experiments. Two high resolution CCD cameras are mounted stereoscopically above the analogue experiment and are calibrated for the 3D volume of each experiment (fig. 3-2). The cameras are programmed to take one picture for every minute, with every tenth picture used to document surface evolution, fault kinematics and subsidence.

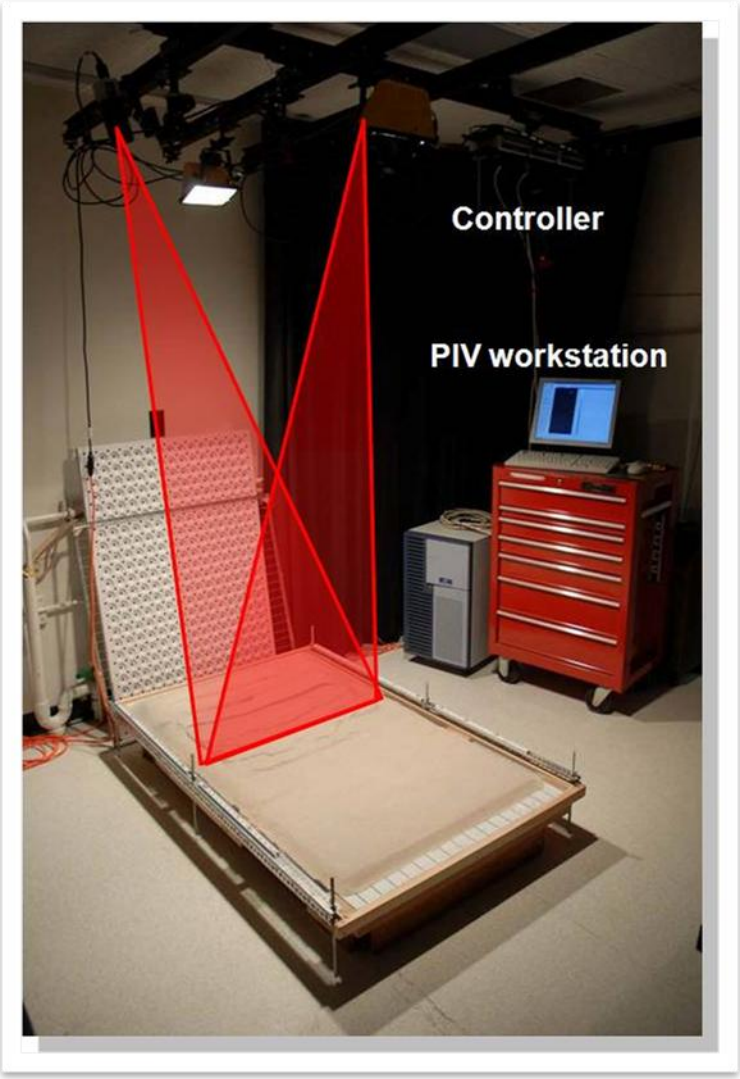

Figure 3-2: Laboratory setup with CCD cameras mounted stereoscopically over the experiment to resolve 3D surface evolution and deformation in topography. (Salt Dynamics Group)

The PIV software (Davis 7.1, LaVision) calculates displacement data by adaptive cross correlation techniques from the shift of particle pattern on the surface in time-series images with sub-millimetre accuracy. This allows for the quantification of incremental and finite strain as seen in fig. 3-3 (Adam, 2005). With the complete displacement field data and the strain history of model structures observed in the analogue model, 3D structural and kinematic models are constructed that document the evolution of structures and sedimentation through time.

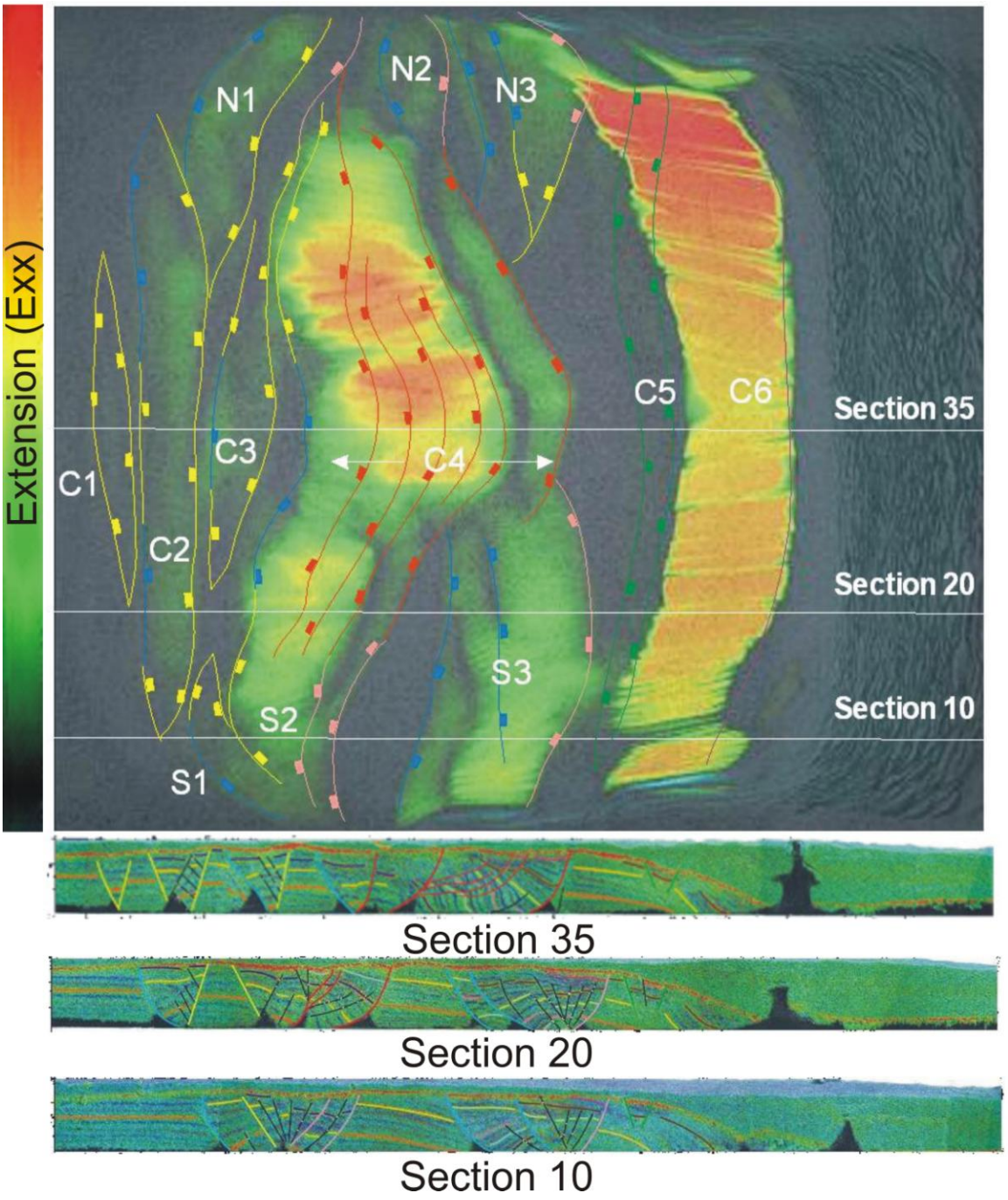

Figure 3-3: Example of final experiment surface with overlay of PIV total horizontal strain (Exx) data, structural interpretation and cross section data. Yellow and green lines indicate planar normal faults, blue indicates basinward dipping listric faults, pink indicates early landward dipping listric faults, red indicates mature landward dipping listric faults and purple indicates diapir/expulsion rollover contact. C2 and C3 are basinward rollovers, S1-3 and N1-3 are basinward rollovers with late roller fall, C5 is a keystone graben. (After Krezsek, et al., 2006b)

3.6 Experimental Base

The honours project consists of two sets of experiments. Set 1 is comprised of pilot experiments which are conducted in glass-sided tanks to test the role of sedimentation and basement morphologies in narrow rift basins with thick syn-rift salt, such as what is expected in the Abenaki and Sable area, offshore Nova Scotia.

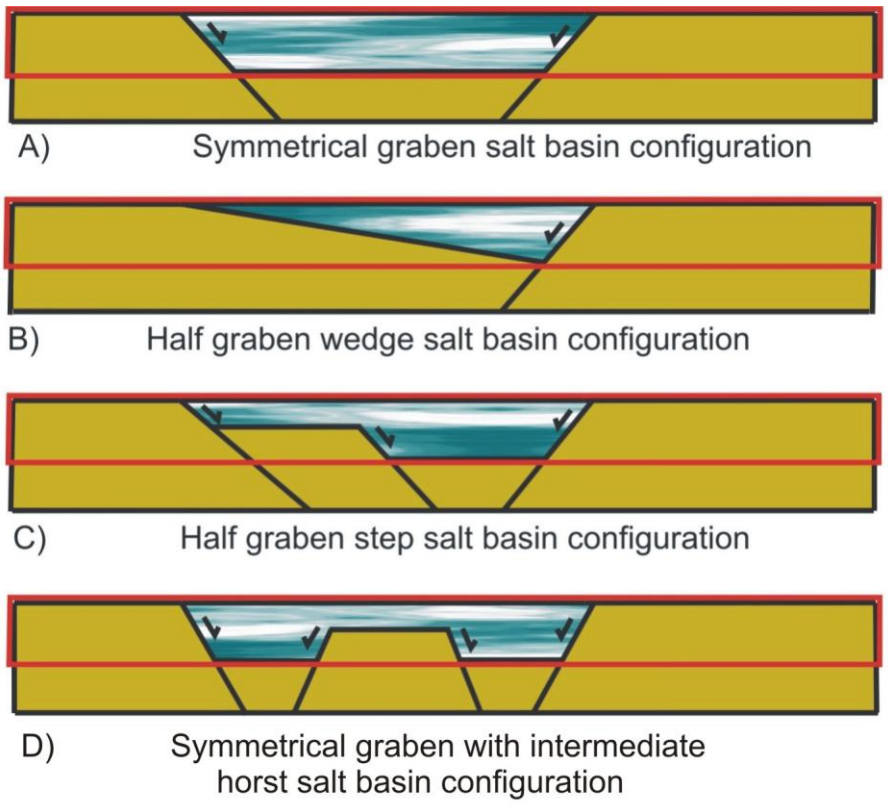

Figure 3-4: Basement morphologies used in analogue experiments. A: Experiments 5-1, 5-2 and 5-7. B: Experiments 5-3, 5-8 and 5-10. C: Experiments 5-5, 5-9 and 5-11. D: Experiment 5-6. The red box in each configuration displays the area modelled in the experiments. Blue/white fill is representative of salt.

For some pilot experiments (exp. 5-1 to 5-6) nightly breaks of sedimentation were allowed as these experiments are only meant to test input conditions and provide an understanding of the overall structural evolution for each setting. Set 2 consists of the larger (120 cm by 90 cm), experiments with scaled basin geometries comparable to

typical sub-basin geometries of the Scotian Margin. These experiments are monitored by the PIV system. Basin and basement morphologies used in these larger experiments are chosen from the pilot experiment results completed in set 1. The silicone thickness (2 cm) is based on literature data and seismic data available from the GSC and is thought to represent an initial salt basin with 2 km of salt. No sedimentation breaks are allowed in the large scale experiments that run continuously to simulate continuous natural sedimentation. The large scale experiments run for approximately ten days with sieving events every four hours. Table 3-2 gives the details of each experiment.

Experiment	Setup	Basin Geometry	Shelf Buildup	Sedimentation Rate	Modelled Sediment input: km^3/km of margin in 150,000 years	Sieve Intervals	Duration
5 - 1	Full Graben	Full Graben; 35 cm length. 2 cm of salt	4.0 cm	0.25 cm/2 hours	3.13	1 hour	144 hours
5 - 2	Full Graben	Full Graben; 35 cm length. 2 cm of salt	4.0 cm	0.25 cm/2 hours	1.57	2 hours	187 hours
5 - 3	Wedge	Half Graben Wedge; 35 length. 2 cm of salt	4.0 cm	0.25 cm/2 hours	1.57	2 hours	234 hours
5 - 4	Compressional Reactivational/ Tilt	Full Silicon Basement; 1 cm of salt	4.0 cm	0.25 cm/2 hours	1.57	2 hours	~244 hours
5 - 5	Basement Steps	Half Graben Steps; 35 cm length. 2 cm of salt with no step. 1 cm of salt with step	4.0 cm	0.25 cm/2 hours	1.57	2 hours	218 hours
5 - 6	Intermediate Horst	Full Graben with Intermediate Horst; 35 cm length. 2 cm of salt with no horst. 1 cm of salt with horst	4.0 cm	0.25 cm/2 hours	1.57	2 hours	220 hours
5 - 7	Full Graben	Full Graben; 60 cm length. 2 cm salt	4.0 cm	0.25 cm/4 hours	1.95	4 hours	224 hours
5 - 8	Wedge	Half Graben Wedge; 60 length. 2 cm of salt	4.0 cm	0.25 cm/4 hours	1.82	4 hours	176 hours
5 - 9	Basement Steps	Half Graben Steps; 60 cm length. 2 cm of salt with no step. 1 cm of salt with step	4.0 cm	0.25 cm/4 hours	1.82	4 hours	188 hours

Table 3-2: Experiment setups detailing: basin geometry, shelf buildup, sedimentation rate, progradation rate, sieve intervals and durations. Experiments 5-1 to 5-6 are pilot experiments. Experiments 5-7 to 5-9 are large scale experiments.

Chapter 4: Experimental Results

4.1 Work Flow

Interpretation of the experiments were done jointly by Clarke Campbell and myself as experiments used for the honours projects are conducted by multiple members within the Salt Dynamics Group at Dalhousie University. As it makes no sense to interpret only the autochthonous and allochthonous regions of a particular experiment separately it has been decided that individual experiments would be assigned to each person. With complete interpretations and restorations of the experiments, each member may discuss areas which relate to their thesis topic. The experiments and their respective interpreter are presented in table 4-1.

Experiment	Setup	Basin Geometry	Interpreter
5 - 1	Full Graben	Full Graben; 35 cm length. 2 cm of salt	Training
5 - 2	Full Graben	Full Graben; 35 cm length. 2 cm of salt	Clarke Campbell
5 - 3	Wedge	Half Graben Wedge; 35 length. 2 cm of salt	Cody MacDonald
5 - 4	Compressional Reactivational/ Tilt	Full Silicon Basement; 1 cm of salt	Test
5 - 5	Basement Steps	Half Graben Steps; 35 cm length. 2 cm of salt with no step. 1 cm of salt with step	Clarke Campbell
5 - 6	Intermediate Horst	Full Graben with Intermediate Horst; 35 cm length. 2 cm of salt with no horst. 1 cm of salt with horst	Cody MacDonald
5 - 7	Full Graben	Full Graben; 60 cm length. 2 cm salt	TBA
5 - 8	Wedge	Half Graben Wedge; 60 length. 2 cm of salt	TBA
5 - 9	Basement Steps	Half Graben Steps; 60 cm length. 2 cm of salt with no step. 1 cm of salt with step	TBA

Table 4-1: Experiments and their respective interpreter.

As seen in the table, experiments: 5-1, 5-4, and 5-8 will not be included as part of the honours project. Experiment 5-1 was conducted as orientation to lab techniques, experiment 5-4 was conducted by Csaba Krezsek to test compressional diapirism with

inversion of the salt basin and was not prepared for cross sectioning, and experiment 5-8 had cross section images which were unusable. Experiment 5-9 will be interpreted in future projects.

4.2 Overview of Results

The structural evolution of the experiments (fig. 4-1, etc.) varies significantly with basement morphology. In each experiment different structural regimes were identified. In particular, the extensional and translational regimes in the shelf and slope area were examined in detail as they correspond to salt and sediment structures that developed during early mobilization of autochthonous salt in the original salt basin area.

4.2.1 Early Stage

In all experiments deformation begins with the onset of basinward dipping growth normal faults at the landward limit of the salt basin "BGF", marking the initiation of salt mobilization and dominantly vertical subsidence from the imposed differential load of sand on the silicone. This faulting is observed in all lateral sections of the experiments and is commonly associated with a set of antithetic faults that accommodate subsidence in the hangingwall block. The duration of this fault system typically extends to the end of shelf buildup, marking the beginning of salt withdrawal basin welding to the basin floor. As this structure occurs in every experiment it will not be described independently for each. The basinward growth strata are a relatively undeformed package of strata subsiding in the silicone during shelf aggradation which is bounded basinward by a passive diapir or inflated silicone complex. After shelf buildup, with the onset of sediment progradation the basins may eventually evolve to have expulsion rollovers

"ER". The extent of this undeformed region varies with the basement configuration in the various experiments.

The compressional regime of the experiments is first seen in the early stage and comprises buckle folding and silicone inflation in the basinward part of the autochthonous salt basin.

4.2.2 Intermediate Stage

Major passive diapirism occurs in the inflated salt complex of all experiments after the end of shelf buildup with the onset of sediment progradation (intermediate stage) where the basinward limit of the salt basin acts as a buttress to the ductile flow within the silicone. The experiment with the half graben steps is characterized by downbuilding of sand, allowing for more passive diapirs. Sedimentation breaks during the pilot experiments have influenced the geometry of passive diapirs and canopy evolution; though entrapment of silicone and the location of the passive diapirs are considered to be mainly controlled by the basement morphology. Associated with this diapirism is considerable rafting of stratigraphic packages "R" in the experiments: half graben wedge and symmetrical graben with horst (figure 4-1). With the sedimentation breaks during the pilot experiments there are also landward and seaward canopies associated with passive diapirism in all experiments (see diapirs "D" in the half graben step experiment). This is most notable in the two half graben experiments, so much so in the latter that there is a significant canopy system that formed in the late stage of its evolution, causing much lateral flow and making typical structural restoration difficult.

4.2.3 Late Stage

A silicone nappe is present in the deepwater region of all pilot experiments and is a direct result of silicone expulsion. The silicone, like salt in nature, is able to act like a glacier and flow over the basinward limit and subsequent strata. However, if progradation continues the nappe will undergo extension, resulting in basinward and landward listric faults, and various rollovers. This deepwater extension is seen most obviously in the experiment testing the half graben wedge.

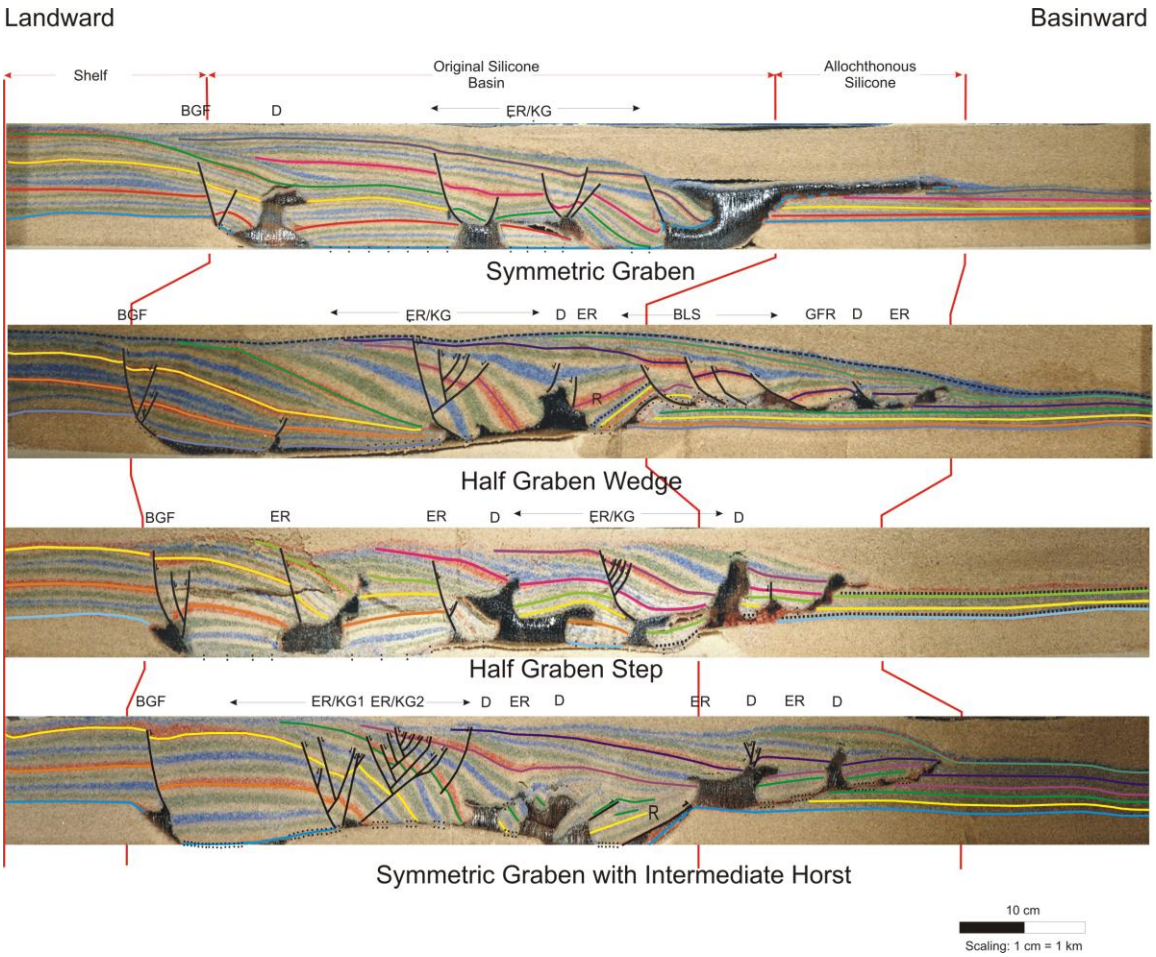

Figure 4-1: Overview of pilot results. BGF: Basinward growth normal fault. ER/KG: Expulsion rollover/keystone graben. D: Diapir. ER: Expulsion rollover. GFR: Growth fault rollover. R: Raft.

4.3 Symmetric Graben Pilot Experiment

4.3.1 Overview

The evolution, interpretation and restoration for the pilot experiment, 5-2 with the symmetrical graben basement configuration is presented in figures 4-2, 4-4 and 4-5.

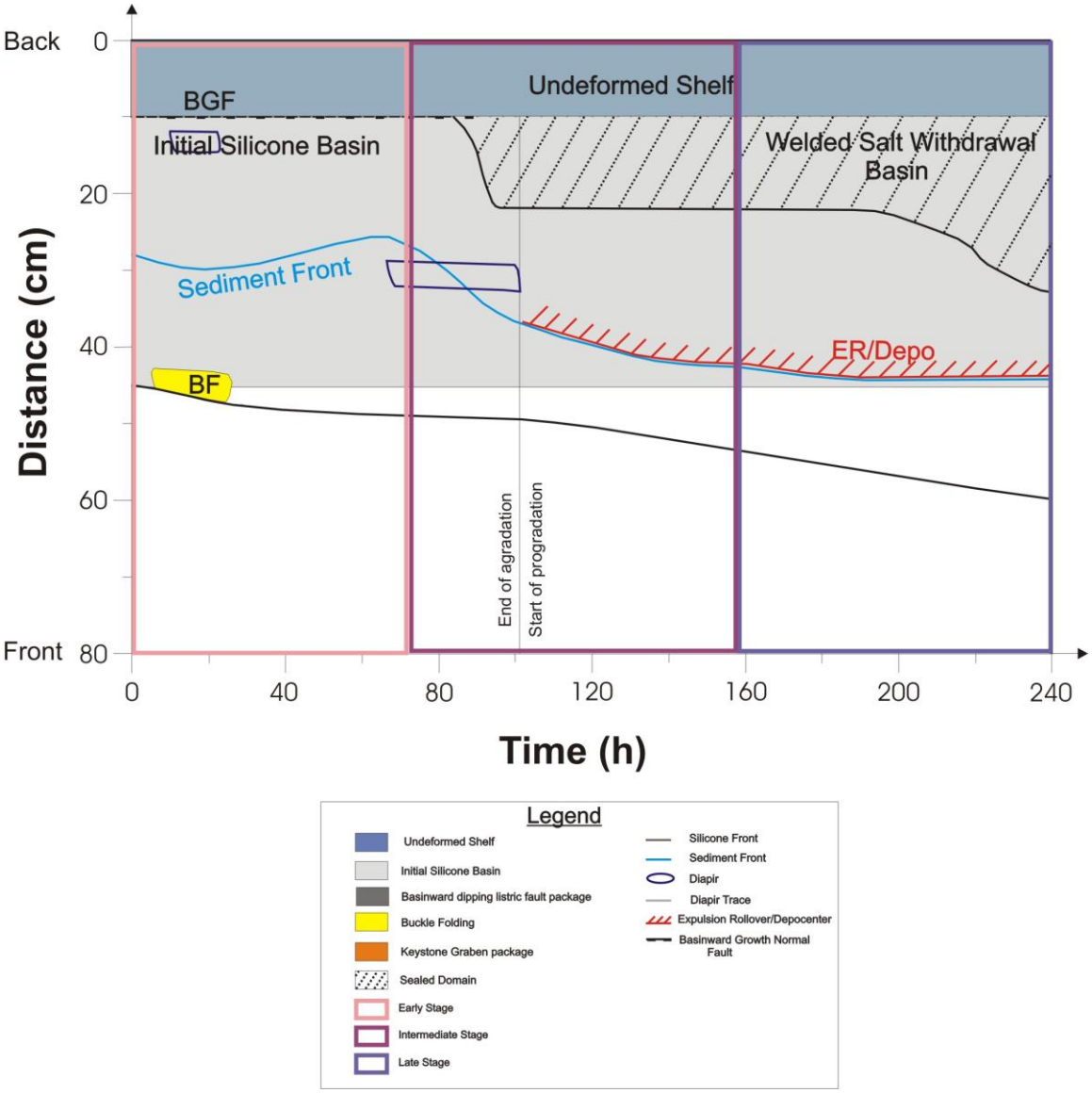

Figure 4-2: Schematic diagram of the symmetric graben structural evolution with time. The diagram represents the central cross-section of the experiment while displaying the timing and position of structures as they appear. In this case the front and back annotations represent the basinward and landward limits of the models respectively.

From the landward to basinward limit there are four major regional elements which are presented in figure 4-4: 1) a basinward dipping major growth fault "BGF" situated at the landward limit of the silicone basin with antithetic faults, 2) a major diapir

"D" flanked by a basinward downbuilding expulsion rollover system "ER", 3) a mid-basin diapir/canopy "D" with a basinward downbuilding expulsion rollover system, and 4) a thick inflated silicone massif/allochthonous nappe system.

Adjacent to the basinward dipping growth normal fault is a major diapir "D" which is present in all lateral sections of the experiment. However, the position of this diapir is not constant throughout the entire base and appears to be continuously moving basinward from one lateral limit to the other; i.e. from section 2.5 cm – 27.5 cm (Appendix B1). This diapir also began its evolution during the early stage (between 6 and 18 hours) and continued to rise passively until the intermediate stage (approximately 112 hours) when the overburden welded on the basin floor. This large diapir is flanked on its landward boundary by a basinward expulsion rollover "ER" system which began during the early stage (18 hours) of the experiment. This rollover system continued with downbuilding until the diapir was shutdown by salt withdrawal. There is minor faulting present in the rollover structure; however it is not very extensive in comparison to other experiments and natural settings.

Further basinward there is a mid-basin diapir with an associated canopy system "D", linking it to a remnant of what was the front of the major inflated silicone body. This diapir became passive during the early stage, at approximately the same time as the first (between 6 and 18 hours) and began to flow passively at the surface, even with later sedimentation. The silicone canopy developed freely until approximately 62 hours when it merged with the front of the inflated silicone body. This process was driven by continuous downbuilding occurring in front of the mid-basin passive diapir "D", creating

enough accommodation space to protect the flowing silicone from being overridden with sediments.

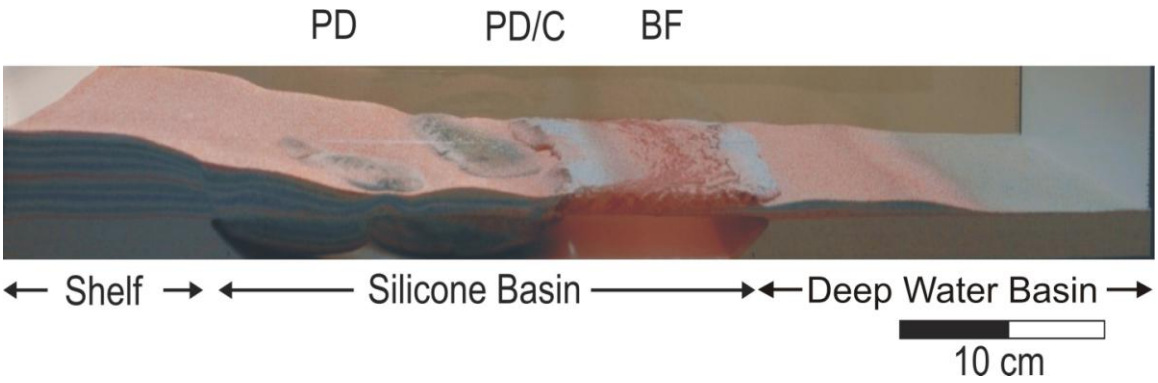

Figure 4-3: Image showing the silicone flowing freely at the surface of the experiment (62 hours). At this time the silicone at the surface is almost in contact with the inflated silicone further basinward. PD: Passive diapir, C: Canopy, BF: Buckle folding.

The canopy allowed silicone to be sourced to the inflated front from the mid-basin diapir until approximately 112 hours (intermediate-stage) when it was shutdown from welding on both sides. However, this allochthonous silicone supported late-stage diapiric growth at the front for the remainder of the experiment. This resulted in the adjacent strata being translated basinward as extension was accommodated in the diapir. With late-stage downbuilding of strata, most of the silicone that preferred to flow into the new diapir system was trapped after welding. The canopy-turned-diapir system is flanked by a basinward expulsion rollover which began at approximately 112 hours (late-stage), as sediments overrode the second diapir and canopy and began to downbuild in the new accumulation of silicone. The remainder of the silicone from the original salt basin was displaced horizontally into the large nappe system.

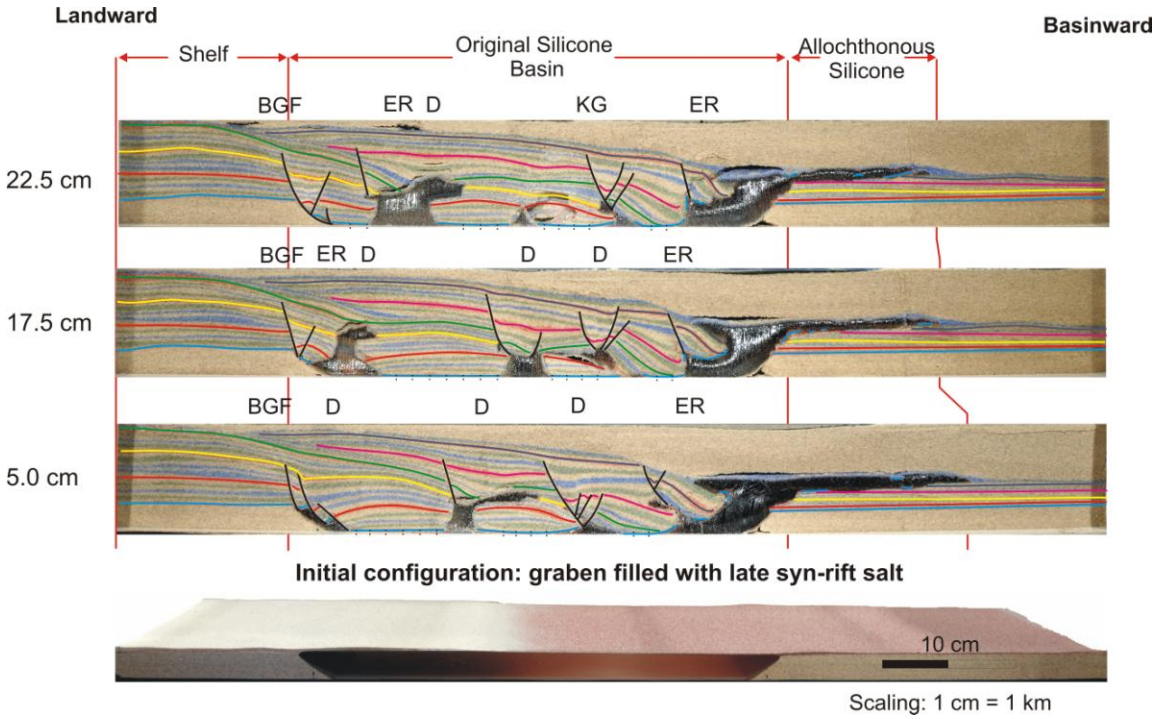

Figure 4-4: Cross-sections of the symmetric graben experiment. Sections detail lateral changes through the extent of the experiment base. BGF: Basinward dipping growth normal fault. ER: Expulsion rollover. D: Diapir. KG: Keystone graben.

4.3.2 Structural Restoration

The structural restoration of the experiment testing the symmetric graben basement morphology is presented in fig. 4-5.

Restored to 24 hours

The first structure to form is the basinward dipping growth normal fault "BGF". Minor extension created by this fault was accommodated by buckle folding at the basinward margin of the silicone basin. There is a diapir "D" present at this time which accommodated space created by extension in the brittle overburden. A silicone roller is also seen in the mid basin area indicating reactive rise of silicone.

Restored to 67 hours

At this time the diapir at the landward limit has grown larger, though is becoming overridden with further sedimentation and decreasing volume in underlying silicone. The mid-basin silicone roller has evolved into a passive diapir "PD" and sourced silicone at the surface to form an extensive canopy system with the basinward inflated silicone massif. Sediments trapped between this silicone canopy system are now isolated as a rafted package.

Restored to 101 hours

In this section the diapir adjacent to the BGF has been shutdown with overriding sedimentation and silicone withdrawal. The canopy system present in mid-basin region has become covered with sediments, and extensional faulting has resulted from silicone evacuation. Extension in the sediments overlying the canopy has also resulted in another passive diapir "PD". The canopy is still significant in size however, and continues to feed the inflated the inflated silicone complex. Downbuilding of sediments into this inflated silicone has begun in the form of an expulsion rollover "ER" (Appendix B1).

Restored to 146 hours

With advancement of the prograding sedimentary wedge and further loading, the canopy system is efficiently being evacuated. Consequently numerous faults occur in the overlying sediments thought little horizontal translation takes place. Basinward, the expulsion rollover continues to significantly downbuild into the inflated silicone which is forcing the advancement of the allochthonous silicone nappe. Some silicone is also flowing in the landward direction, on top of the rolling sediment front.

Restored to 191 hours

At this time there is continued expulsion of silicone from the canopy, as well as downbuilding of the expulsion rollover into the inflated silicone front. Minor faulting is also occurring in the rollover structure but not as significantly as those found in other keystone grabens. The landward flowing silicone associated with the inflated silicone has been covered by sand, forming a silicone overhang.

Unrestored Section

The final section of the experiment shows that the canopy system welded over the rafted sediment package. The silicone evacuated from this welding became trapped as the basinward expulsion rollover also touched down and welded with the basement. The allochthonous silicone nappe has reached its final position.

Figure 4-5: Structural restoration of center section (15.0 cm) in the symmetric graben experiment; 5-2. BGF: Basinward dipping growth normal fault. ER: Expulsion rollover. D: Diapir. PD: Passive Diapir. (Next page)

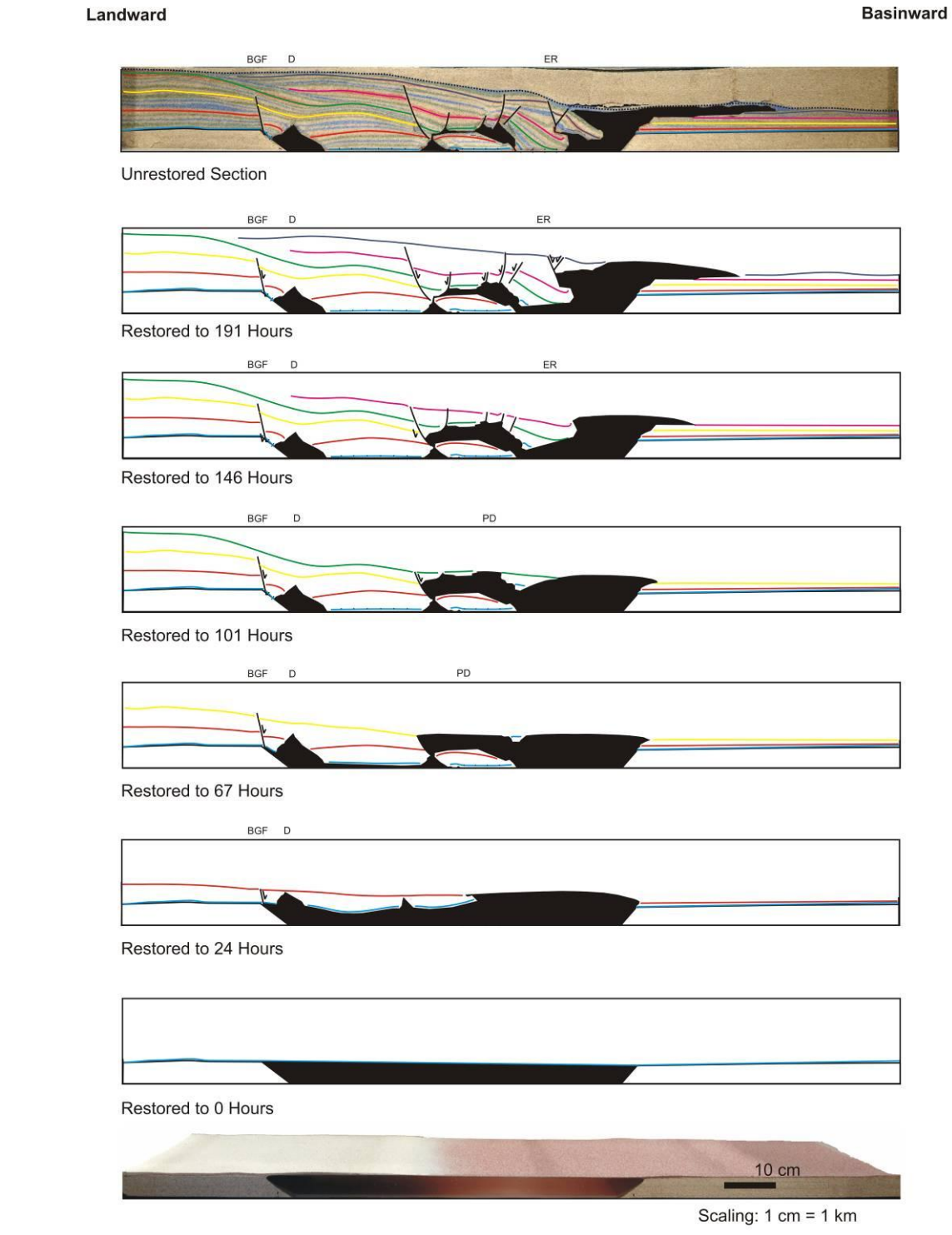
Landward
Basinward
BGF
D
ER
Unrestored Section
BGF
D
ER
Restored to 191 Hours
BGF
D
ER
Restored to 146 Hours
BGF
D
PD
Restored to 101 Hours
BGF
D
PD
Restored to 67 Hours
BGF
D
Restored to 24 Hours
Restored to 0 Hours
10 cm
Scaling: 1 cm = 1 km
Legend
Experiment Cover Layer
Marker Horizon
Salt Weld
Sedimentation Break
Former Marker
Fault with Displacement Vector
Former Fault with Displacement
Salt

4.4 Half Graben Wedge Pilot Experiment

4.4.1 Overview

The evolution, interpretation and restoration for the pilot experiment 5-3; with the half graben wedge basement morphology, are presented in figures: 4-6, 4-7 and 4-8.

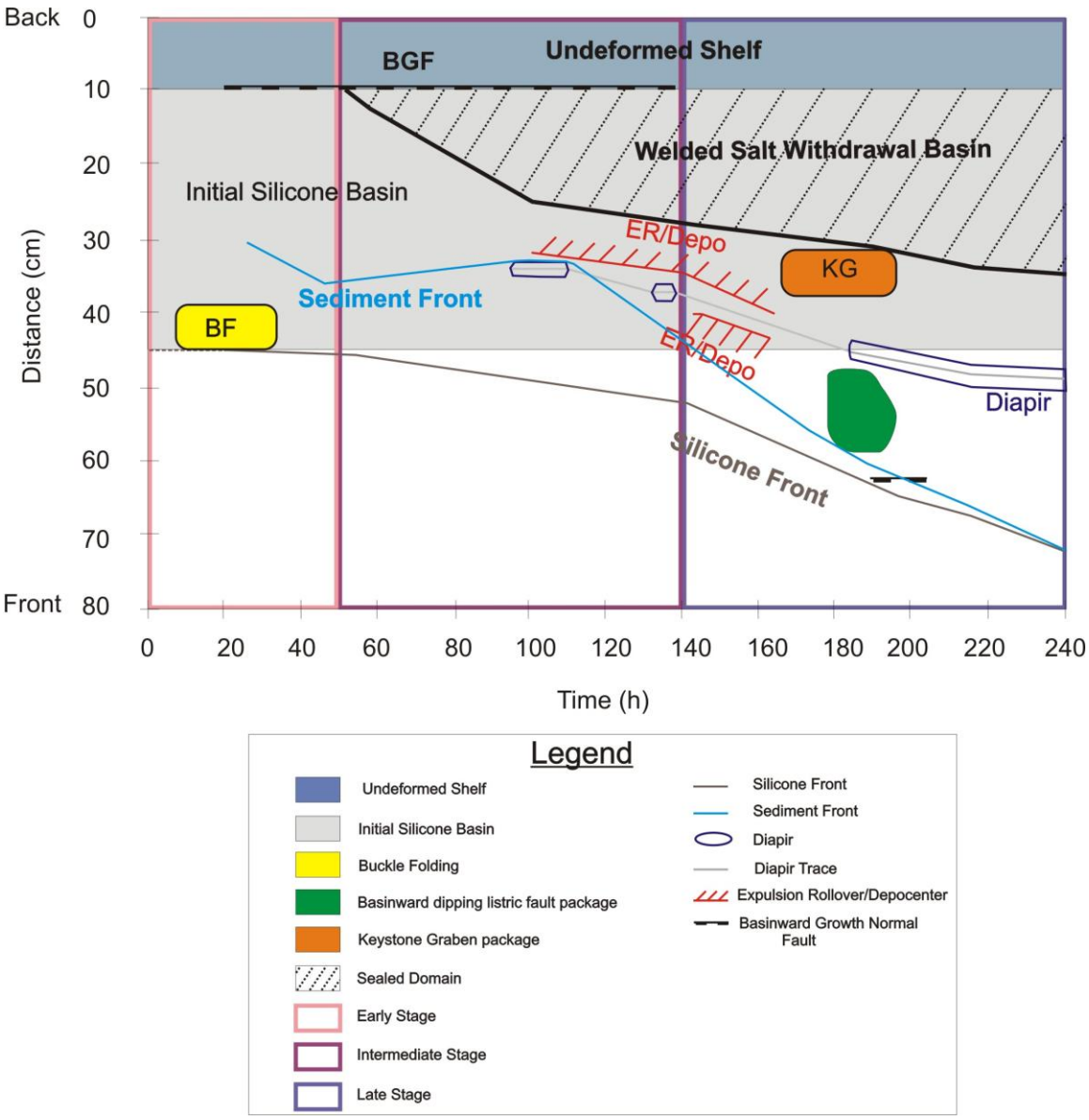

Figure 4-6: Schematic diagram of the half graben structural evolution with time. The diagram represents the central cross-section of the experiment while displaying the timing and as position of structures as they appear. In this case the front and back annotations represent the basinward and landward limits of the models respectively.

From the landward to basinward limit there are three major regional elements, presented in figure 4-7: 1) a half-graben wedge-shape silicone withdrawal basin with a major basinward growth normal fault with secondary antithetic faults “BGF”, 2) a central diapir “D” flanked by expulsion rollovers “ER” and associated keystone grabens “KG”, and 3) an allochthonous salt nappe province.

The diapir province is marked by the major diapir “D”, which is substantial in size (max height: 3 km by max length: 6.5 km). This diapir extends laterally in all sections except for section 0 cm, which is close to the glass wall of the experiment. The geometry of the diapir changes significantly along strike, showing late-stage diapir fall in most instances, but active rise in others (5.0 cm and 22.5 cm) where it is still being supplied by feeders. On both sides of the main diapir are expulsion rollovers “ER”, which were active during the intermediate to late stage ,approximately 100 – 164 hours (basinward downbuilding) and 143 – 164 hours (landward downbuilding). Extension created in the hangingwall by the bending of the basinward downbuilding expulsion rollover anticline was accommodated by a major keystone graben “KG”. The landward downbuilding rollover contains a raft “R” which was part of the toe of the sedimentary wedge, but was detached during early reactive and passive rise of the diapir. This raft was also thrusted onto the allochthonous silicone nappe later in the experiment.

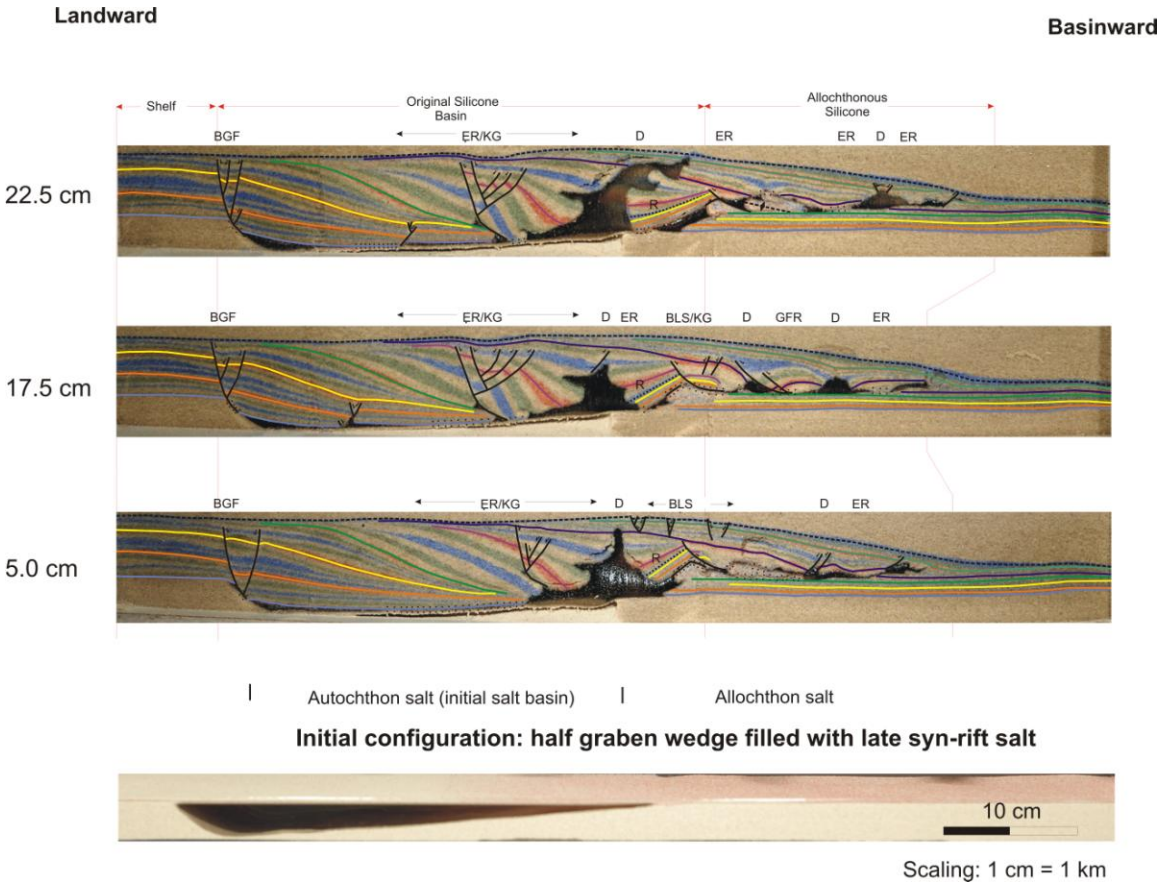

Figure 4-7: Cross sections of the half graben wedge experiment. Sections detail lateral changes through the extent of the experiment base. BGF: Basinward dipping growth normal fault system. ER/KG: Expulsion rollover/keystone graben. D: Diapir. GFR: Growth fault rollover. R: Raft.

4.4.2 Structural Restoration

The structural restoration of this experiment (fig. 4-8) reveals that there was 8.0 cm of horizontal extension, equating to 8.0 km in nature.

Restored to 28 hours

The first structure formed is the basinward dipping growth normal fault "BGF". Extension associated with this fault was accommodated by early basinward compression in the form of buckle folding and minor salt inflation.

Restored to 56 hours

Following the BGF is an antithetic fault that accommodates extension in the mid basin region. Up to this point there is a relatively low amount of extension observed (approximately 0.5 cm).

Restored to 101 hours

During this time it is evident that initiation of a reactive diapir in the lower slope triggered separation of the toe of the sedimentary wedge as the major raft "R". This main diapir "PD" is now in the passive stage, with a max thickness of 2.77 cm. It is also at this time that the inflated silicone starts to form an allochthonous nappe at the basinward margin of the silicone basin, thrusting the raft over deep water equivalents.

Restored to 143 hours

In this section it is evident that most of the silicone has been evacuated from the basinward margin of the original silicone basin with any silicone left behind being trapped between primary welds. Basinward strata have also begun to downbuild and roll into the main diapir "PD" creating expulsion rollovers "ER". The nappe continues to flow into the deepwater region, extending 6.58 cm past the basinward margin of the original silicone basin.

Restored to 189 hours

At this time keystone grabens "KG" are present due to downbending of the growth strata. The main diapir has finally reached its final geometry in this section of the experiment, although it continues to rise passively in other lateral sections (Appendix B2). The thrust leading into the nappe is now welded at this time, leaving it isolated from further rejuvenation.

Restored to 218 hours

Further loading of the nappe has lead to extension which is accommodated by basinward listric faults, growth fault rollovers, and expulsion rollovers. The extension faulting in the nappe has also resulted in multiple welds. The nappe has reached its final position at this time at 20.1 cm from the basinward margin of the original silicone basin.

Unrestored Section

Little deformation has occurred from the last time step as most of the system has already shutdown. The end of the allochthonous silicone nappe has advanced very slightly, offsetting some of the adjacent sediments.

Figure 4-8: Structural restoration of (center) section 12.5 cm in the half graben wedge experiment; 5-3. BGF: Basinward dipping growth normal fault. ER/KG: Expulsion rollover/keystone graben. D: Diapir. PD: Passive Diapir. R: Raft. GFR: Growth fault rollover. (Next page)

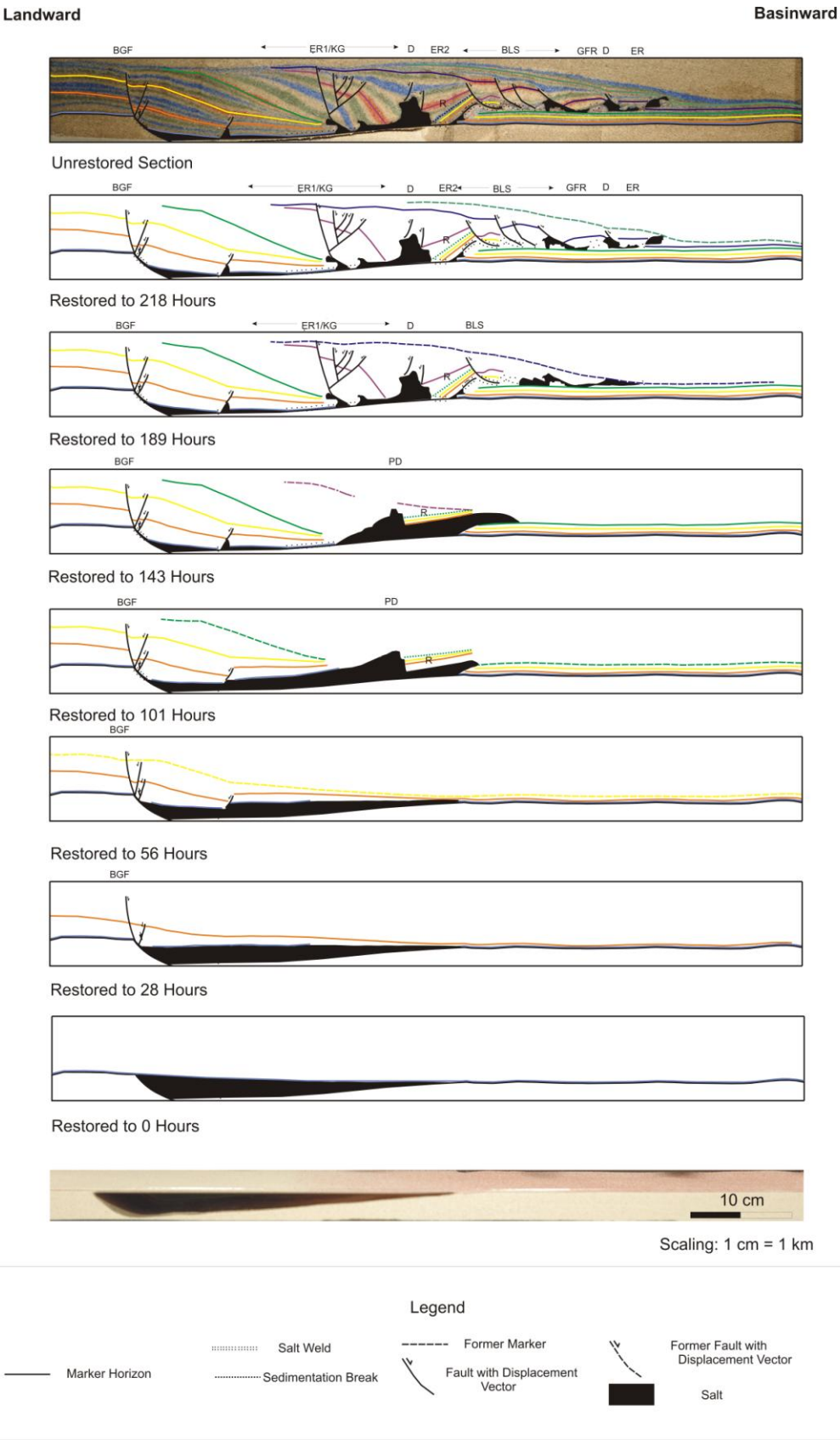
Landward
Basinward
BGF
ER1/KG
D
ER2
BLS
GFR
D
ER
R
Unrestored Section
Restored to 218 Hours
Restored to 189 Hours
PD
Restored to 143 Hours
Restored to 101 Hours
Restored to 56 Hours
Restored to 28 Hours
Restored to 0 Hours
10 cm
Scaling: 1 cm = 1 km
Legend
Marker Horizon
Salt Weld
Sedimentation Break
Former Marker
Fault with Displacement Vector
Former Fault with Displacement Vector
Salt

4.5 Half Graben Step Pilot Experiment

4.5.1 Overview

The evolution, interpretation and restoration for the pilot experiment 5-5; with the half graben steps basement morphology are presented in figures, 4-9, 4-12 and 4-13.

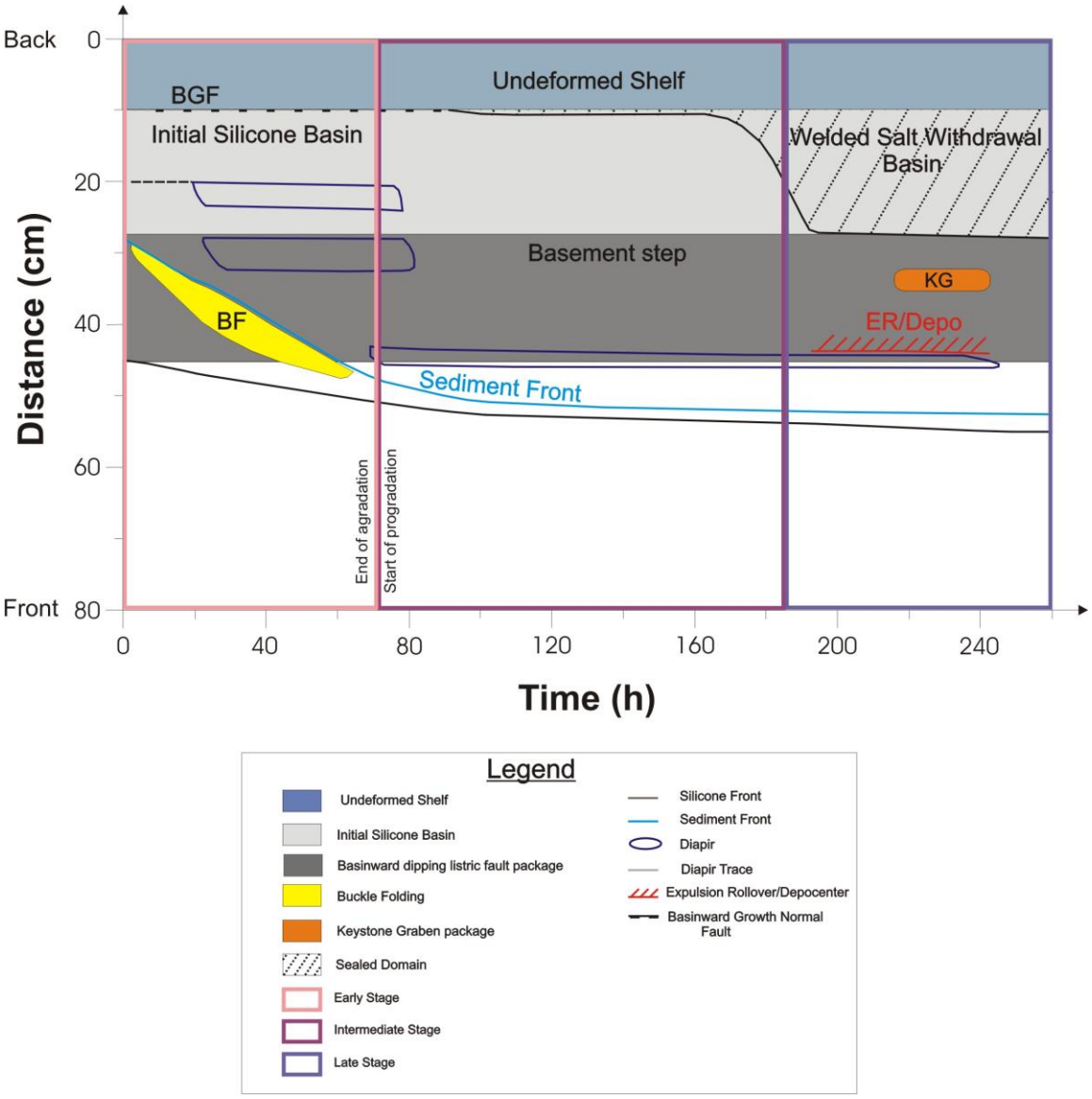

Figure 4-9: Schematic diagram of the structural evolution of the half graben steps experiment with time. The diagram is centered on the central cross-section of the experiment while displaying the timing and position of structures as they appear. The front and back listed here are the basinward and landward limits of the experiment respectively.

From the landward to basinward limit there are five major regional elements which are presented in figure 4-12: 1) a basinward dipping growth normal fault with trapped silicone, 2) a major diapir "D" with a varying tongue system, 3) a mid-basin diapir "D" with multiple tongues, 4) a minor diapir/canopy system "D", and 5) a complex nappe system with extensive diapirism.

The diapir province, marked by the major diapir "D" initiated during the early stage (between 8 and 24 hours). This diapir is present in all lateral sections with exception to sections 2.5 cm and 0 cm (Appendix B3), which are close to the boundary of the experiment. The shape of this diapir varies laterally showing more passive flow in some sections than others; i.e. section 17.5 cm versus 5.0 cm (Appendix B3). One time in which notable passive flow associated with this diapir occurred between 32 and 48 hours. On the landward side of the diapir is an expulsion rollover system which started at 24 hours when sedimentation was re-established. This rollover system shut down at approximately the same time as the diapir; 124 hours.

The mid-basin diapir with multiple tongue systems, marked by the following basinward diapir "D" initiated at the same time as that aforementioned. As it was further from the sedimentary wedge front it had more chances to flow passively at surface, contributing to its complex tongue system. It was also able to flow freely at surface at the sedimentation break between 32 and 48 hours. During this sedimentation break the first diapir was able to flow far enough at surface to suture with it and form a canopy system as seen in figure 4-10 and section; 25.0 cm (Appendix B3).

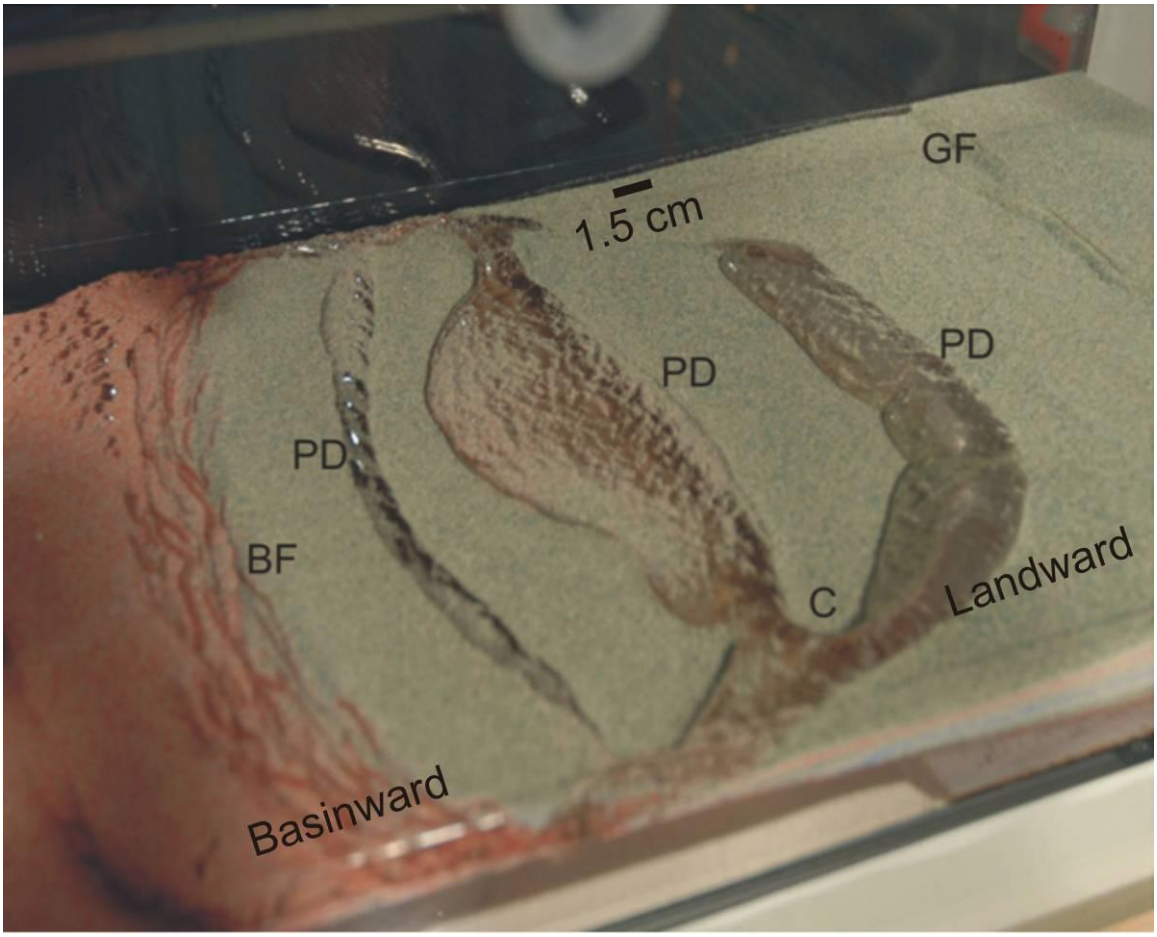

Figure 4-10: Image showing the passive silicone at surface forming a canopy system at the boundary of the experiment. This event occurred during a sedimentation break between 32 and 48 hours. GF: Growth fault, PD: Passive diapir, C: Canopy, BF: Buckle folding.

The canopy system formed here was short lived and was shutdown almost immediately at approximately 50 hours when sedimentation resumed. This diapir was able to grow passively into the late stage (to 150 hours), outlasting the first.

The last autochthonous feature, the minor diapir canopy system "D" was at the surface for a relatively short time but was crucial in the formation of diapirs in the nappe system as it acted as a feeder. This diapir formed at the same time as the others; however, it grew at a slower rate with less pressure being imposed on immediate silicone as the bulk of the sedimentary wedge was further away. Eventually it was able to flow

semi-passively (with a very thin sedimentary cover) to the basinward limit of the original basin and to the inflated silicone during the intermediate stage (between 104 and 120 hours; figure 4-11).

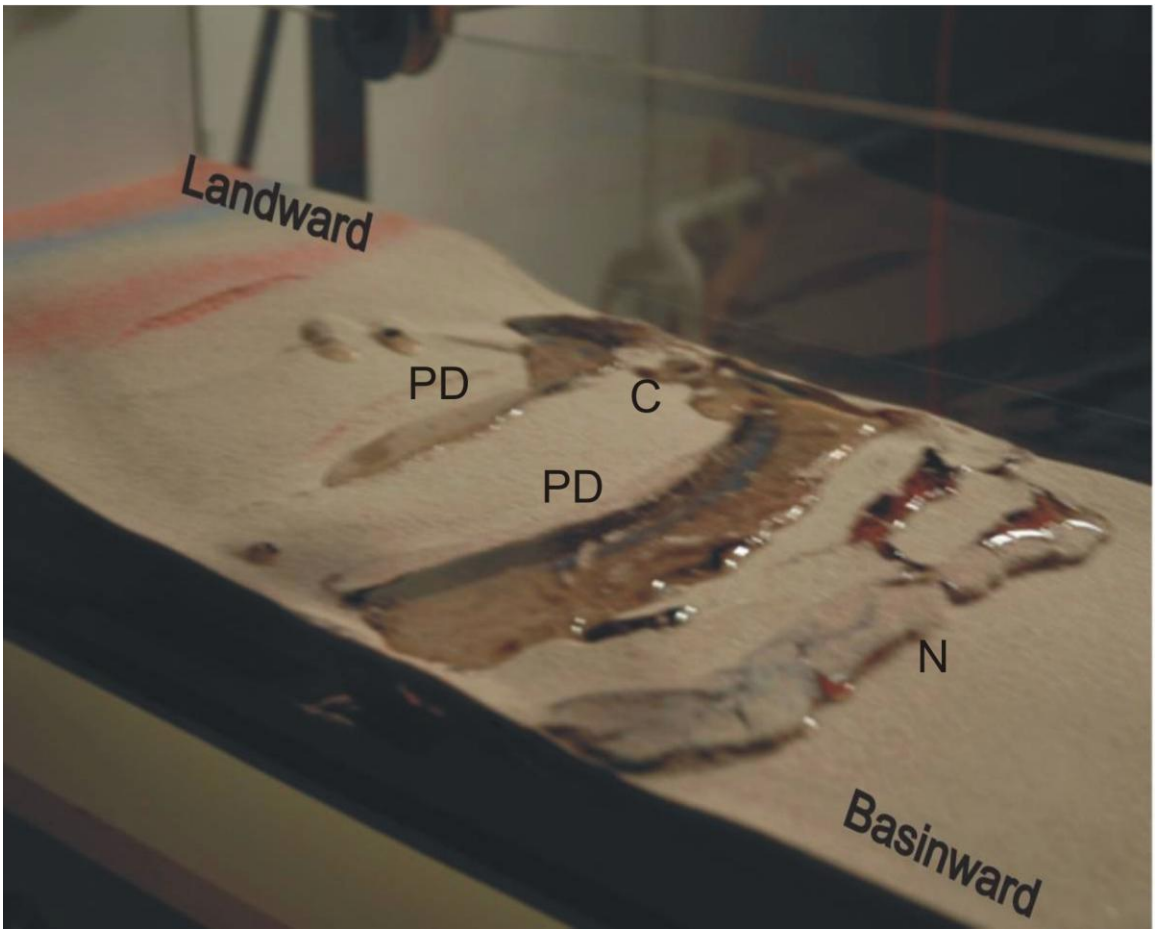

Figure 4-11: Image displaying semi-passive silicone flow between 104 and 120 hours enabling the formation of the canopy system. PD: Passive diapir, C: Canopy, N: Nappe.

The canopy that formed from this merging of silicone was quickly shut down at approximately 122 hours with further sedimentation; however it was still able to source silicone to the front of the inflated silicone and contributed to the diapiric features seen in the nappe system.

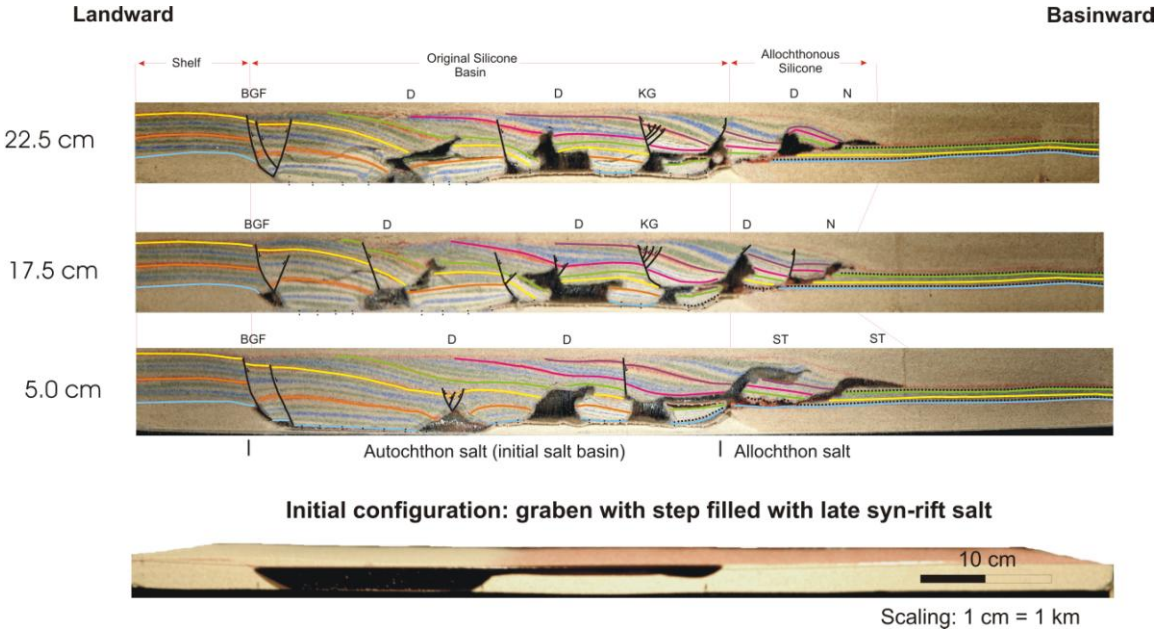

Figure 4-12: Cross sections of the half graben step experiment. Sections show lateral variability throughout the extent of the experiment base. BLS: Basinward dipping listric growth fault system. ER/KG: Expulsion rollover/keystone graben. D: Diapir. PD: Passive diapir.

4.5.2 Structural Restoration

The structural restoration of experiment 5-5 is present in fig. 4-13.

Restored to 28 hours

The first feature to form was the basinward dipping growth normal fault "BGF" at the landward limit of the experiment. The extension associated at the landward portion of the experiment induced compression at the basinward limit which led to buckle folding of the sediments above the step in the graben system, which acted as a buttress to silicone flow. Downbuilding of sediment blocks (~0.8 cm) and the formation of diapirs "D" occurred as silicone migrated vertically in response to differential pressure. Silicone trapped in the landward limit of the basin could not create passive diapirs as sediment coming from the shelf overrode and suppressed vertical migration of silicone. Small canopy systems are also present at the slope limit of the basin, though less than 1 cm long. As mentioned in the overview these canopy systems are associated with nightly

sedimentation breaks, but still yields important information as they correlate with low periods of sedimentation in nature.

Restored to 72 hours

By the intermediate stage silicone had begun to move out of the basin to a distance of 5 cm, forming an allochthonous sheet with related passive diapirs "PD". The reactive diapir "D" had also reached its passive stage and pierced the overburden during this time and formed a basinward migrating tongue extending approximately 1 cm long.

Restored to 102 hours

Subsidence of overlying sediments continued until they reached the basin floor and created primary welds. Sediments were later able to prograde over the tongue here and the overlying sediments caused welding on the landward portion. At this time an expulsion rollover "ER" initiated and continued to develop until the basinward block of sediments associated with the canopy also welded.

Restored to 146 hours

The diapir "D" which had formed by reactivation of the old diapir became passive "PD" and formed a landward oriented canopy system approximately 2 cm long. The landward block of sediments associated with this system in turn began to fault and rotate, creating the expulsion rollover/keystone graben system "ER/KG". A small sedimentary package was also able to fully subside to the bottom of the basin at this time, forming a weld. This package later was able to weld with new sediment by the end of the experiment.

Restored to 176 hours

The sedimentary package extends the entire length of the silicone in this time step, although the passive diapir "PD" continues to flow at the surface.

Unrestored Section

No deformation has occurred during this time step as the system is essentially shut down. The passive diapir has been covered with sand and is no longer at the surface.

Figure 4-13: Structural restoration of the center section in the half graben step experiment; 5-5. BGF: Basinward dipping growth normal fault. KG: keystone graben. D: Diapir. PD: Passive Diapir. (Next Page)

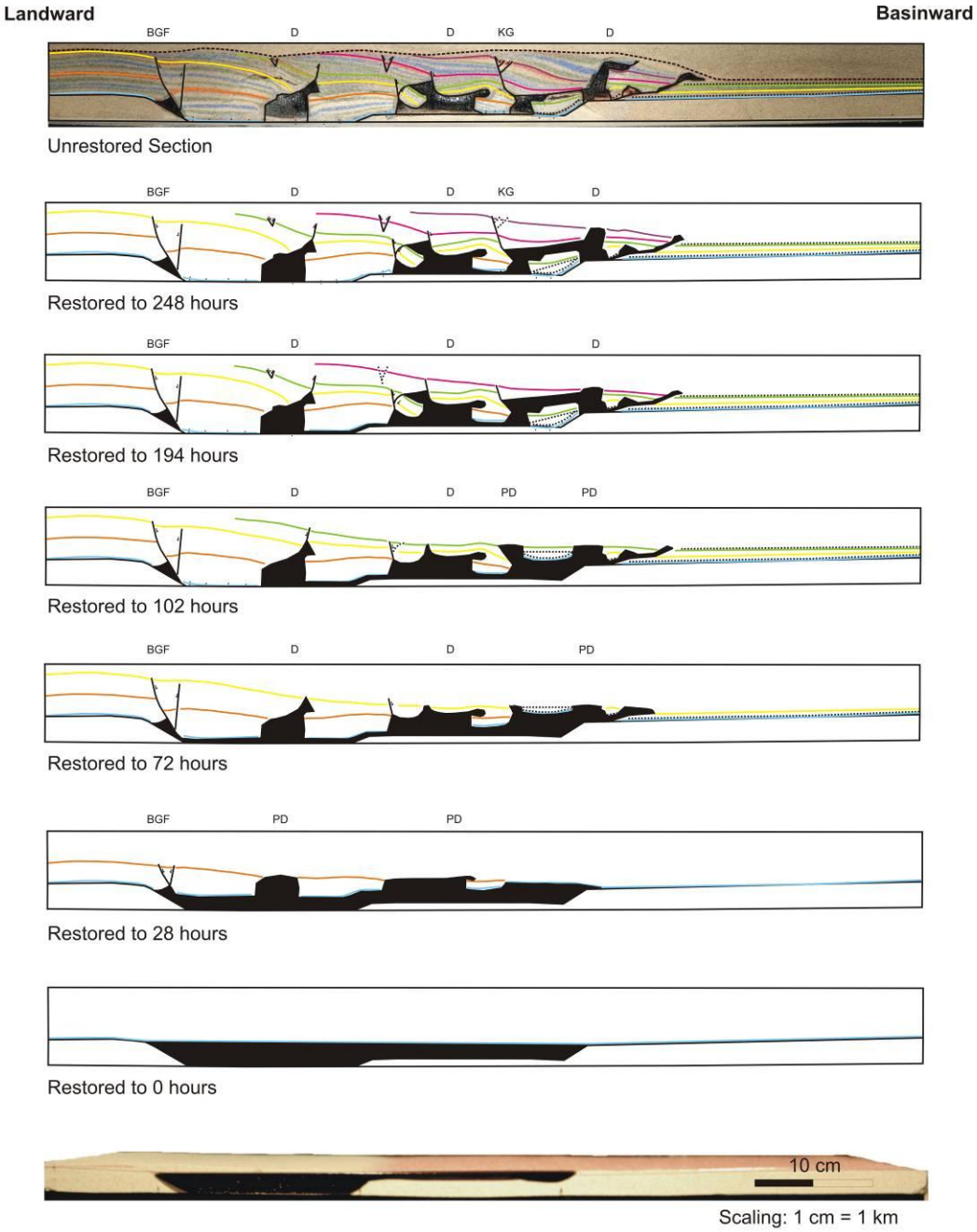
Landward
Basinward
BGF
D
D
KG
D
Unrestored Section
BGF
D
D
KG
D
Restored to 248 hours
BGF
D
D
D
Restored to 194 hours
BGF
D
D
PD
PD
Restored to 102 hours
BGF
D
D
PD
Restored to 72 hours
BGF
PD
PD
Restored to 28 hours
Restored to 0 hours
10 cm
Scaling: 1 cm = 1 km
Legend
Marker Horizon
Salt Weld
Sedimentation Break
Former Marker
Fault with Displacement Vector
Former Fault with Displacement
Salt

4.6 Symmetric Graben with Intermediate Horst Pilot Experiment

4.6.1 Overview

The evolution, interpretation and restoration for the pilot experiment 5-6; with the symmetric graben with intermediate horst basement morphology, are presented in figures 4-14, 4-16 and 4-17.

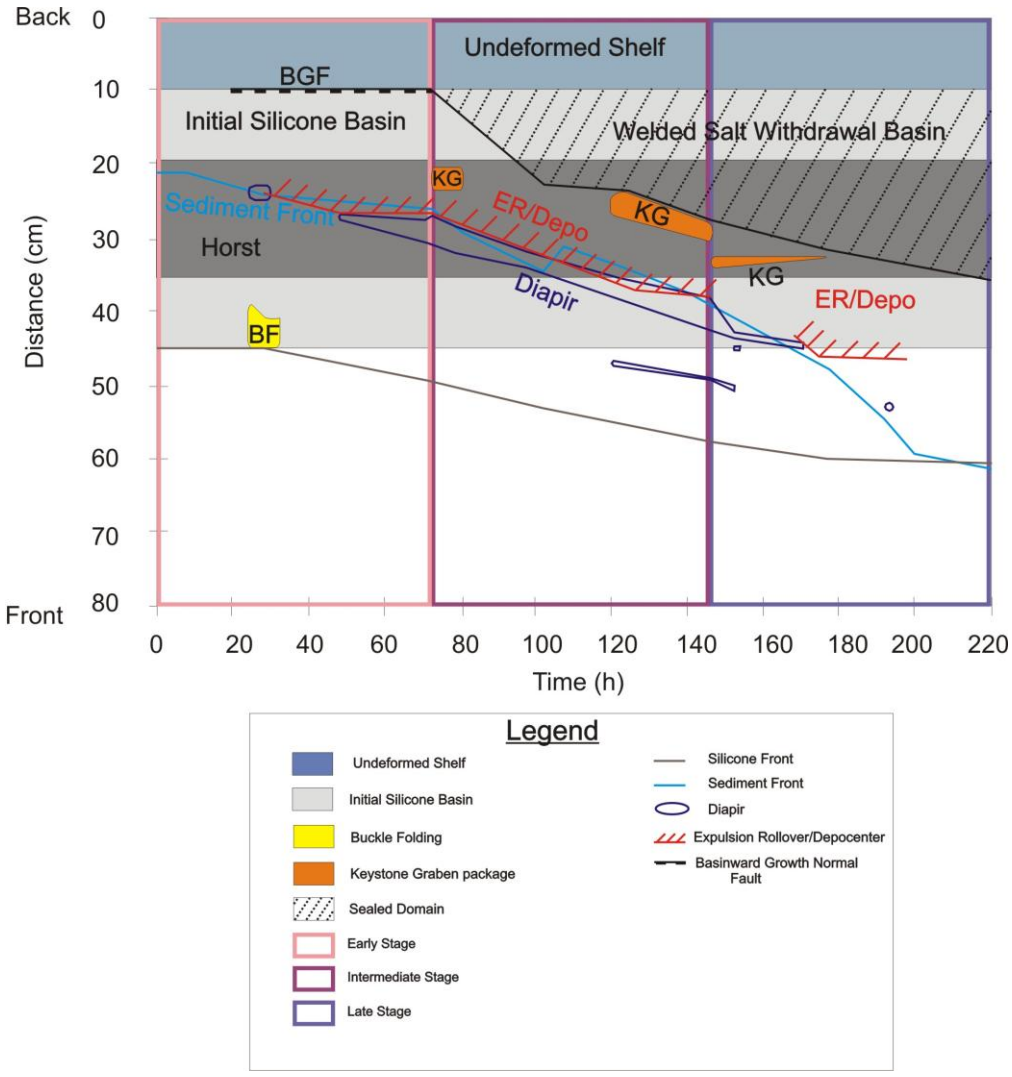

Figure 4-14: Schematic diagram of the symmetric graben with intermediate horst structural evolution with time. The diagram is centered on the central cross-section of the experiment while displaying the timing and position of structures as they appear. The front and back listed here are the basinward and landward limits of the experiment respectively.

From the landward to basinward limit there are four major elements, as presented in figure 4-16: 1) a former symmetrical graben silicone basin with a major basinward dipping growth normal fault “BGF” which is in contact with an intermediate horst, 2) a diapir “D” with a trapped salt massif flanked by an expulsion rollover and associated keystone grabens, 3) a major raft “R” and diapir/canopy “D” which is situated between the basinward limit of the intermediate horst and the basinward graben hangingwall, and 4) an allochthonous salt nappe province.

The diapir “D” became passive during the early stage (approximately 24 hours) and is now a trapped salt massif, which ranges greatly in position, extent and geometry. This diapir was connected to the raft “R” and diapir/canopy “D” early in the experiment and in some sections; sections 2.5 cm and 25.0 cm (Appendix B4), there is a canopy system still connecting the two domains. This diapir-diapir canopy system has also trapped significant rafted sedimentary packages in many areas. The translation in position of this diapir is evident via the extent of the major rollover/keystone graben system flanking its landward boundary, which began during the early stage (approximately 28 hours) of the experiment and ended in the late stage (approximately 146 hours). Horizontal displacement of this diapir is approximately 13.75 cm equating to 13.75 km in nature. The rolling of strata caused three sets of keystone graben systems, all which account for extension created by bending of the downbuilding overburden.

The major raft “R” and diapir/canopy “D” also varies in position, extent and geometry throughout the lateral sections of the experiment. At the lateral boundaries of the experiment (sections 2.5 cm and 27.5 cm, Appendix B4) there is a significant canopy

system which contributed to considerable lateral flow of passive silicone during the evolution of the experiment (figure 4-15).

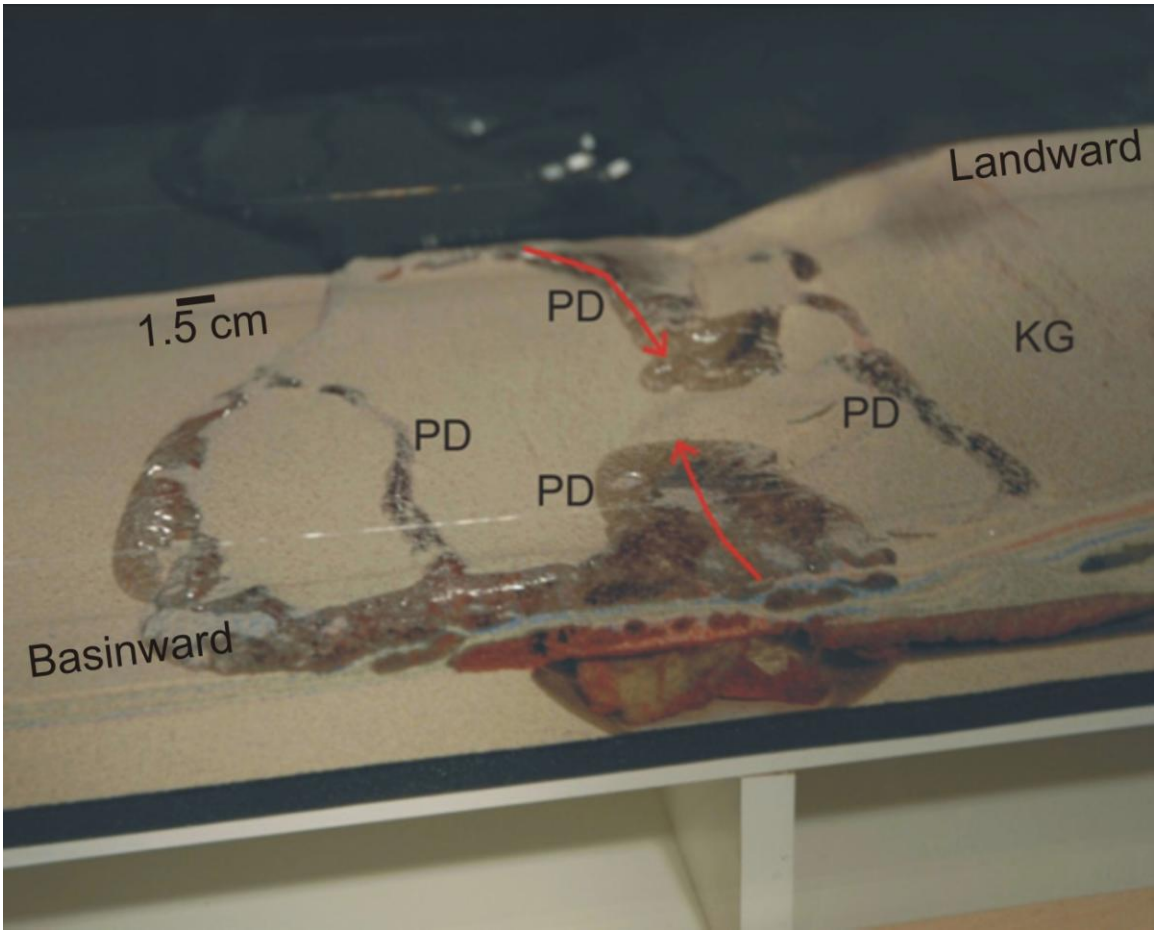

Figure 4-15: Picture showing direction of lateral flow of silicone in the raft and diapir/canopy province at time, 120 hours. Red arrows show the direction of passive silicone flow. PD: Passive diapir, KG: Keystone graben.

However, in some central sections (i.e. sections 17.5 cm and 20.0 cm, Appendix B4) this canopy system is not seen in cross-section at all. As a result, diapir structures which fed silicone to this canopy system also vary laterally in section with its max size being located at the experiment boundaries. In these areas the basinward limit of the initial silicone basin has provided such an effective barrier to flow that much of the silicone had become trapped as it could not flow fast enough to compete with overriding

sedimentation. In the central sections (sections 12.5 cm – 20.0 cm) of the experiment where there was less inflation of silicone, faster flow may have occurred as a significant amount of silicone is seen to have been evacuated efficiently to the allochthonous nappe system. In some cases however, much of this silicone is linked to the passive canopy system (section 15.0 cm, Appendix B4) showing the complicated nature of silicone mobilization associated with this setup. In most of the lateral sections a second basinward expulsion rollover "ER" system is associated with the diapir/canopy "D" system as sediments passive pushed underlying silicone forward. This rollover system initiated in the late stage (approximately 168 hours) of the experiment, ending at approximately 198 hours and gives a horizontal displacement of the diapir system of about 3.5 cm or 3.5 km in nature. The rafting evident in this area is complex and not coeval throughout all sections. The greatest displacement of the rafted sediments is seen in sections where inflated silicone is greatest and where the canopy system is more prevalent.

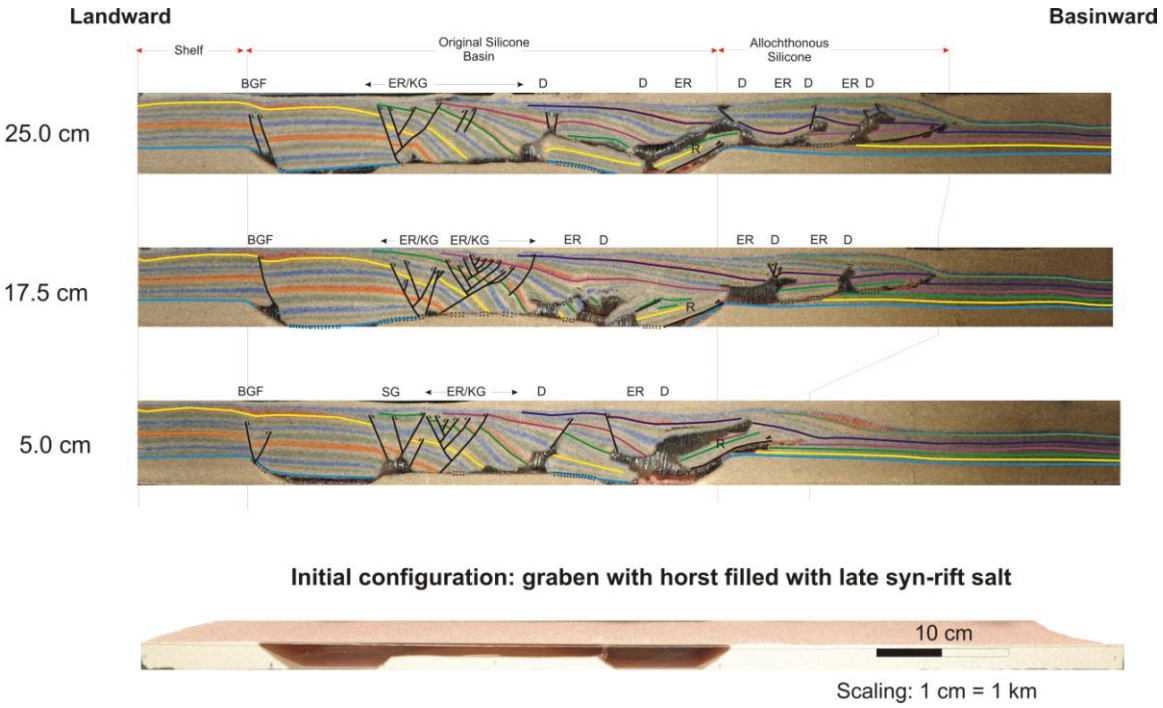

Figure 4-16: Cross sections of the symmetric graben with intermediate horst experiment. Sections detail lateral changes through the extent of the experimental base. BGF: Basinward dipping listric growth fault system. SG: Symmetric graben. ER/KG: Expulsion rollover/keystone graben. D: Diapir.

4.6.2 Structural Restoration

The structural restoration for experiment 5-6 is presented in fig. 4-17.

Restored to 28 hours

The first structure to form was the basinward dipping growth normal fault (BGF). Extension associated with this structure was accommodated by early basinward compression in the form of buckle folding. Downbuilding of the overburden into the silicone at the landward portion of the experiment created 0.93 cm of silicone inflation above the intermediate horst feature. With further deposition on this area strata had subsided and rolled enough to result in the expulsion rollover/keystone graben system "ER/KG1".

Restored to 72 hours

By this time (intermediate stage) the sedimentary package at the landward limit of the original silicone basin has become primarily welded to the basin floor. With this further evacuation silicone inflation over the intermediate horst has reached a vertical height of 1.67 cm. Sediments subsiding into this silicone massif resulted in another expulsion rollover/keystone graben system "ER/KG2. Rafted packages of sand "R" from the toe of the slope of the sedimentary wedge associated with this basinward evacuation of silicone are also seen to have been translated horizontally. The allochthonous silicone nappe is now present at the basinward limit of the experiment.

Restored to 102 hours

In this stage of the restoration it is apparent that the dominant process is basinward silicone evacuation. Passive diapirs "PD" are now becoming defined as sediments downbuild into the inflated silicone massif. The diapir "D" at the basinward margin of the original silicone basin is present though not yet passive. With the basinward basement low beyond the intermediate horst, silicone is flowing relatively un-hindered by the buttress present as the basinward margin of the original silicone basin. The rafted package "R" which was translated to its current location at the last time step is no longer being translated horizontally, but is subsiding vertically. This vertical displacement of rafted material agrees with the concept of poiseuille (channel) flow, where the horizontal velocity vectors at the base of the sediments are very small. With this increase in silicone evacuation the nappe has advanced 7.17 cm.

Restored to 146 hours

At this time primary welding of the sedimentary wedge has now advanced to over half the length of the intermediate horst. The passive diapirs seen in restored section: 102 hours are now overridden "D" with prograding sediments and have begun to undergo diapir fall. The rafted material "R" continues to only subside with little horizontal displacement. Silicone is still being evacuated under this rafted package and contributes to the passive diapir on the basinward margin of the original silicone basin. This is not the only source for silicone supply to the passive diapir however; as there is significant lateral flow from adjacent sections (sections 5.0 cm and 27.5 cm Appendix B4). This lateral flow of silicone causes discordant area above the typical 15% allowance for using 2D structural restoration techniques for extensional settings with salt influence. Therefore, the equal area of silicone was not kept when doing restored section: 102 hours. Another passive diapir "PD" is now present at the front of earlier deposited sediments, as they formed a minor buttress which hampered flow at the nappe front.

Restored to 176 hours

During this time step the first mid-basin diapir has become a remnant salt structure as it has undergone significant fall. There is also more rolling into the second mid-basin diapir as seen in the expulsion rollover "ER". The rafted material "R" continues to subside with little horizontal translation, and both diapirs "D" in the nappe system have been overridden with sediments. The nappe has reached its final position at this time and extends 15.46 cm past the basinward margin of the original silicone basin.

Restore to 220 hours

During this time very minor deformation happened as the system has already been shut down due to welding and very low salt thickness/sedimentation.

Unrestored Section

No further deformation has occurred at this time of the experiment as the system has already been shutdown.

Figure 4- 17: Structural restoration of section 17.5 cm in the symmetric graben with intermediate horst experiment; 5-6. BGF: Basinward dipping growth normal fault. ER/KG: Expulsion rollover/keystone graben. D: Diapir. PD: Passive Diapir. R: Raft. (Next page)

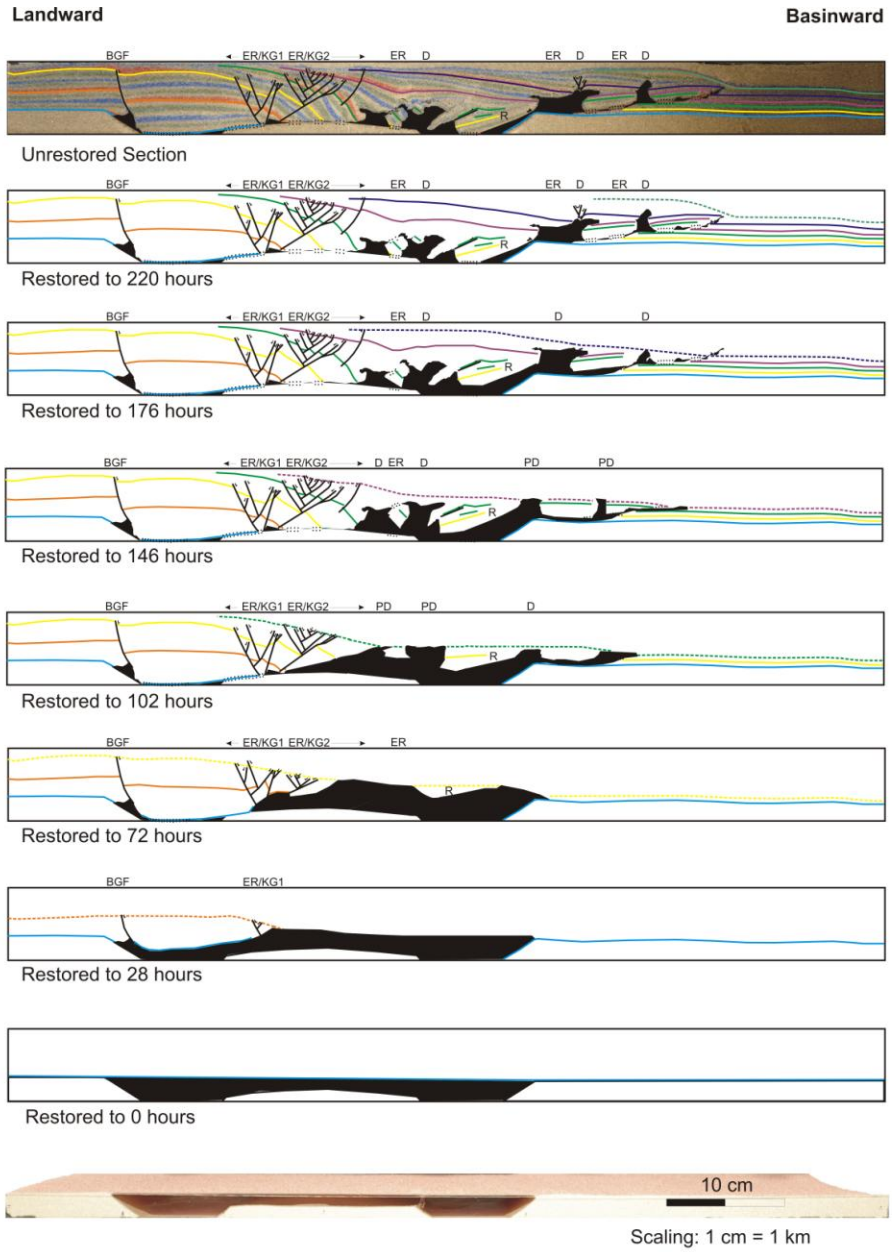
Landward
Basinward
BGF
ER/KG1 ER/KG2
ER
D
PD
R
Unrestored Section
Restored to 220 hours
Restored to 176 hours
Restored to 146 hours
Restored to 102 hours
Restored to 72 hours
Restored to 28 hours
Restored to 0 hours
10 cm
Scaling: 1 cm = 1 km

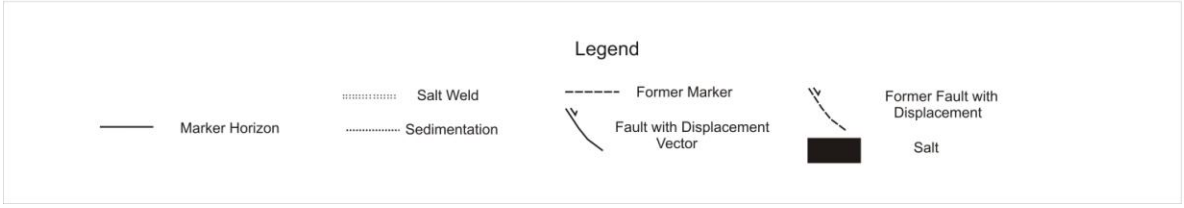
Legend
Marker Horizon
Salt Weld
Sedimentation
Former Marker
Fault with Displacement Vector
Former Fault with Displacement
Salt

4.7 Symmetric Graben Large Scale Experiment

4.7.1 Overview

An interpreted center section of the large scale experiment testing the symmetric graben basement morphology is presented in fig. 4-18.

Like all pilot experiments, it displays an early stage basinward dipping growth normal fault at the landward limit of the silicone basin "BGF". However, in the autochthonous region there are only expulsion rollovers "ER" and keystone grabens "KG" present as silicone was evacuated efficiently by downbuilding of the sedimentary wedge into the thick silicone layer. These structures indicate minor horizontal translation and that silicone flow was dominantly channel (Poiseuille) flow. Like the pilot experiment testing the symmetric graben setup, silicone was mobilized towards the basinward margin rapidly where it inflated as a large silicone massif. As a result, the most significant growth strata/expulsion rollover packages are found in this region. Unlike the pilot experiment, progradation continued until this expulsion rollover package of sand welded to the basement and as a consequence the inflated silicone eventually became overridden with sediments. A significant amount of silicone became trapped over the basinward rift shoulder, though there is an extensive but thin allochthonous nappe. Associated with this silicone nappe is a symmetric graben in the overburden as well as extensive buckle folding and block rotation of sand layers.

Figure 4-18: Central section of the large scale experiment testing symmetric graben basement morphology. BGF: Basinward growth normal fault. ER: Expulsion rollover. KG: Keystone graben. SG: Symmetric graben. (Next Page)

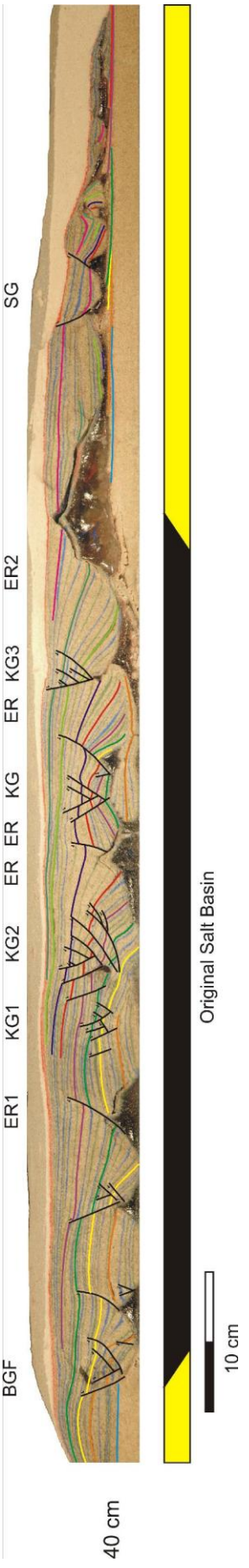
BGF
ER1
KG1
KG2
ER
ER
KG
ER
KG3
ER2
SG
Original Salt Basin
10 cm
40 cm

4.7.2 Symmetric Graben PIV Analysis

To quantify the relative timing and extent of interpreted structures in the central section, PIV data is used (Appendix C; fig. 4-19). Selected images are arranged to show the relationship of surface structure, incremental strain, incremental velocity and finite subsidence to the surface image. All structures are cross-identified with red lines. The lines are not all straight between images as time intervals are not exactly the same, but close enough to illustrate aspects of the structural evolution. Of particular note is the incremental velocity, which is uniform laterally. This proves that there is very little or no boundary affects from the lateral margins of the experimental salt basin.

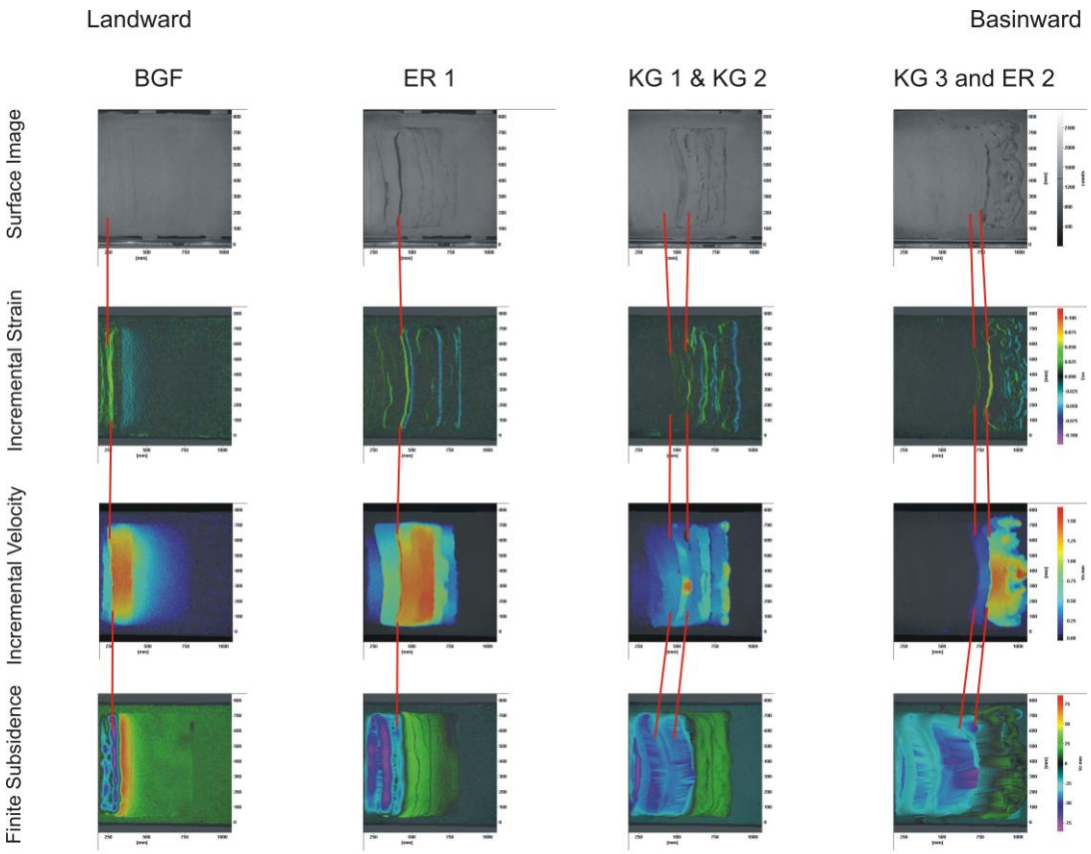

Figure 4-19: Select Particle Imaging Velocimetry (PIV) images showing structures with the surface image, incremental strain, incremental velocity and finite subsidence. Red lines connect structures between images.

Chapter 5: Conclusions

Three main conclusions can be drawn from the experiments with variable salt basin geometries:

1) The dominant mechanism for initial salt mobilization in rift basins with thick salt (2 km and greater) is channel flow within the salt layer (Poiseuille flow) driven by passive downbuilding of the landward salt withdrawal basins.

2) Initial landward mobilization and position of basinward salt inflation depends on mainly salt thickness controlled by the basin floor geometry, rather than the geometry of the basinward rift shoulder.

3) The timing and extent of allochthonous salt nappe advancement depends on the efficiency of early salt evacuation in the landward salt basin and sediment progradation on top of the inflated salt complex.

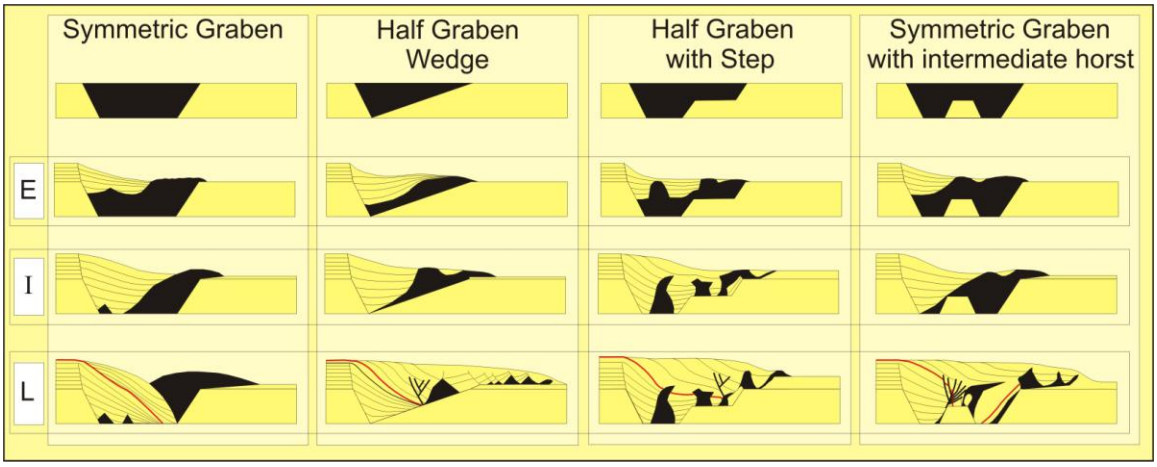

Figure 5-1: Overview of experiment evolution. E: Early stage, I: Intermediate stage, L: Late Stage. The red line in the late stage for all experiments marks the end of aggradation and the beginning of progradation.

In all experiments it is clear that salt mobilization in the landward part of the salt basin occurs during the early stage of development (stage E, fig. 5-1) as aggradation of sediments during the shelf build-up stage causes differential loading. Salt primarily undergoes channel flow during this stage, with most significant flow rates occurring in the middle of the salt layer (fig. 5-2). As a result of this channelized flow, the overburden directly overlying the area of the evacuated salt subsides with little horizontal translation or extension (absence of internal normal faulting). The downbuilding of salt withdrawal basins results in a basinward dipping growth normal fault at the landward margin of the original salt basin with associated growth strata that is active during the entire aggradation stage (stages E & I, fig. 5-1). When the base of salt withdrawal basins subside enough to form a weld to the basement (stage I, fig. 5-1) sediment progradation begins, and downbuilding and salt mobilization migrates further basinward onto the inflated salt massif. This process of salt evacuation and passive downbuilding repeats itself in all experiments until the salt has either been trapped in diapir structures or has been expelled from the initial salt basin to the allochthonous nappe system (stage L, fig. 5-1).

The style of initial salt withdrawal and the position of early salt inflation are strongly controlled by rift basin basement morphology. This primarily occurs as changes in topography cause variations in salt thickness and consequently alterations to the flow regime in the salt layer. It is found that the geometry of the basinward rift shoulder is not the principal factor in withdrawal efficiency, but the thickness of salt in proportion to basin floor geometry. With this understanding it can be stated in a regional framework that salt inflation and formation of allochthonous salt nappes is hindered with basin floor

morphologies that have gradational basinward margins tapering out in the basinward direction (half grabens) than rift basins with continuous salt thickness but steep rift shoulders (symmetrical graben). Although seemingly counter-intuitive this relationship can be easily expressed in fig. 5-2:

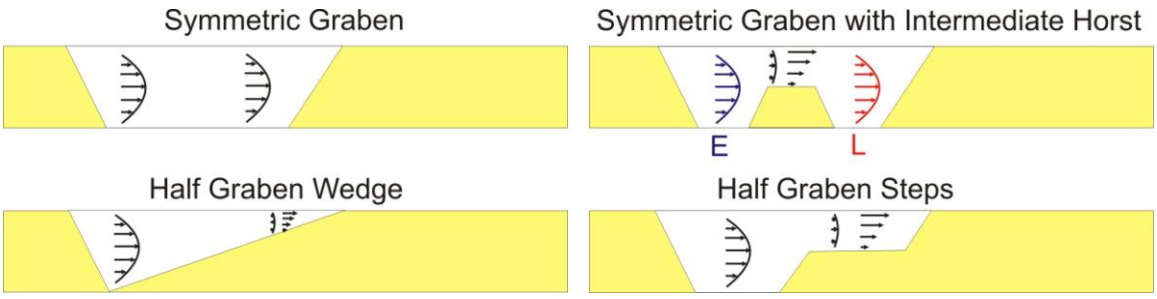

Figure 5-2: Relationship of salt flow regimes with basement (yellow) morphology. Initial salt (white) withdrawal is associated with poiseuille flow, whereas areas with low salt thickness show Couette flow or a combination of both. In the symmetric graben with an intermediate horst blue indicates early stage processes while red indicates late stage processes.

As seen in both symmetric graben setups, salt thickness at the landward and basinward limit of the original salt basin yield channel flow with large vectors. In the case of the symmetric graben, initial salt inflation occurs at the basinward limit with no intermittent impedance to flow. However, in the symmetric graben with an intermediate horst initial inflation occurs directly above the horst block (stage I, fig. 5-1), as salt thickness is decreased and therefore salt flow vectors are shorter. This development divides the rift basin into two sub-basins with individual evolution; early and late stage (E & L, fig. 5-2).

In contrast, both the half graben wedge and half graben step experiments differ from the symmetric graben experiments in that the basinward thinning of the original salt basin strongly slows down basinward salt inflation. In these experiments, the mobilized

salt prefers to inflate in the mid-basin (half graben wedge and half graben step) and landward areas (half graben steps) of the initial salt basin.

The importance of the efficiency of initial salt mobilization in the landward salt basin and position of early salt inflation in the autochthonous basinward area are revealed when quantifying the timing of allochthonous nappe emplacement. Both symmetric graben experiments with abrupt basinward rift shoulders evacuate salt to the basinward region earlier and more extensively than those with gradational limits. For the symmetric graben, early mobilization was most significant as salt was translated to the basinward margin very quickly. With further downbuilding and formation of expulsion rollovers into the inflated salt massif, flow was great enough to initiate an extensive nappe between early and intermediate stages (fig. 5-2). The symmetric graben with an intermediate horst reveals a similar evolution but lags slightly in timing of nappe emplacement. This is mainly a result of early inflation occurring over the horst block in the mid-basin area rather than continuous flow into the basinward sub-basin. On top of the horst there is strong mechanical coupling causing extensive domino style faulting and block rotation in the overlying sand "KG" (Appendix B4) indicating that there is an added component of Couette flow associated with low salt thickness and overburden translation. As salt from this area flows into the thick salt past the horst block and loading continues major inflation occurs at the basinward margin, indicating that Poiseuille flow becomes dominant once more (half graben with intermediate horst, stage I, fig. 5-1). Further loading of inflated salt by sediment progradation then evacuates salt into the nappe system very quickly and efficiently as seen in the experiment without the horst block.

In the experiments with half graben setups evacuation occurs later than those involving symmetric grabens; intermediate and late stage (stage I and L, fig. 5-1). In the case of the half graben wedge experiment major inflation remained focused in the mid basin area for most of the experiment duration (stages E & I). With dominantly basinward sediment progradation over the huge diapir, the nappe system began to form at the intermediate stage. As the sedimentary wedge prograded basinward, a symmetric expulsion rollover "ER" (Appendix B2) developed in both basinward and landward directions, as seen in growth strata and keystone grabens "KG" (Appendix B2). This forced an accelerated flow of salt in the diapir that rapidly moved into the allochthonous position, though trapping a significant amount in the basinward area. This is coeval with sediment progradation on top of the allochthonous salt nappe during late stage expulsion. The thin salt experienced high mechanical coupling and underwent extensive faulting in the asymmetric grabens with basinward listric growth faults and salt rollers indicating dominant Couette flow. In the experiment with half graben steps salt is trapped due to diapir formation in both the mid-basin and landward areas. With the sedimentary wedge advancing over the landward diapir much of the salt was trapped in this position. Expulsion rollover formation in the mid-basin position caused passive diapirism and salt evacuation over the step. However, decreasing salt thickness in the basinward region of the salt basin together with trapping salt in passive diapirs had major implications on the size and emplacement of the salt nappe system. Most evacuated salt inflated over this high instead of flowing basinward (stage I, fig. 5-1). Later with more loading, the inflated salt in this area was mobilized again.

Chapter 6: Discussion

Numerous structures observed in seismic data Offshore Nova Scotia infer the former presence of thick salt which was initially mobilized by mechanisms similar to those observed in the experiments. At the landward portion of the central Scotian Basin there are regional scale basinward dipping growth normal faults hanging wall strata that is relatively undeformed (fig. 6-1).

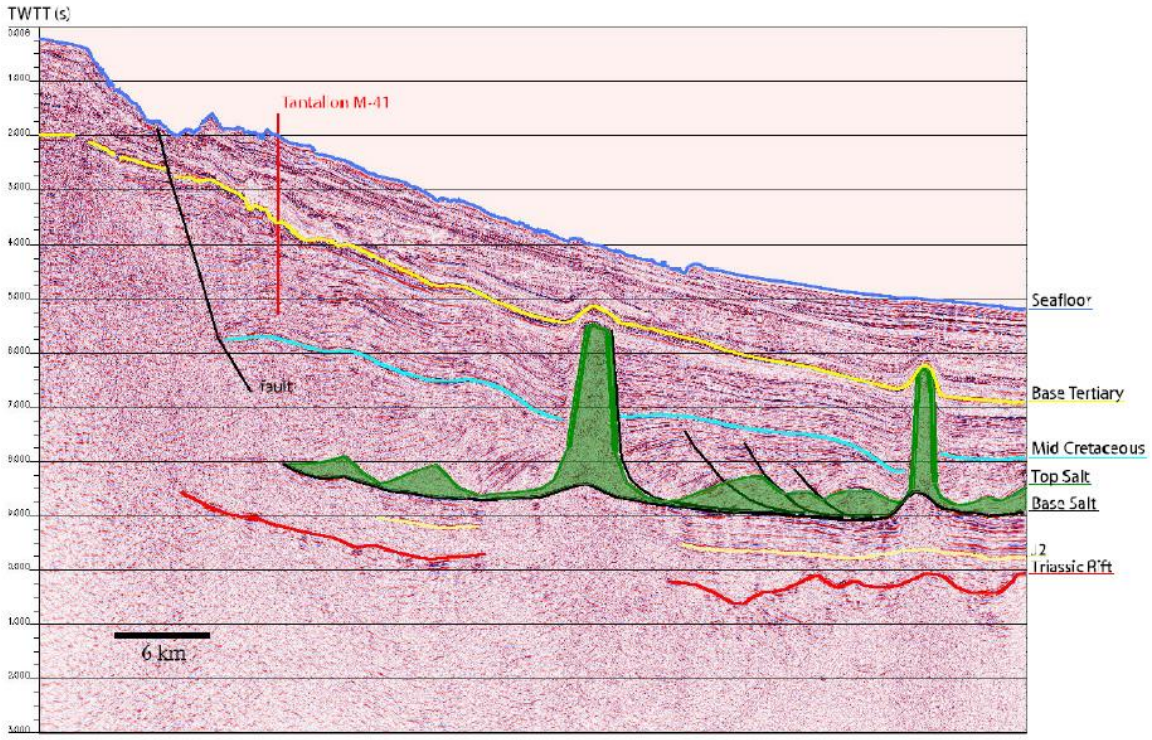

Figure 6-1: Seismic section showing typical salt structures present in the landward portion of the Scotian Margin. (Kidston et al., 2002)

As in the experiments, this indicates passive downbuilding of sediments during initial salt mobilization in the basin. Close to the shelf, little horizontal extension had occurred resulting in the lack of major faulting. There are also diapirs in the landward portion of the basin effectively rafting packages of sediments. Diapirs in this area

correlate with similar structures observed in the experiment testing the half graben steps basement floor geometry. This may indicate that there was early impedance to salt flow due to a structural high, with overlying thin salt causing a low flow velocity zone.

With the degree of variability of salt structures present between salt subprovinces III and IV it is inferred that the basement morphology is complex in this region, even in this regionally small scale. In Subprovince III, which includes the Sable Subbasin, there are major differences in salt structures between the eastern and western regions. Most notable is the presence or lack of feeders to the allochthonous tongue canopy systems (fig. 6-2). In the western region there are multiple feeders present, whereas in the eastern region there are none. In the eastern region however, there is a salt nappe which extends up to 100 km seaward.

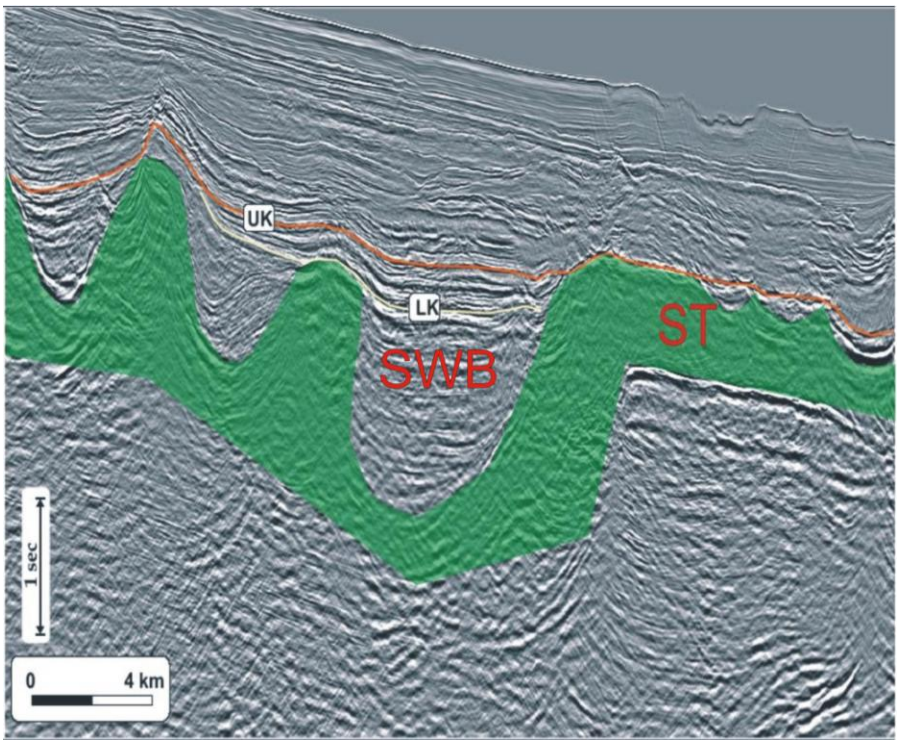

Figure 6-2: Allochthonous tongue canopy system as seen in Subprovince III. ST: Salt tongue. SWB: Salt Withdrawal Basin. Green fill: Salt. (Modified from Shimeld, 2004)

The difference between structural styles may be an indicator of salt thickness variations due to rift basin morphology. The western portion with extensive feeders and tongue canopy systems resembles the experiment testing the half graben wedge with a gradual termination seaward of the salt basin and multiple small abrupt variations in salt thickness. In the eastern portion the lack of feeders indicates that there was possibly a more continuous, thick salt layer with an abrupt basinward rift shoulder termination. The experiment testing the symmetric graben with an intermediate horst may be analogous to this area, with the sable high having the same effect on salt flow as the experimental horst block.

In Subprovince IV there are relatively little salt structures in proximity to the shelf and Subprovince III, as salt is further outboard than other areas. However, closer to Subprovince V is the deformed sedimentary package known as the Banquereau Wedge. At the termination of this structure is a thrusted package of sediments characterized by landward dipping reflectors (fig. 6-3).

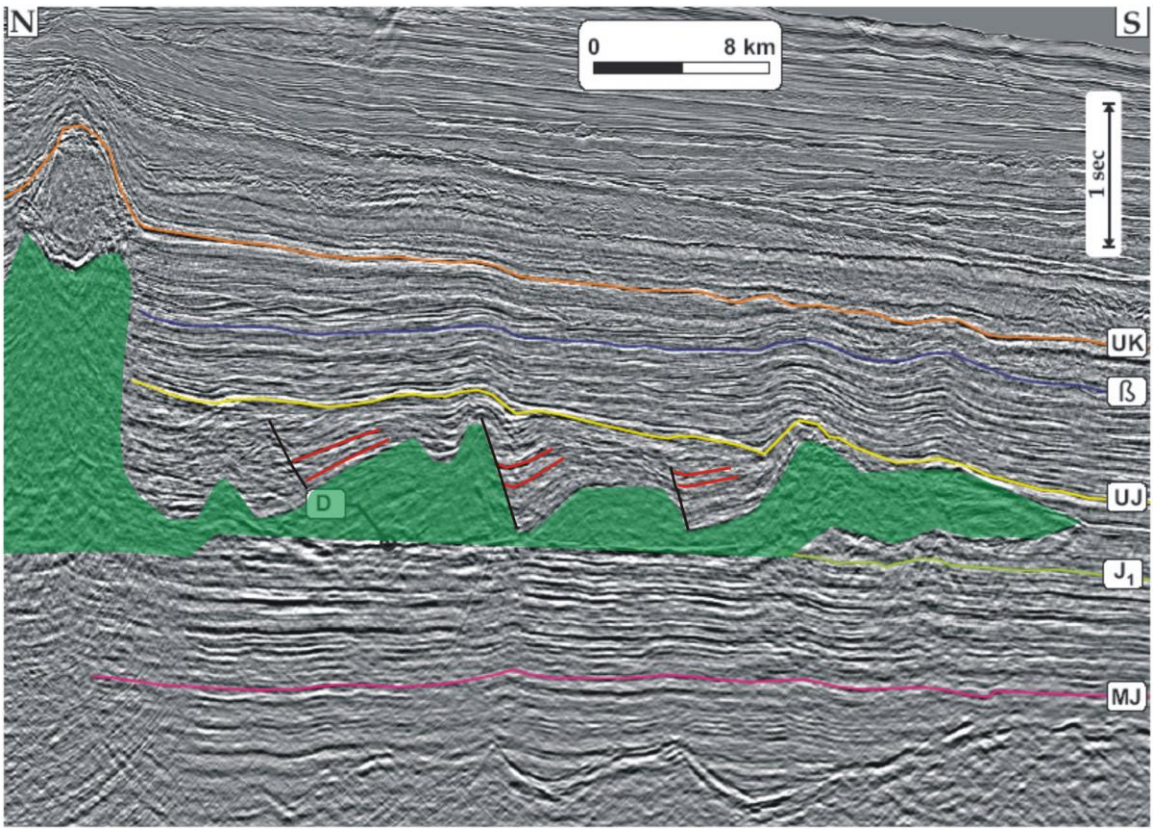

Fig. 6-3: Interpreted structures in the thrusted portion of the Banquereau Wedge. Black lines: basinward dipping faults. Red lines: landward dipping reflectors. Green fill: Salt. (Modified from Shimeld, 2004)

In the relatively undeformed region of Subprovince IV it is apparent that salt has been evacuated very efficiently. This withdrawal is seen in the symmetric graben experiment, where salt had a continuous thickness in the basin until abruptly thinning out on the basinward rift shoulder. Flow of the salt in this setting continued seaward with little or no impedance until meeting this basinward limit where it inflates and is later evacuated from the basin with loading from prograding sediments. The Banquereau Wedge overlying an allochthonous salt detachment is a sedimentary package that is analogous to the faulted overburden with basinward listric growth faults “BLS” in the half graben wedge experiment (Appendix B2). This feature is often called a Roho structure and is typical of rapid shear flow of thin salt into the allochthonous position.

This structural style is good evidence that the basinward termination becomes more gradual in this area and that most evacuation occurred during late stage development.

All of these hypotheses are first order and are mainly discussions about salt thickness in relation to basement topography. However, with the inspection of more seismic data it will be possible to apply these structural concepts to refine the variable basement structures present in the Scotian Margin. With an understanding of the salt tectonics evolution based on the differences in timing of deformation it will also be possible to better understand reservoir development, migration systems and potential plays for hydrocarbons. Therefore, future projects will be continued within the Salt Dynamics Group at Dalhousie University which will focus more on the interpretation of available seismic data, while still improving and testing current ideas. In these future projects there will be more PIV monitored experiments as the pilot experiments have given insights into first order affects of basement morphology.

References

Adam, J., Shimeld, J., Krezsek, C., and Grujic, D., 2006. How Sedimentation Controls Structural Evolution and Reservoir Distribution in Salt Basins. Nova Scotia's Energy Research and Development Forum, May 24-25, 2006, Antigonish, Canada (on CD).

Adam, J., Urai, J.L., Wieneke, B., Oncken, O., Pfeiffer, K., Kukowski, N., Lohrmann, J., Hoth, S., Van der Zee, W., and Schmatz, J., 2005. Shear localisation and strain distribution during tectonic faulting--new insights from granular-flow experiments and high-resolution optical image correlation techniques. *Journal of Structural Geology* 27, 283–301.

Bally, A.W., 1981. Thoughts on the tectonics of folded belts., in McClay, K.R., and Price., N.J. eds., Thrusting and Nappe Tectonics. *Spec. Publs geol. Soc. Lond. 9:*13-32

Barton, D.C., 1933. Mechanics of formation of salt domes with special reference to Gulf Coast salt domes of Texas and Louisiana. *Bull. Am. Ass. Petrol. Geol. 17:*1025-1083

Bates, R.L., and Jackson, J.A., 1987, Glossary of geology, 3rd ed.: Alexandria, Virginia, American Geological Institute, p. 788

Costa, E., and Vendeville, B.C. 2002. Experimental insights on the geometry and kinematics of fold-and-thrust belts above weak, viscous evaporitic decollement. *Journal of Struc. Geol.* 24, 1729-1739

Coward, M.P., and Stewart, S., 1995. Salt-influenced structures in the Mesozoic-Tertiary cover of the southern North Sea, U.K., in Jackson, M.P.A., Roberts, D.G., and Snelson, S., eds., Salt Tectonics: a global perspective. *AAPG Memoir 65:* 229-250.

Enachescu, M. and Wach, G., 2005. Exploration Offshore Nova Scotia: Quo Vadis? *ocean-resources: 23-35*.

Fort, X., and J. P. Brun, et al., 2004. Salt tectonics on the Angolan margin, synsedimentary deformation processes. *AAPG Bulletin 88(11):* 1523-1544.

Ge, H., Jackson, M.P.A., and Vendeville, B.C., 1997. Kinematics and dynamics of salt tectonics driven by progradation. *AAPG Bulletin 81*(3), 398-423.

Gemmer, L., C. Beaumont, et al. (2005). Dynamic modelling of passive margin salt tectonics: effects of water loading, sediment properties and sedimentation patterns. *Basin Research 17: 382-402, doi: 10.1111/j.1365-2117.2005.00274.x.*

Harrison, J.C., and Bally., A.W., 1988. Cross-section of the Parry Islands fold belt on Melville Island, Candian Arctic Islands: implications for the timing and kinematic history of some thin-skinned décollement systems. *Bull. Can. Petrol. Geol. 36:* 311-332.

Haq, B.U., Hardenbol, J. and Vail, P.R., 1987. Chronology of Fluctuating Sea Levels Since the Triassic. *Science*, Vol.235, p.1156-1167.

Hubbert, M.K., 1937. Theory of scale models as applied to the study of geologic structures" *Geological Society of America Bulletin* 48(10), 1459-1519.

Ings ,S.J., and Shimeld, J.W., 2006. Structural evolution of a regional salt detachment on the northeast Scotian Margin, offshore eastern Canada: A new conceptual model. *Bull. Am. Ass. Petrol. Geol.*

Jackson, M.P.A., 1995. Retrospective salt tectonics, in M.P.A. Jackson, Roberts, D.G., and Snelson, S. eds., Salt Tectonics: a global perspective. *AAPG Memoir 65:* 1-28.

Jackson, M.P.A., and Vendeville, B.C., 1994. Regional extension as a geologic trigger for diapirism. *Geological Society of America Bulletin*, Vol. 106: 57-73

Jackson, M.P.A. and Talbot, C.J. 1991. A Glossary of salt tectonics: The University of Texas at Austin, Bureau of Economic Geology Geological Circular, No. 91-4, p. 44

Jackson, M.P.A., and Talbot, C.J., 1986. External shapes, strain rates, and dynamics of salt structures: *Geological Society of America Bulletin*, v. 97, p. 305-328

Jansa, L.F., and Wade, J.A., 1975. Geology of the continental margin off Nova Scotia and Newfoundland. In: W.J.M. van der Linden, J.A. Wade (eds.): *Offshore geology of Eastern Canada*, Vol. 2, Regional geology: Geological Survey of Canada, Paper 74-30, 51-106.

Kidston, A.G., Brown, D.E., Altheim B., and Smith B.M., 2002. Hydrocarbon Potential of the Deep-water Scotian Slope, Canada-Nova Scotia Offshore Petroleum Board, Open Report, 111 p.

Kidston, A.G., Brown, D.E., Altheim B., and Smith B.M., 2002. Hydrocarbon Potential of the Deep-water Scotian Slope, Canada-Nova Scotia Offshore Petroleum Board, Open Report, 111

Krezsek, Cs., Adam, J., Grujic, D., 2006a. Mechanics of Fault and Expulsion Rollover Systems Developed on Passive Margins Detached on Salt: Insights from Analogue Modelling and Optical Strain Monitoring. *Geological Society of London Special Publication.* (In Press)

Krezsek, Cs., Adam J., Grujic, D., 2006b. Structural Evolution Driven by Sedimentation: Experimental Insight in the Kinematics and Growth Fault/Rollover Systems.

Lohrmann, J., Kukowski, N., Adam, J., and Oncken, O., 2003. The impact of analogue material parameters on the geometry, kinematics, and dynamics of convergent sand wedges. *J. Struc. Geol.* 25(10), 1691-1711.

Mauduit, T. and Brun, J.P., 1998. Growth fault/rollover systems: Birth, growth, and decay. *Journal of Geophysical Research*. Vol. 103, No. B8, p. 18, 119-18, 136, August 10, 1998

Nettleton, L.L, and Elkins, T.A., 1947. Geologic models made from granular materials: *American Geophysics Union Transactions*. v. 28, p. 451-466

Nettleton, L.L., 1934. Fluid mechanics of salt domes. Bull. Am. Ass. Petrol. Geol.
Vol.18, 1175-1204

Palmer, A.R. and Geissman, J., 1999. Geologic Time Scale. Geological Society of America Website: http://www.geosociety.org/science/timescale/timescl.htm

Peel, F. J., C. J. Travis, et al. (1995). Genetic Structural Provinces and Salt Tectonics of the Cenozoic Offshore U.S. Gulf of Mexico: A Preliminary Analysis. *Salt tectonics: a global perspective: AAPG Memoir*. In M. P. A. Jackson, D. G. Roberts and S. Snelson, *AAPG*. 65: 153-175.

Rowan, M.G., 2005. Salt Tectonics and Sedimentation: A Structual and Sedimentary Framework for Petroleum Systems in Salt Basins.

Schultz-Ela, D.D., and Jackson, M.P.A., 1996. Relation of subsalt structures to suprasalt structures during extension. *AAPG Bulletin*, Vol. 80: 1896-1924.

Shimeld, J.W., 2004. A comparison of salt tectonic sub-provinces beneath the Scotian Slope and Laurentian Fan. In: P.J. Post, D.L. Olson, K.T. Lyons, S.L. Palmes, P.F. Harrison, N.C. Rosen (eds.): *Salt-sediment interactions and hydrocarbon prospectivity: Concepts, applications and case studies for the 21st century*, 24th Annual GCSSEPM Foundation Bob F. Perkins Research Conference proceedings, 291-306. (On CD Rom - ISSN: 1544-2462).

Stonely, R., 1981. Petroleum: the sedimentary basin. Economic Geology and Geotectonics. p. 51-71

Truscheim, F., 1960. Mechanism of salt mobilization in northern Germany. *Bull. Am. Ass. Petrol. Geol. 44:*1519-1540.

Twiss, R.J., and E.M. Moores. 2007. Structural Geology 2nd edition. New York: W.H. Freeman and Company.

Twiss, R.J., and E.M. Moores. 1992. Structural Geology. New York: W.H. Freeman and Company.

Vendeville, B.C and Cobbold, P.R., 1988. How normal faulting and sedimentation interact to produce listric fault profiles and stratigraphic wedges. *J. Struc. Geol.* 10, 649-659.

Vendeville, B.C., and Jackson, M.P.A., 1993. Rates of extension and deposition determine whether growth faults or salt diapirs form, in Armentrout, J.M., Bloch, R., Olson, H.C., and Perkins, B.F., eds. Rates of Geological Processes: Fourteenth Annual Research Conference, Gulf Coast Section, SEPM Foundation, Program with Papers, p. 263-268

Vendeville, B.C., Jackson, M.P.A., 1992. The fall of diapirs during thin-skinned extension. *Marine and Petroleum Geology* 9(4), 354-371.

Wade, J.A., MacLean, B.C., and Williams, G.L., 1995. Mesozoic and Cenozoic stratigraphy, eastern Scotian Shelf: new interpretations. *Canadian Journal of Earth Sciences*, Vol.32, No.9, p.1462-1473.

Wade, J. A. and B. C. MacLean., 1990. The geology of the southeastern margin of Canada. *Geology of the Continental Margin of Eastern Canada*. In: M. J. Keen and G. L. Williams (editors). Geological Survey of Canada. *Geology of Canada*, no 2 (also Geological Society of America, *the Geology of North America*, vI-1), p. 167-238.

Weijermars, R., Jackson, M.P.A., and Vendeville, B., 1993. Rheological and tectonic modelling of salt provinces. *Tectonophysics* 217(1-2), 143-174.

APPENDIX A: TIME SERIES IMAGES

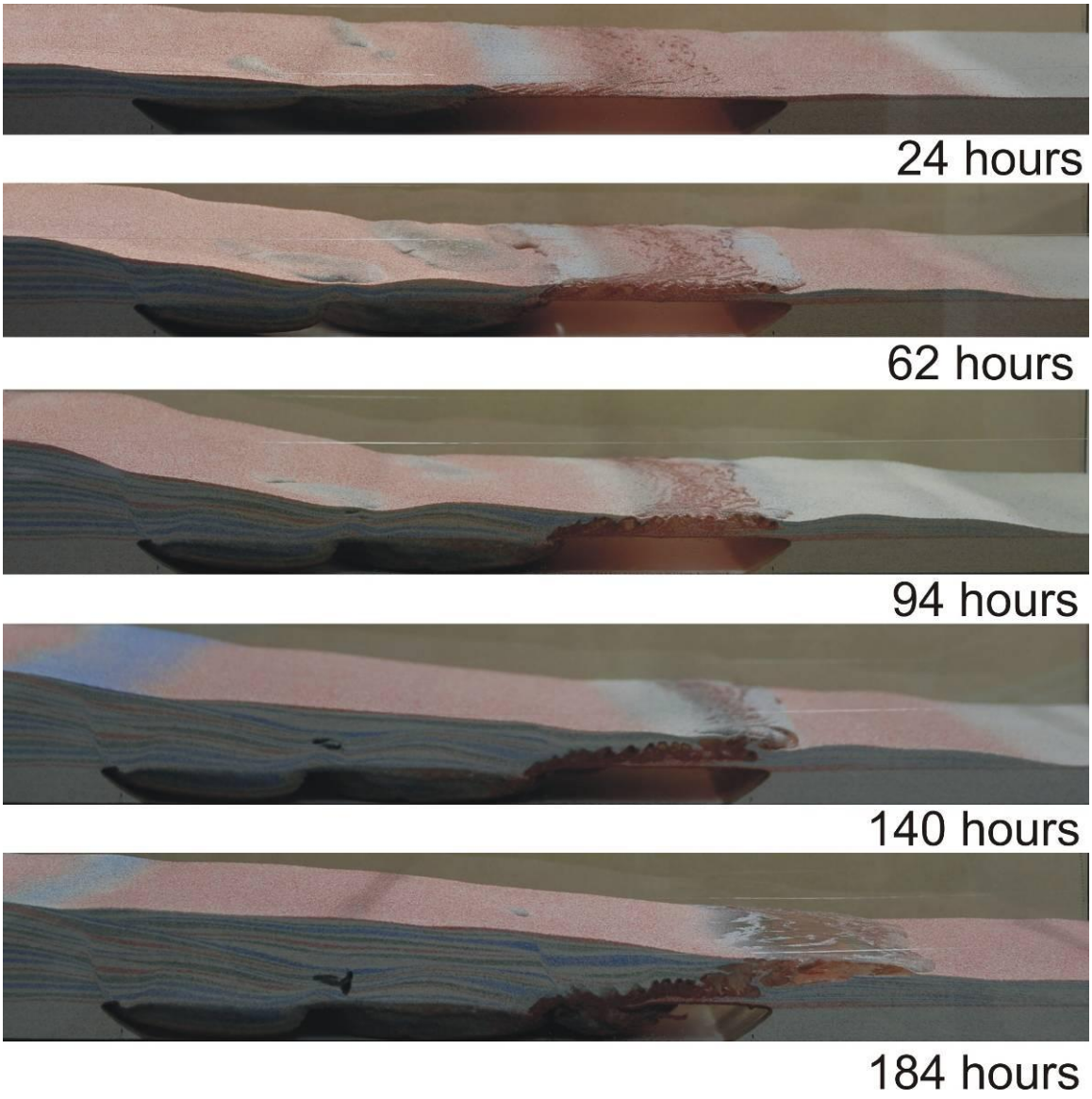

Appendix A1: Select time series images of the experiment testing the symmetric graben basement morphology.

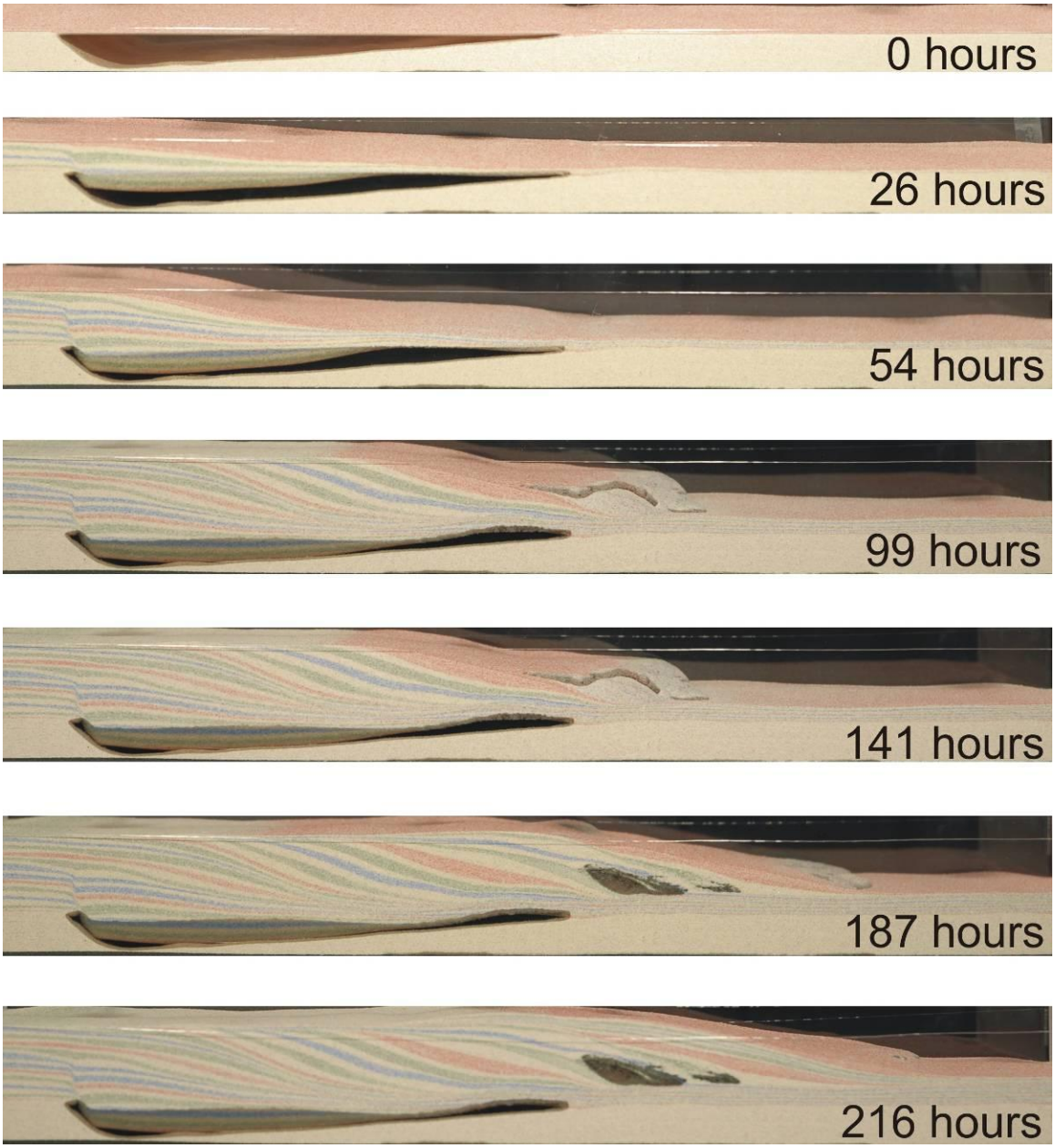

Appendix A2: Select time series images testing the half graben wedge experiment basement morphology.

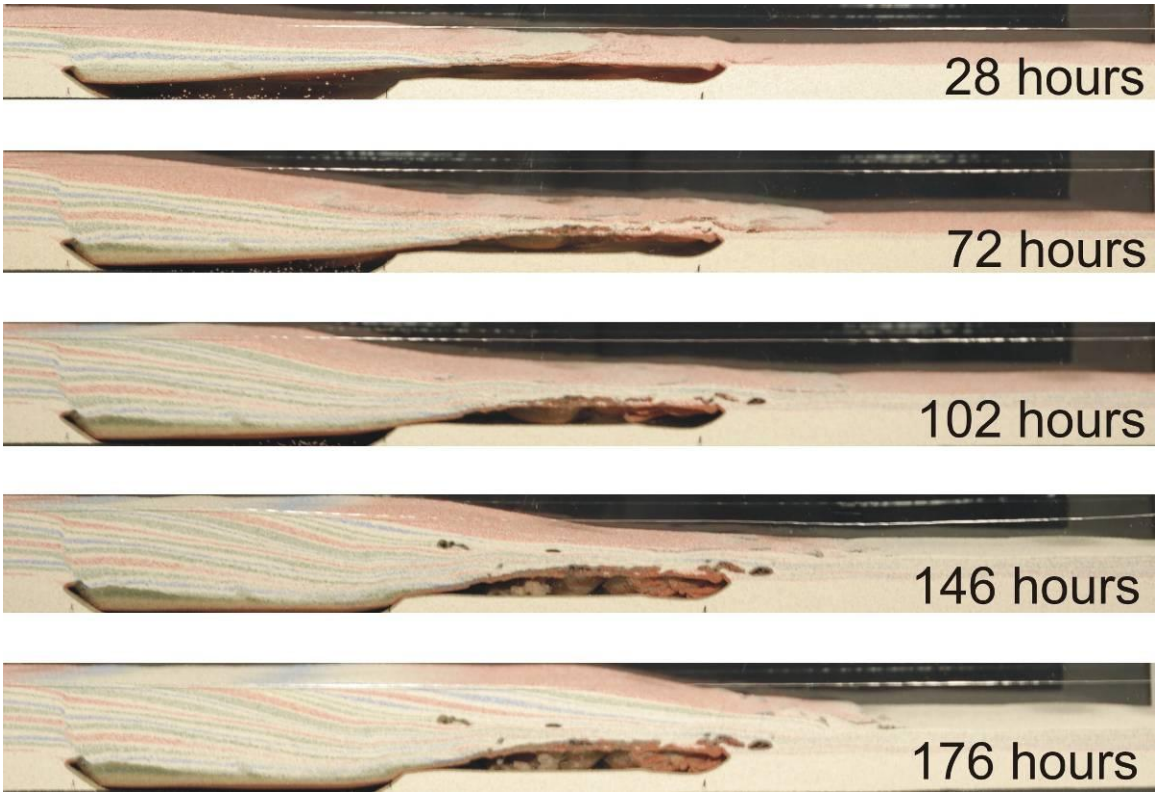

Appendix A3: Select time series images testing the half graben steps basement morphology.

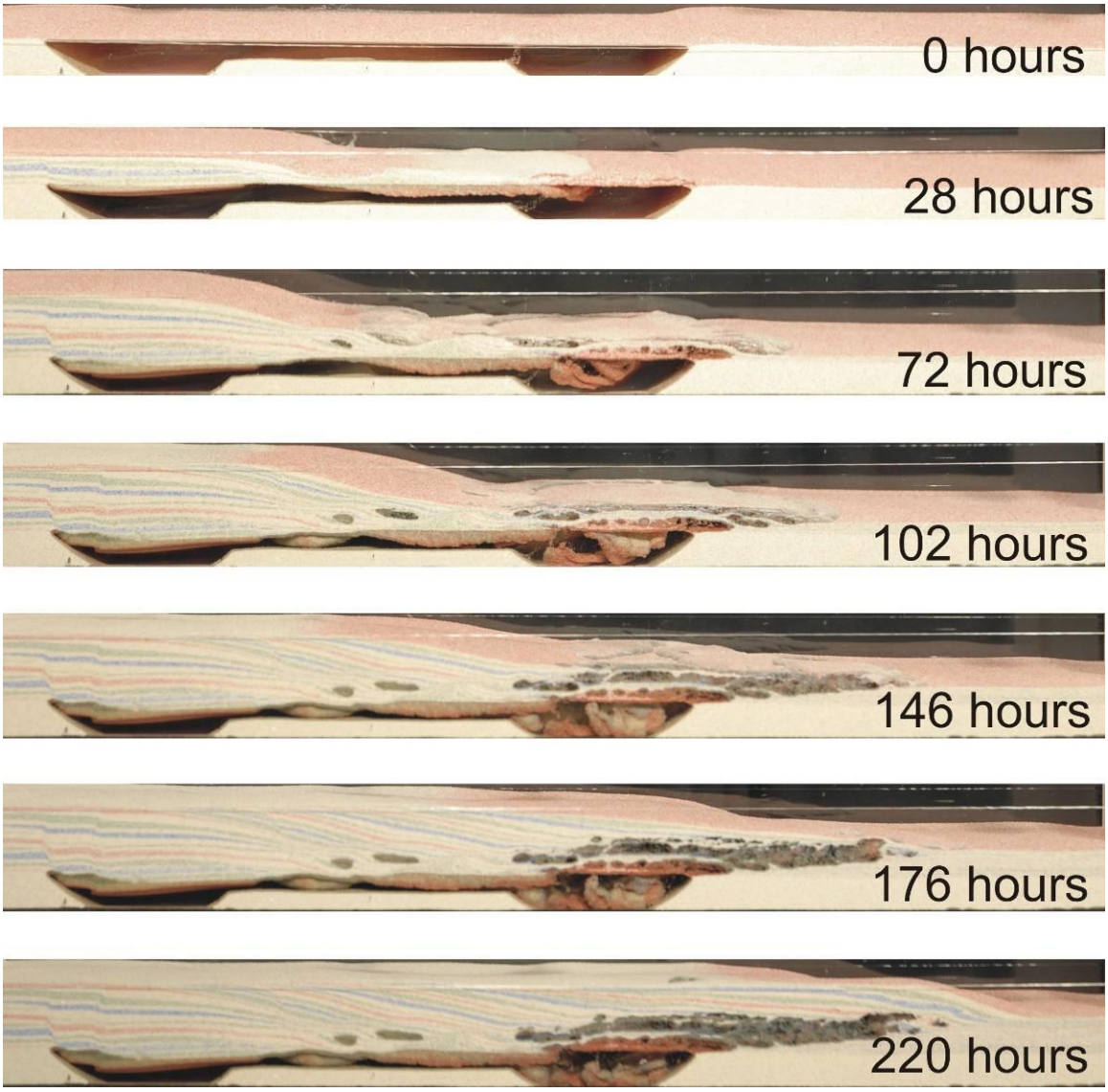

Appendix A4: Select time series images testing the symmetric graben with intermediate horst basement morphology.

APPENDIX B: COMPLETE INTERPRETATIONS OF EXPERIMENTS

Appendix B1: Cross-sections of the symmetric graben experiment. Sections detail lateral changes through the extent of the experiment base. BGF: Basinward dipping growth normal fault. ER: Expulsion rollover. D: Diapir. KG: Keystone graben. (Next Page)

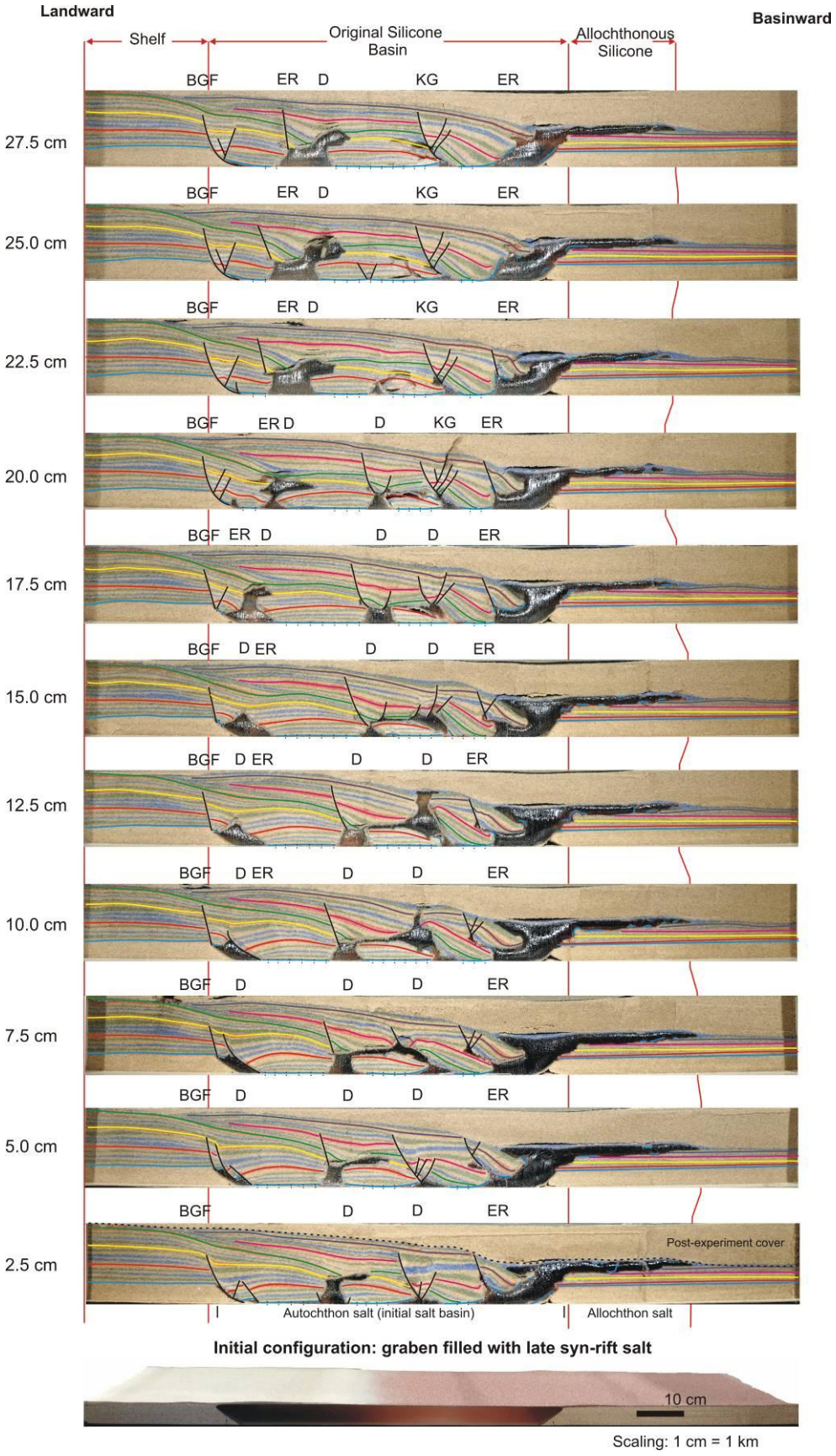
Landward
Basinward
Shelf
Original Silicone Basin
Allochthonous Silicone
BGF ER D KG ER
27.5 cm
25.0 cm
22.5 cm
20.0 cm
17.5 cm
15.0 cm
12.5 cm
10.0 cm
7.5 cm
5.0 cm
2.5 cm
Post-experiment cover
Autochthon salt (initial salt basin)
Allochthon salt
Initial configuration: graben filled with late syn-rift salt
10 cm
Scaling: 1 cm = 1 km

Appendix B2: Sections of the half graben wedge experiment. Sections detail lateral changes through the extent of the experiment base. BGF: Basinward dipping growth normal fault system. BLS: Basinward listric growth fault system. ER/KG: Expulsion rollover/keystone graben. D: Diapir. GFR: Growth fault rollover. R: Raft. (Next Page)

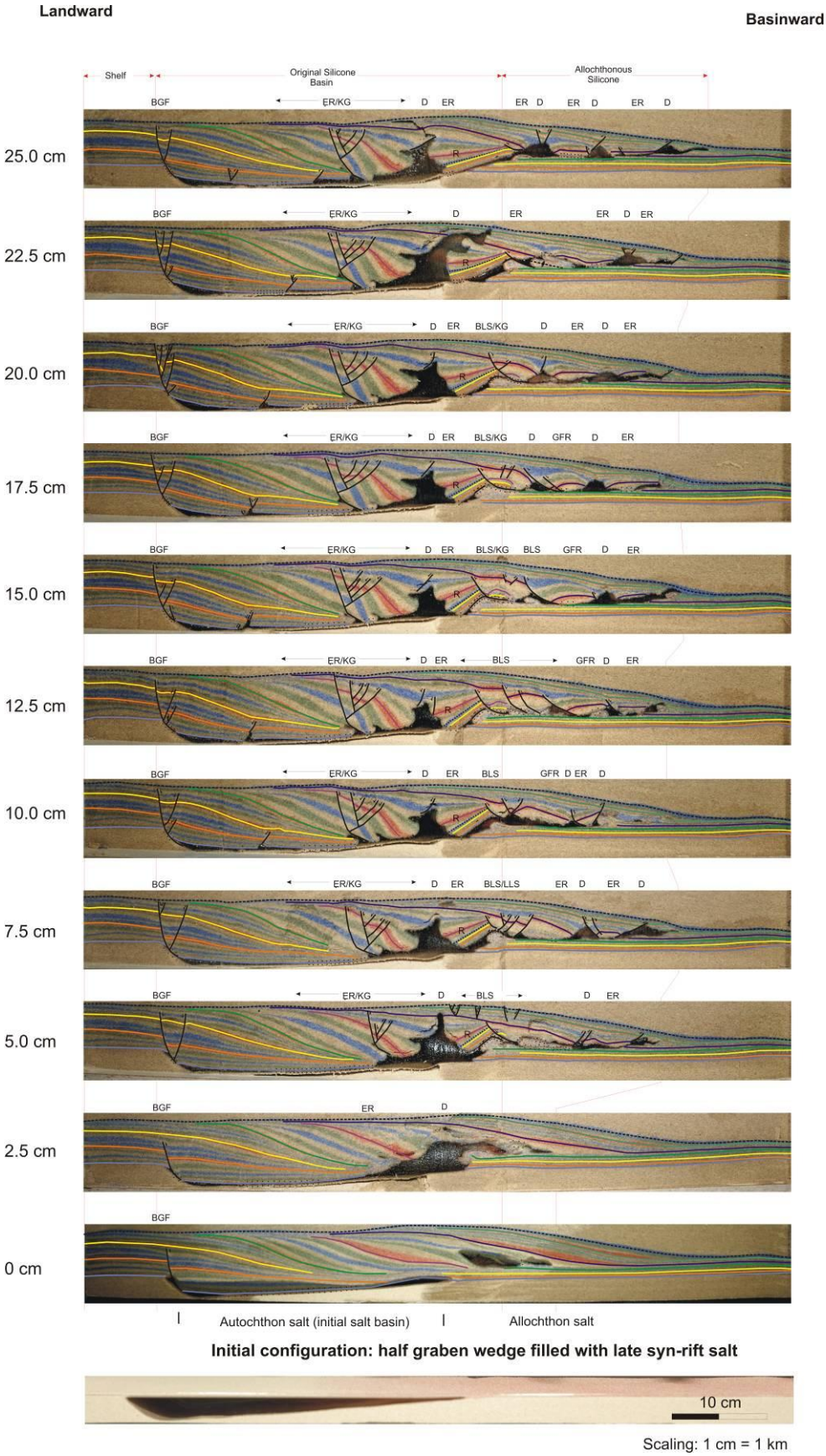
Landward
Basinward
Shelf
Original Silicone Basin
Allochthonous Silicone
25.0 cm
22.5 cm
20.0 cm
17.5 cm
15.0 cm
12.5 cm
10.0 cm
7.5 cm
5.0 cm
2.5 cm
0 cm
BGF
ER/KG
D
ER
BLS/KG
BLS
BLS/LLS
GFR
R
Autochthon salt (initial salt basin)
Allochthon salt
Initial configuration: half graben wedge filled with late syn-rift salt
10 cm
Scaling: 1 cm = 1 km

Appendix B3: Cross-sections of the half graben step experiment. Sections show lateral variability throughout the extent of the experiment base. BLS: Basinward dipping listric growth fault system. ER/KG: Expulsion rollover/keystone graben. D: Diapir. PD: Passive diapir. N: Nappe. ST: Salt tongue. (Next Page)

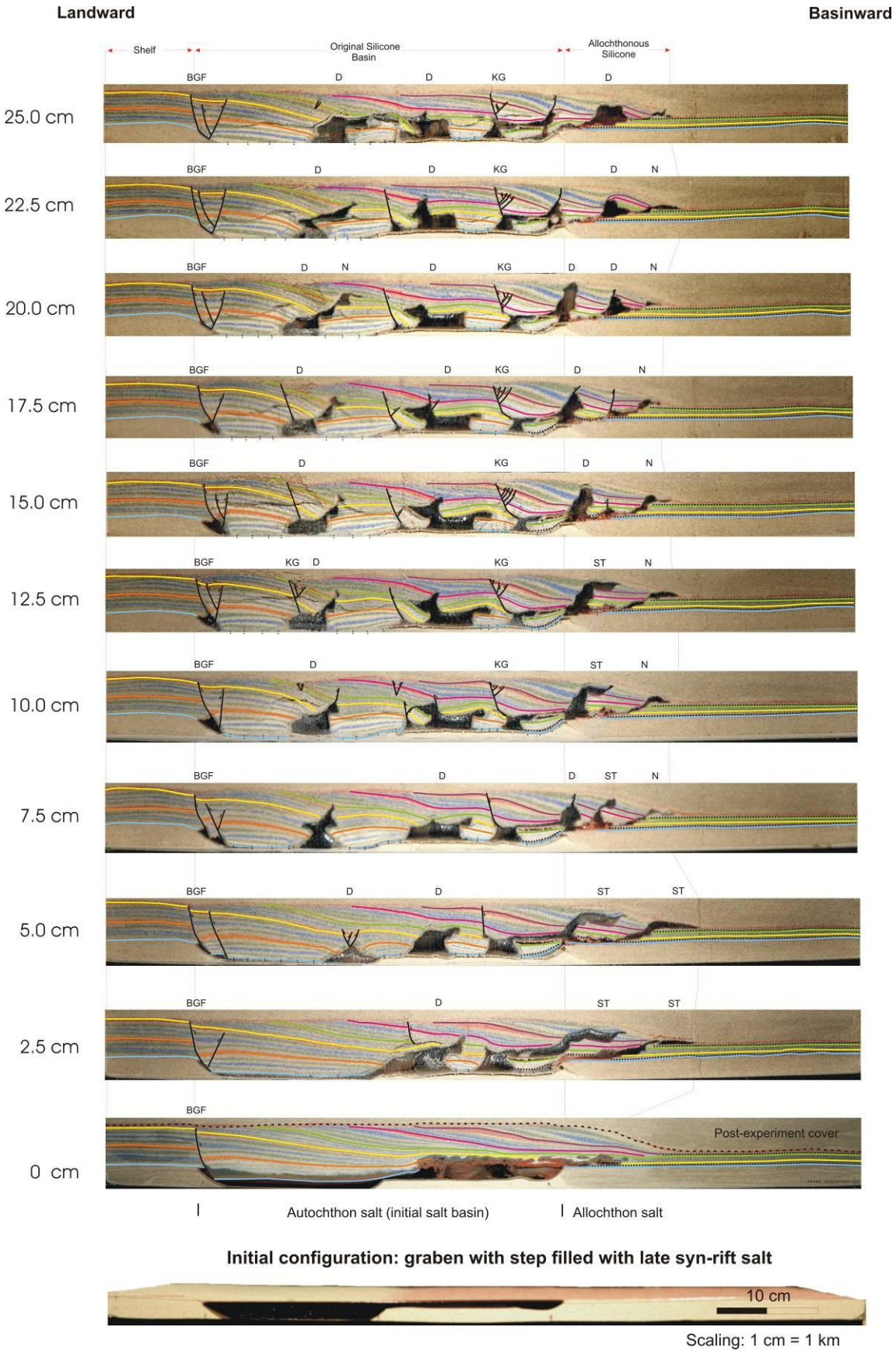
Landward
Basinward
Shelf
Original Silicone Basin
Allochthonous Silicone
25.0 cm
22.5 cm
20.0 cm
17.5 cm
15.0 cm
12.5 cm
10.0 cm
7.5 cm
5.0 cm
2.5 cm
0 cm
BGF
D
KG
N
ST
Post-experiment cover
Autochthon salt (initial salt basin)
Allochthon salt
Initial configuration: graben with step filled with late syn-rift salt
10 cm
Scaling: 1 cm = 1 km

B4: Sections of the symmetric graben with intermediate horst experiment. Sections detail lateral changes through the extent of the experimental base. BGF: Basinward dipping listric growth fault system. SG: Symmetric graben. ER/KG: Expulsion rollover/keystone graben. D: Diapir.
(Next Page)

Dalhousie Analogue Modelling Laboratory

DALHOUSIE UNIVERSITY *Inspiring Minds*

Test experiment 5-6 - Late Jurassic to Early Cretaceous Scotian Basin

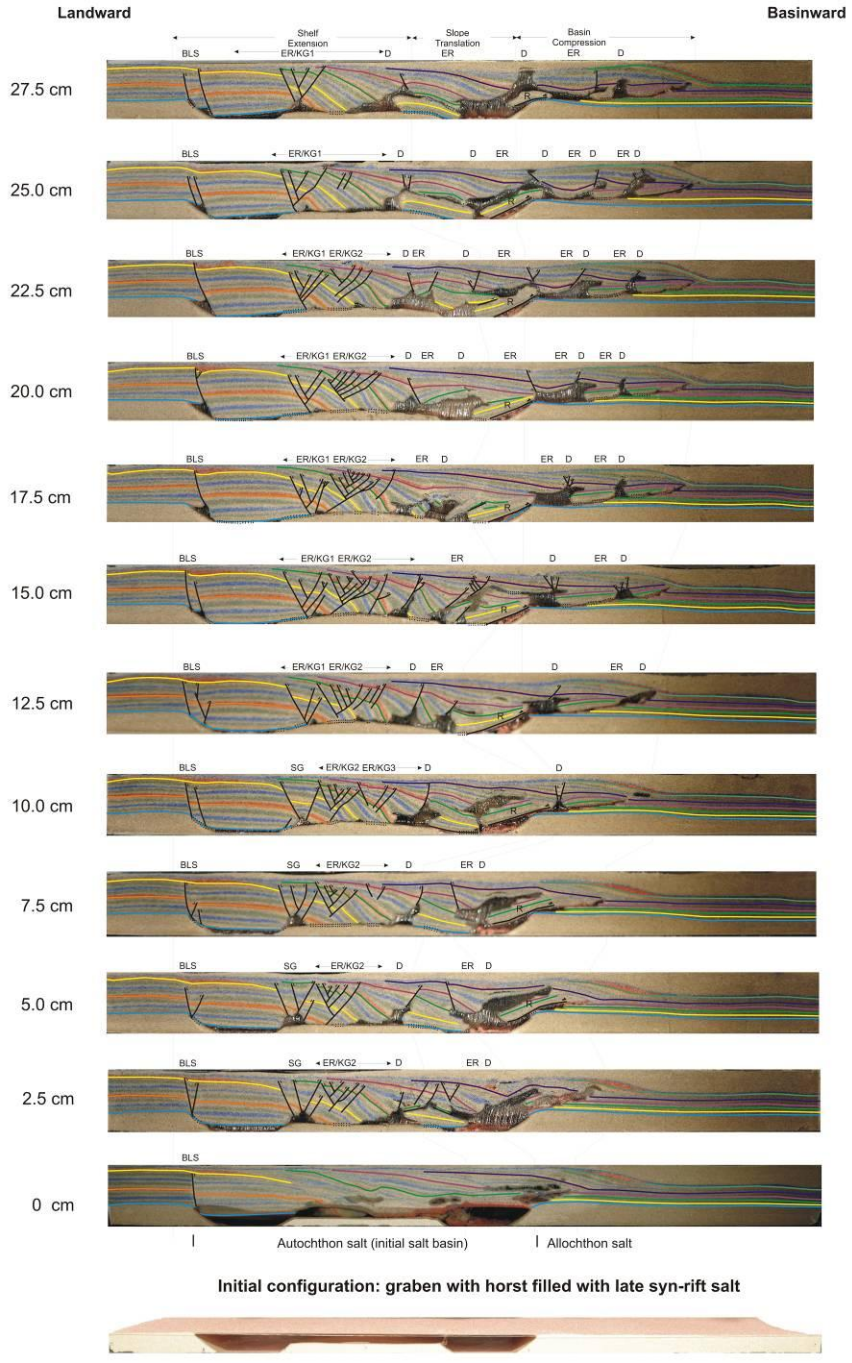

Experiment parameters
Experiment base: flat with horst
Initial salt ("silicone") basin = 30 (width) x 35 (length) x 2 (height) cm - [horst = 30 (width) x 15.5 (length) x 1 (height) cm]
Sedimentation rates = 0.2 cm/2 hours (day time/8 hours) and no sedimentation (night time/16 hours)
Duration of experiment = 222 hours

10 cm
Scaling: 1 cm = 1 km

APPENDIX C: PIV IMAGES FOR INTERPRETED SECTION

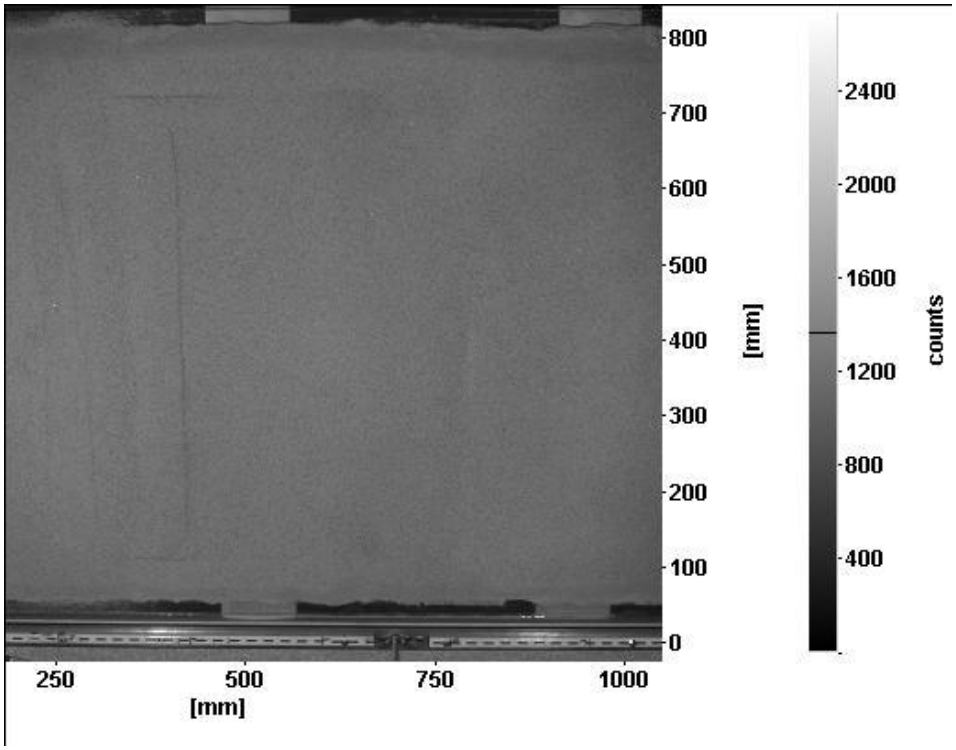

Appendix C1: Surface image of the basinward dipping growth normal fault.

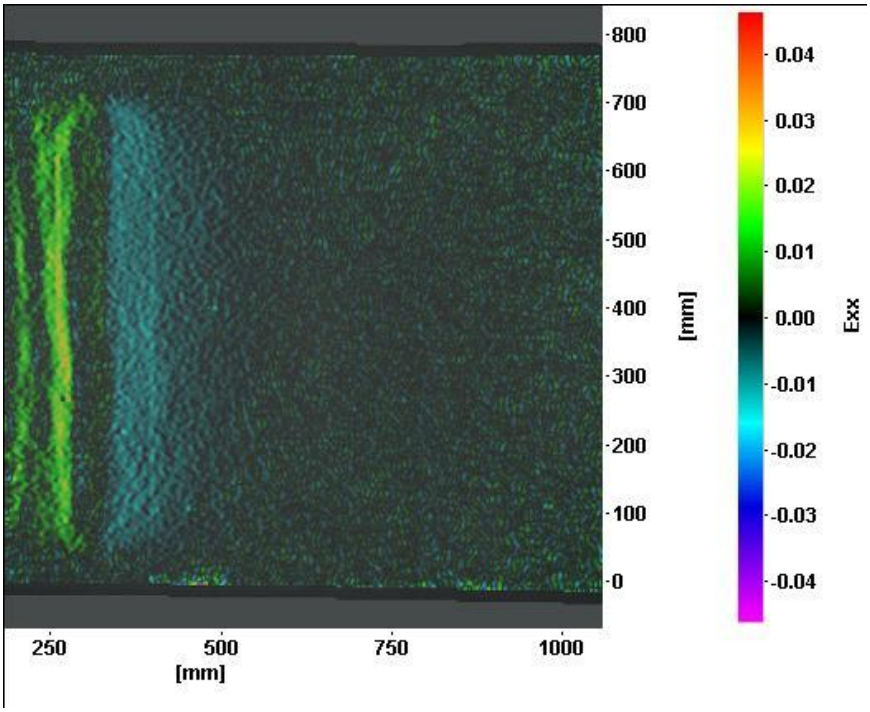

Appendix C2: Incremental strain image of the basinward dipping growth normal fault.

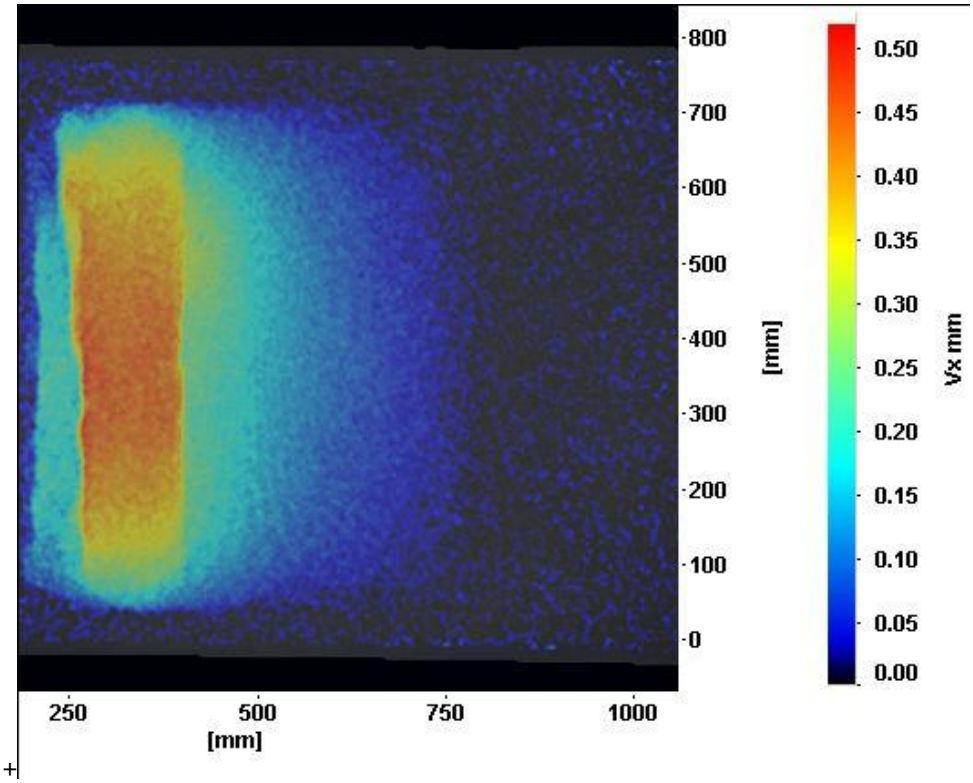

Appendix C3: Incremental velocity image of the basinward dipping growth normal fault.

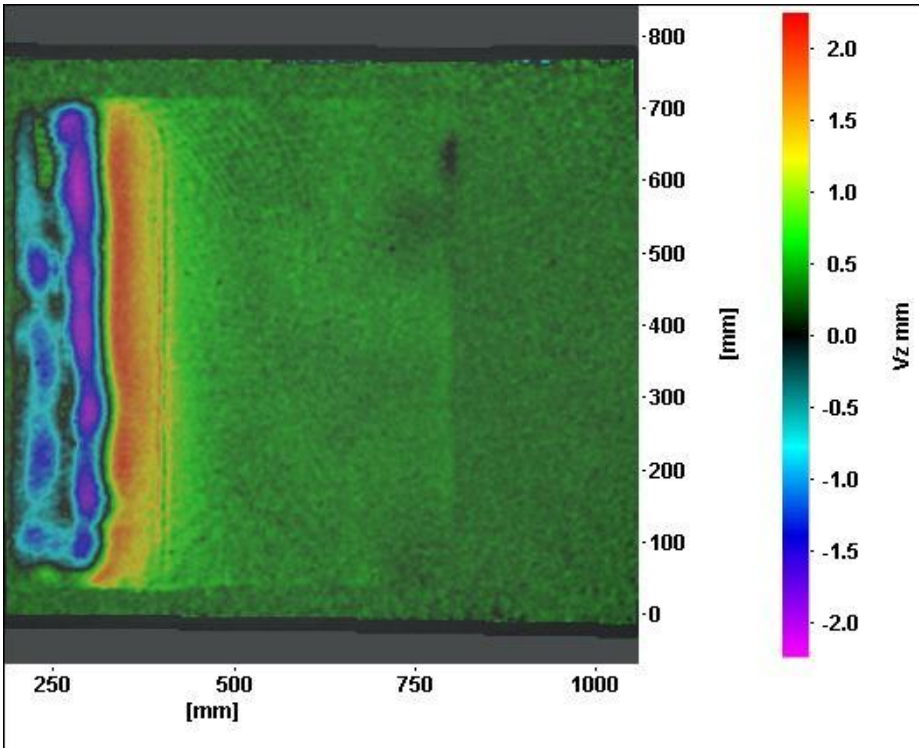

Appendix C4: Finite subsidence image of the basinward dipping growth normal fault.

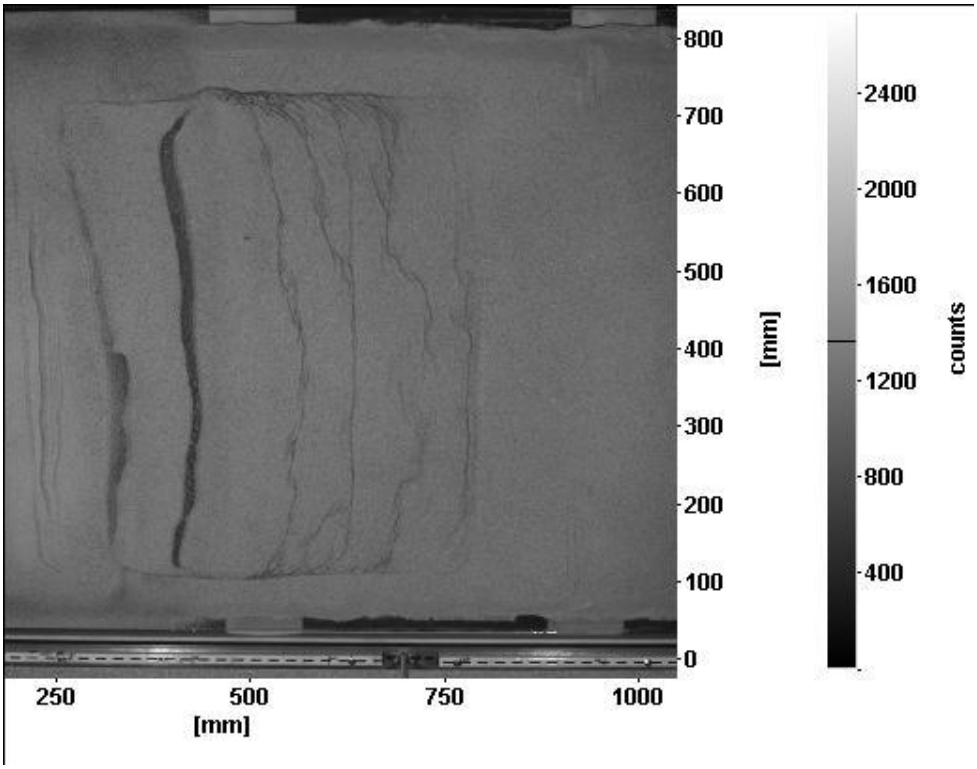

Appendix C5: Surface image of expulsion rollover "ER1".

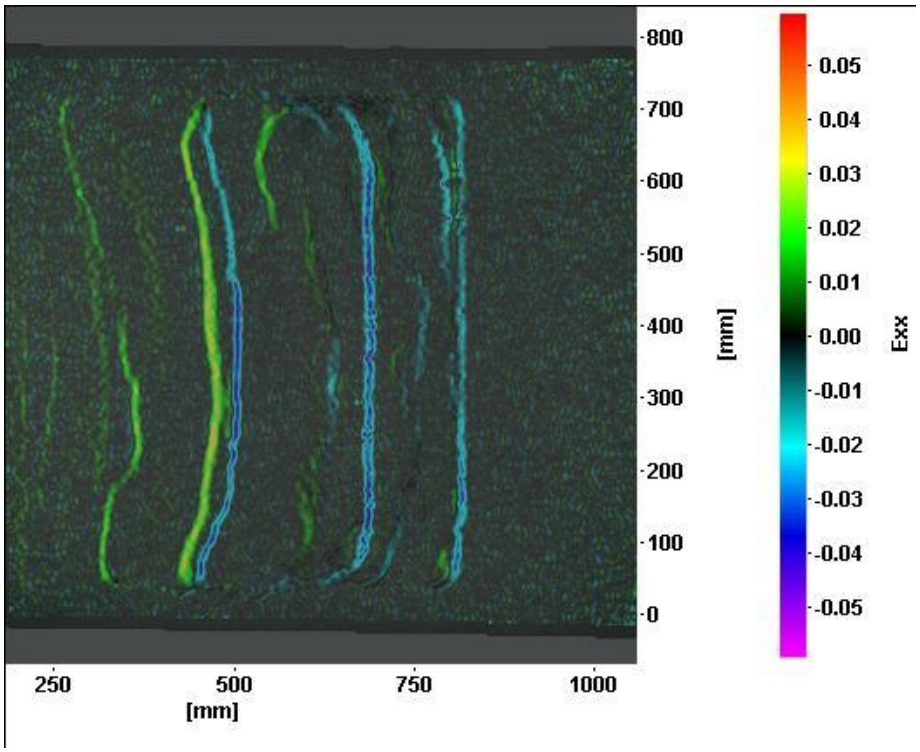

Appendix C6: Incremental strain image of expulsion rollover "ER1".

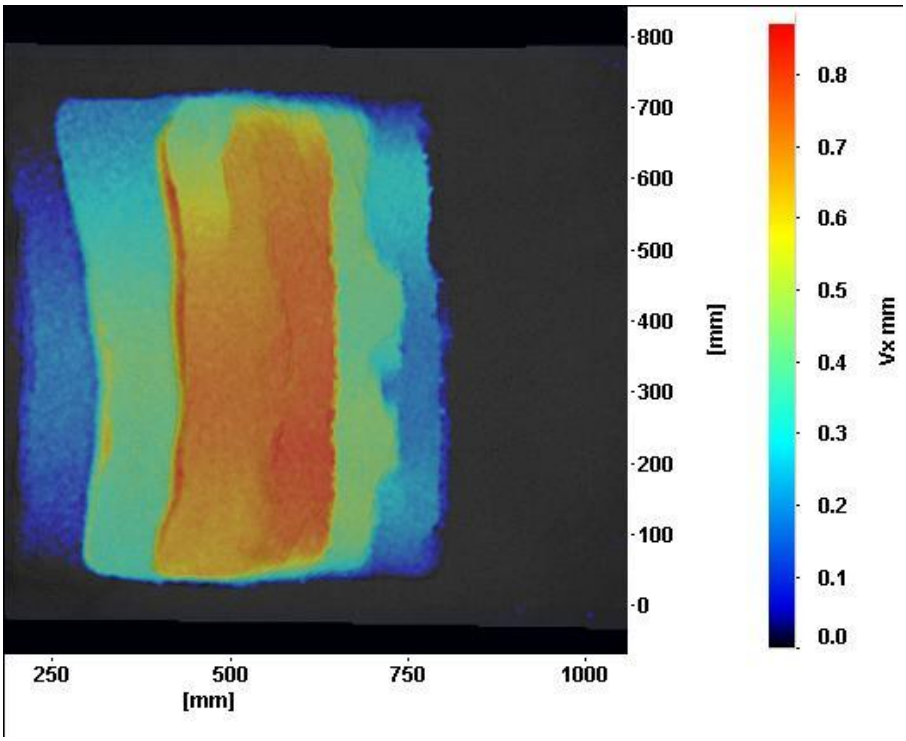

Appendix C7: Incremental velocity image of expulsion rollover "ER1".

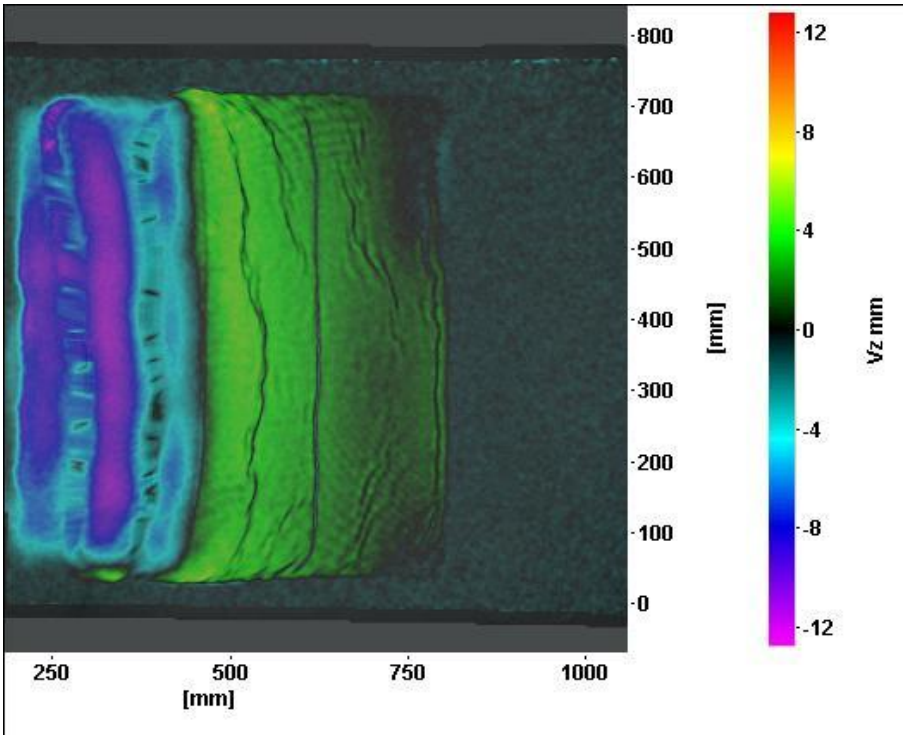

Appendix C8: Finite subsidence image of expulsion rollover "ER1".

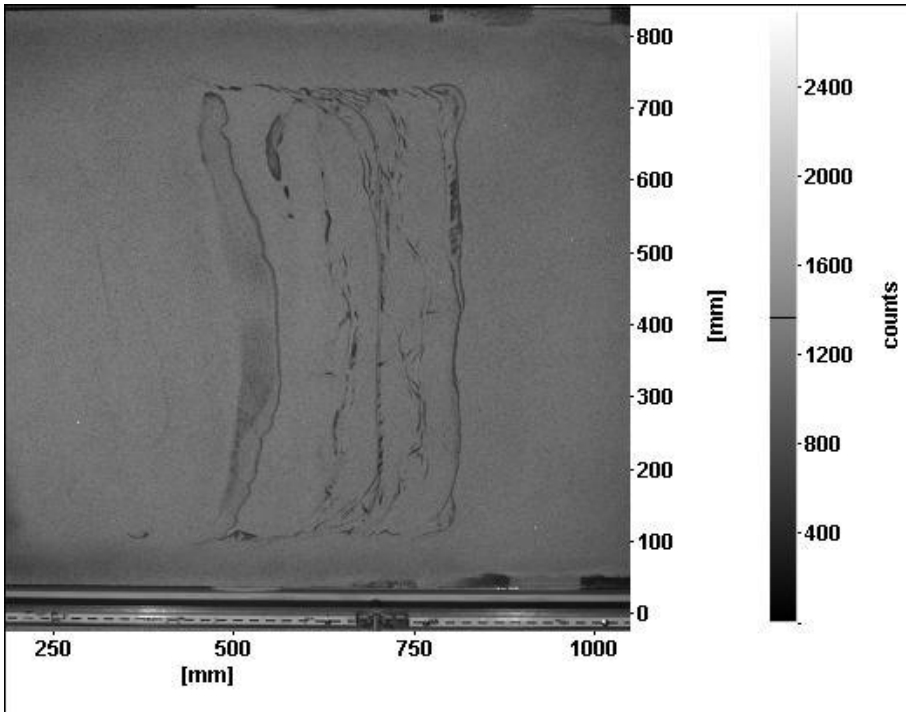

Appendix C9: Surface image of keystone grabens "KG 1 & KG 2".

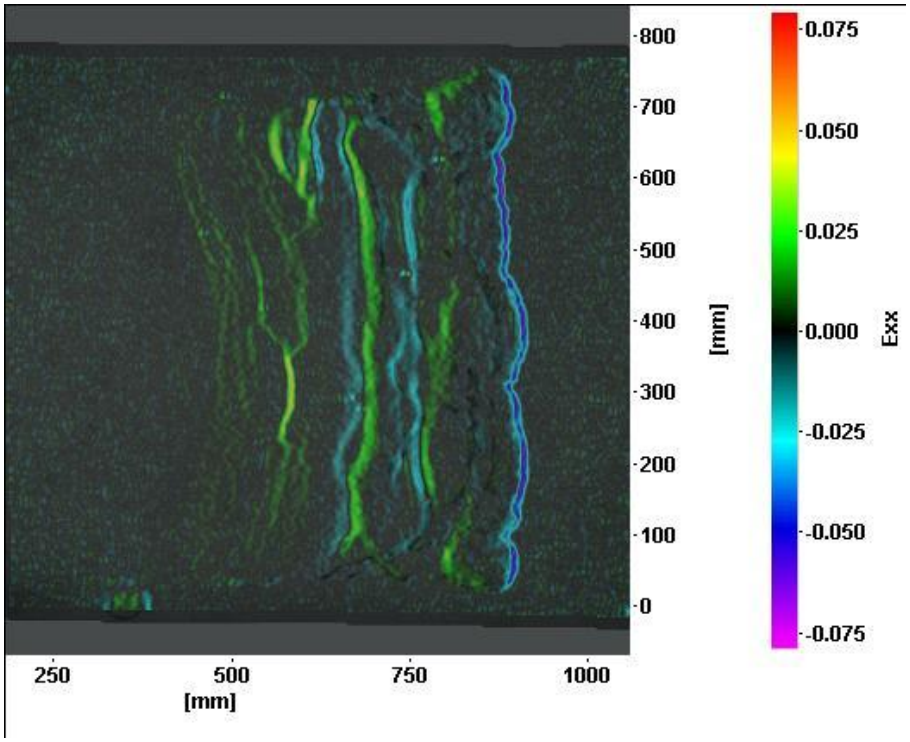

Appendix C10: Incremental strain image of keystone grabens "KG 1 & KG 2".

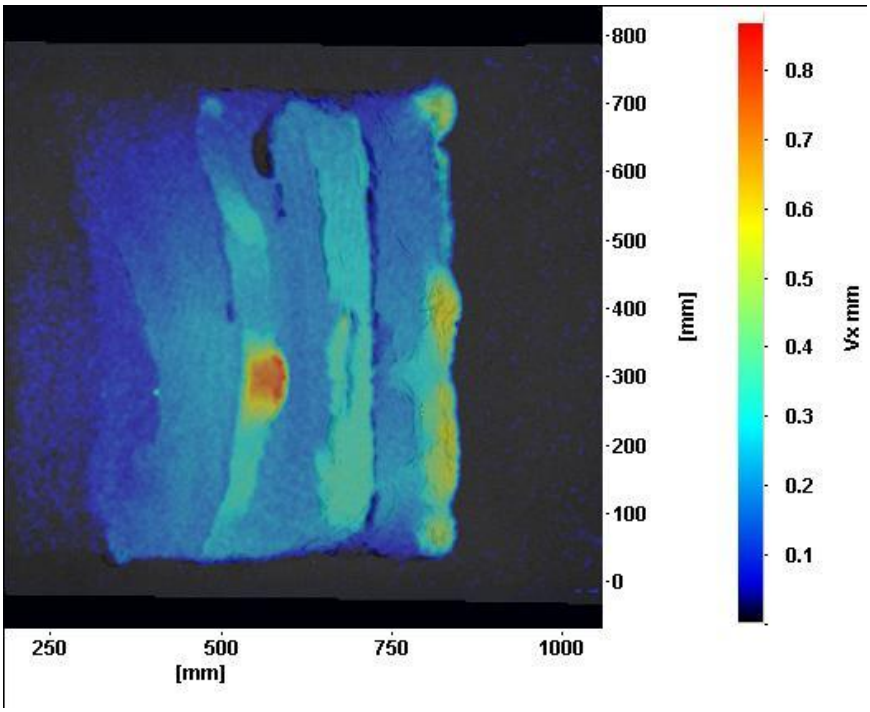

Appendix C11: Incremental velocity image of keystone grabens "KG 1 & KG 2".

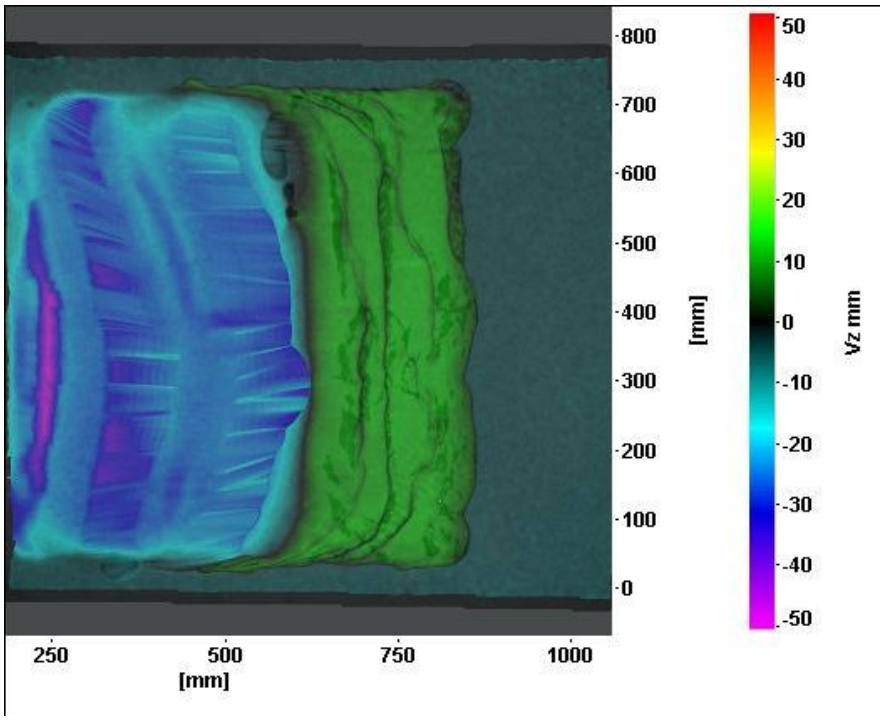

Appendix C12: Finite subsidence image of keystone grabens "KG 1 and KG 2".

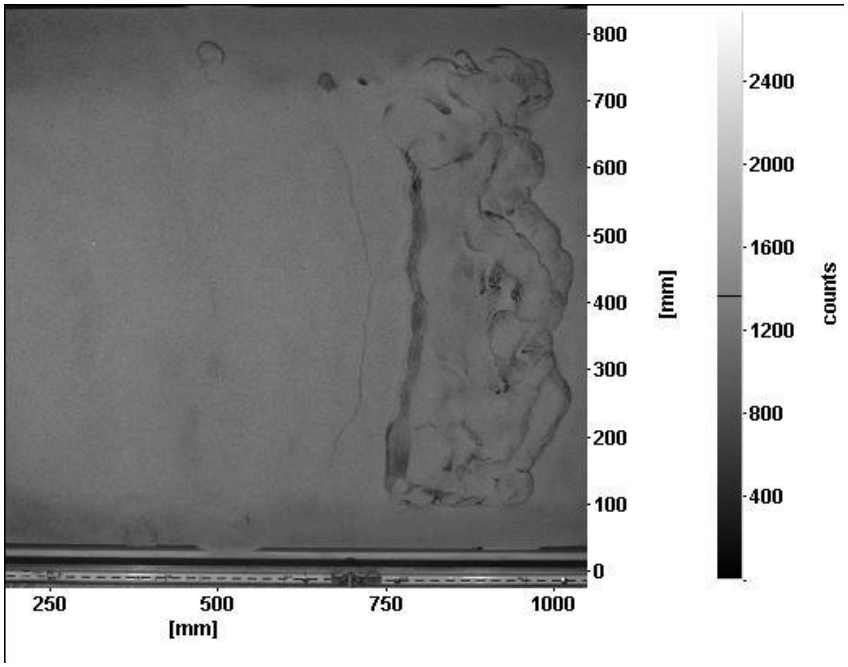

Appendix C13: Surface image of keystone graben "KG 3" and expulsion rollover "ER2".

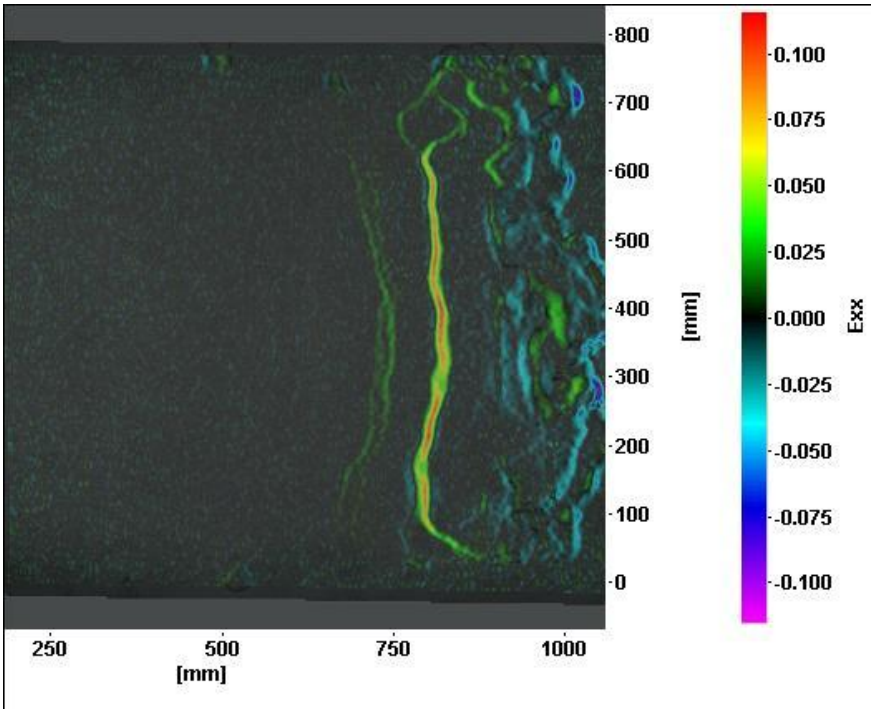

Appendix C14: Incremental strain image of keystone graben "KG 3" and expulsion "ER 2".

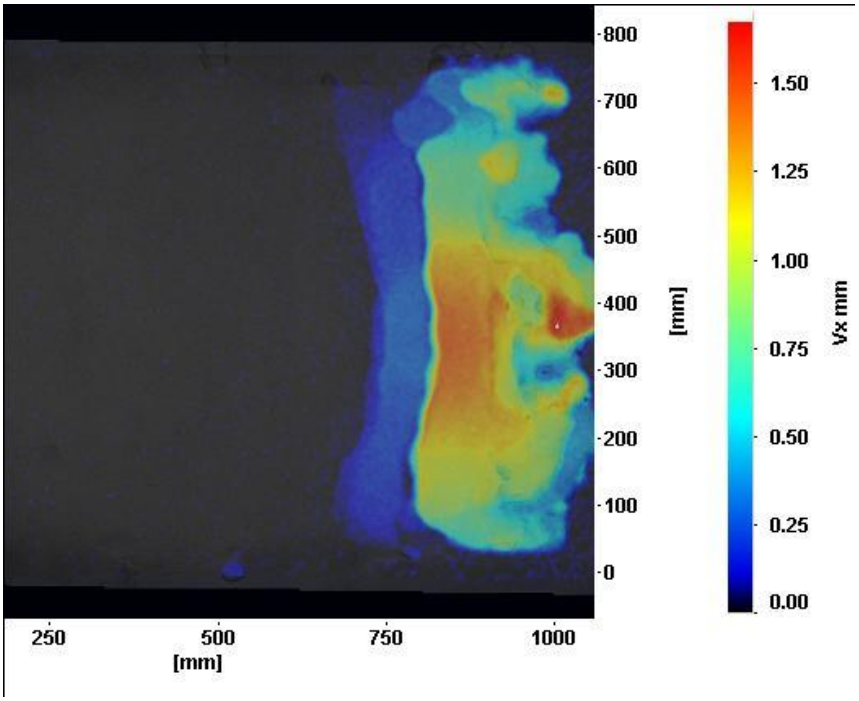

Appendix C15: Incremental velocity image of keystone graben "KG 3" and expulsion rollover "ER 2".

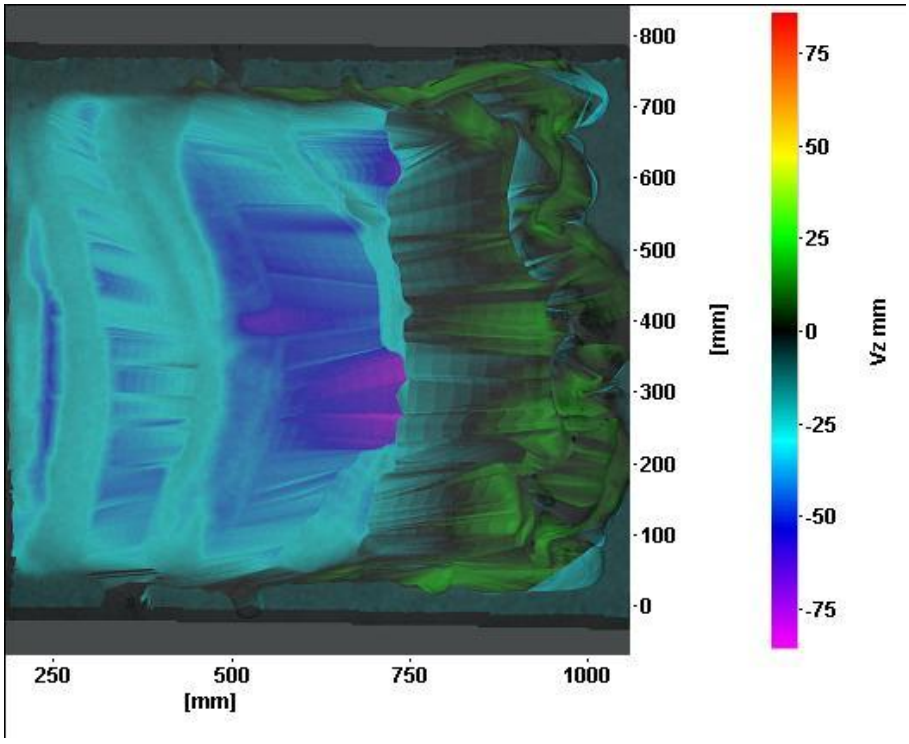

Appendix C16: Finite subsidence image of keystone graben "KG 3" and expulsion rollover "ER 2".